LATERAL-AXIAL COUPLING AND BOUNDARY CONDITIONING OF VIBRATING STRINGS AND CABLES

Chien-Yu Chen

A Thesis

In

The Department

of

Mechanical and Industrial Engineering

Presented in Partial Fulfillment of the Requirements

For the Degree of Master of Applied Science at

Concordia University

Montreal, Quebec, Canada

August 2007

© Chien-Yu Chen, 2007

Library and Archives Canada

Published Heritage Branch

395 Wellington Street
Ottawa ON K1A 0N4
Canada

Bibliothèque et Archives Canada

Direction du Patrimoine de l'édition

395, rue Wellington
Ottawa ON K1A 0N4
Canada

Your file Votre référence
ISBN: 978-0-494-34433-0
Our file Notre référence
ISBN: 978-0-494-34433-0

NOTICE:
The author has granted a non-exclusive license allowing Library and Archives Canada to reproduce, publish, archive, preserve, conserve, communicate to the public by telecommunication or on the Internet, loan, distribute and sell theses worldwide, for commercial or non-commercial purposes, in microform, paper, electronic and/or any other formats.

The author retains copyright ownership and moral rights in this thesis. Neither the thesis nor substantial extracts from it may be printed or otherwise reproduced without the author's permission.

AVIS:
L'auteur a accordé une licence non exclusive permettant à la Bibliothèque et Archives Canada de reproduire, publier, archiver, sauvegarder, conserver, transmettre au public par télécommunication ou par l'Internet, prêter, distribuer et vendre des thèses partout dans le monde, à des fins commerciales ou autres, sur support microforme, papier, électronique et/ou autres formats.

L'auteur conserve la propriété du droit d'auteur et des droits moraux qui protège cette thèse. Ni la thèse ni des extraits substantiels de celle-ci ne doivent être imprimés ou autrement reproduits sans son autorisation.

In compliance with the Canadian Privacy Act some supporting forms may have been removed from this thesis.

While these forms may be included in the document page count, their removal does not represent any loss of content from the thesis.

Conformément à la loi canadienne sur la protection de la vie privée, quelques formulaires secondaires ont été enlevés de cette thèse.

Bien que ces formulaires aient inclus dans la pagination, il n'y aura aucun contenu manquant.

Canada

ABSTRACT

Lateral-Axial Coupling and Boundary Conditioning

of Vibrating Strings and Cables

Chien-Yu Chen

Strings and cables are often used to support loads. Made of stiffer and stronger steel cables, the metal ropes find applications in heavy load bearing situations such as cable supported bridges, elevator, cable car transportation systems, and in overhead transmission line cables. Much more flexible and thin fibres, a key element in textile and optic fibre industry, are wound on high speed bobbins. In most of string and cable studies, very little attention has been given to the boundary condition that may affect their motion. In this thesis, two case studies are analyzed to study the effect of boundary condition on the string behaviour. In the first case, a string with a boundary condition in between fully clamped and free state is studied. The effect of such a partially clamped condition on the natural frequency has been tabulated. The second case investigates the axial-transverse coupled motion of a fixed-fixed string supported at two points. The nonlinearity of the tension during vibration is considered as well as the orbital motion of the excited string. The simulation of string motion is done using numerical finite difference method along with von Neumann and Courant stability conditions to ensure minimum iteration errors. Experiments are conducted by tracking the string's axial motion with a dynamic force sensor and lateral motion with a stroboscope to record the

orbital behavior. In addition fast Fourier transform (FFT) has been performed on sound produced by the vibrating string to obtain the frequency spectrum.

Transcontinental Academic Collaboration

That Attached Many "Heart Strings".

Dedicated to professors and classmates who participated in the visit and two month long stay at the India Institute of Technology, Madras

June-July, 2006

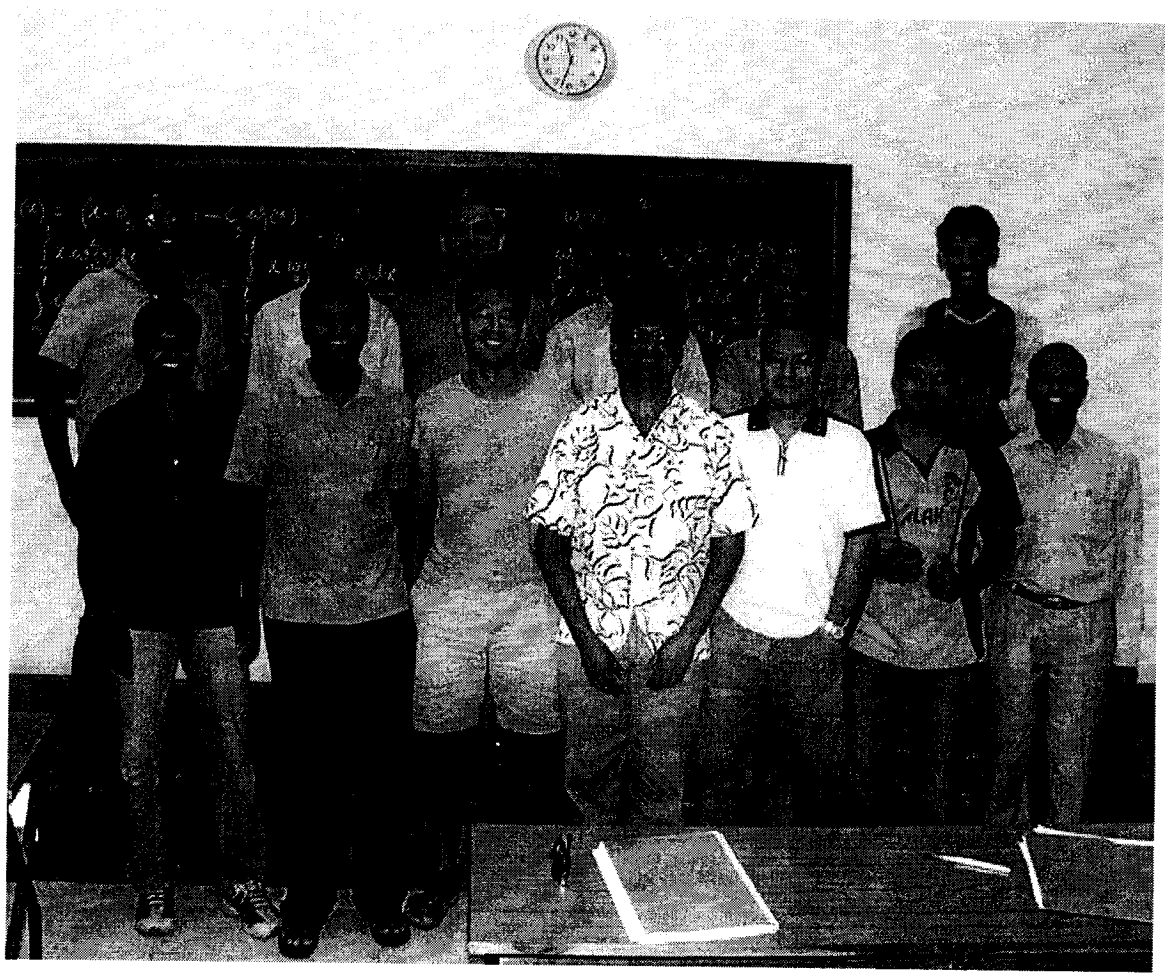

Acknowledgement

The author wishes to express his sincere appreciation to his research supervisor, Dr. Rama Bhat, for his continuous support and guidance during the course of this work. In addition, the author is deeply grateful for the exchange program with India Institute of Technology, Madras initiated by his supervisor. Beyond academic purpose, it was a self-discovering and spiritual trip to unearth the beauty of India. The author is also profoundly thankful for the permission given to pursue an 1800 hours of extra curricular studies in the evening in an automobile mechanics training to gain extra skills.

Special thanks and gratitude are due to Mr. Dainius Juras for his help backed with his vast experience at various stages of this work, especially in the important stage of experiment setup.

Finally, the author would like to thank his family members for the continuous support to whatever he has been able to accomplish so far. The author deeply and sincerely appreciates their understanding throughout some difficult moment in the course of his studies.

Table of Contents

List of Figures ix
List of Tables xiii
List of Symbols xiv
Chapter 1. Introduction 1
1.1 Types of String Vibration 2
1.2 Fundamental and Partials 3
1.3 Literature Review 5
1.3.1 Axial-transverse string model 5
1.3.2 Transmission line cable 6
1.3.3 Suspension bridge 7
1.3.4 Pulley, conveyor and winding systems 9
1.4 Objectives and Scope of Thesis 10
1.5 Thesis Organization 11
Chapter 2. Strings with Classical Boundary Condition 12
2.1 1D Transverse Vibration 12
2.2 2D Transverse Vibration 18
2.3 Axial Vibration 20
2.4 Summary 24
Chapter 3. Boundary Conditioning 26
3.1 Effect of Partial Clamping 27
3.2 3D Coupled String Model 35
3.3 Summary 40

Chapter 4. Beat Phenomenon 42
4.1 Introduction 43
4.2 Beat Equation 44
4.3 Beat Frequency 48
4.4 Wave Interference 49
4.5 Inharmonicity 51
4.6 Summary 59
Chapter 5. Simulation 60
5.1 Finite Difference Method 61
5.2 Digital Waveguide Method 68
5.3 Simulation Results 70
5.4 Summary 81
Chapter 6. Experiments 82
6.1 Experiment Apparatus and Setup 83
6.2 Experimental Results 88
6.3 Data Analyses 109
6.4 Summary 112
Chapter 7. Conclusions 113
7.1 Summary 113
7.2 Conclusions 114
7.3 Recommendations for Future Investigations 116
References 117

List of Figures

Fig. 1.1. Cable car transportation system 2

Fig. 1.2. Types of vibration on a fixed-fixed string 3

Fig. 1.3. Standing waves between two fixed ends 4

Fig. 1.4. Transmission line cables 7

Fig. 1.5. Collapse of Tacoma Narrows Bridge 8

Fig. 1.6. Zarubinskaya and van Horssen's suspension bridge modeled [105, 106] 9

Fig. 2.1. Transverse vibration string segment 13

Fig. 2.2. Motion of a single oscillation cycle of string with an initial impulse displacement at center 17

Fig. 2.3. Different types of string winding 18

Fig. 2.4. Various whirling orbits [94] 19

Fig. 2.5. String at different states 21

Fig. 2.6. Axial vibration string segment 22

Fig. 3.1. String with partial clamped end 27

Fig. 3.2 Graphical solution of transcendental equation 29

Fig. 3.3. Graphical solution of Eq. (3.4) with $L = 0.25m$ 30

Fig. 3.4. Graphical solution of Eq. (3.4) with $L = 5.00m$ 30

Fig. 3.5. String model 35

Fig. 3.6. String segment 36

Fig. 3.7. Spectrum of a piano note with phantom partials marked by circles [3] 40

Fig. 4.1. Two vibrations of same amplitude and close frequencies $(\omega_1 \approx \omega_2)$ 43

Fig. 4.2. Two vibrations of different amplitudes $(G = 1.5, H = 0.5)$ and close frequencies $(\omega_1 \approx \omega_2)$ 46

Fig. 4.3. Graphic representation of beat equation (Eq. (4.5)) 47

Fig. 4.4. Wave interference and phase 50

Fig. 4.6. Fundamental (ω_1) and first harmonic partial (ω_2) of same amplitude, $(\omega_2 = 2\omega_1)$ 52

Fig. 4.7. Fundamental (ω_1) and first inharmonic partial (ω_2) of same amplitude, $(\omega_2 \approx 2\omega_1 \,\&\, \omega_2 < 2\omega_1)$ 52

Fig. 4.8. Fundamental (ω_1) and first inharmonic partial (ω_2) of same amplitude, $(\omega_2 \approx 2\omega_1 \,\&\, \omega_2 > 2\omega_1)$ 52

Fig. 4.9. Fundamental (ω_1) and first two (ω_2, ω_3) harmonic partials of same amplitude, $(\omega_2 = 2\omega_1; \omega_3 = 3\omega_1)$ 53

Fig. 4.10. Fundamental (ω_1) and first two (ω_2, ω_3) inharmonic partials of same amplitude, $(\omega_2 \approx 2\omega_1 \,\&\, \omega_2 > 2\omega_1; \omega_3 \approx 3\omega_1 \,\&\, \omega_3 > 3\omega_1)$ 54

Fig. 4.11. Fundamental (ω_1) and first two (ω_2, ω_3) inharmonic partials of same amplitude, $(\omega_2 \approx 2\omega_1 \,\&\, \omega_2 < 2\omega_1; \omega_3 \approx 3\omega_1 \,\&\, \omega_3 < 3\omega_1)$ 54

Fig. 4.12. Fundamental (ω_1) and first two (ω_2, ω_3) inharmonic partials, of same amplitude, $(\omega_2 \approx 2\omega_1 \,\&\, \omega_2 < 2\omega_1; \omega_3 \approx 3\omega_1 \,\&\, \omega_3 > 3\omega_1)$ 55

Fig. 4.13. Fundamental (ω_1) and first two (ω_2, ω_3) inharmonic partials of same amplitude, $(\omega_2 \approx 2\omega_1 \,\&\, \omega_2 > 2\omega_1; \omega_3 \approx 3\omega_1 \,\&\, \omega_3 < 3\omega_1)$ 55

Fig. 4.14. Fundamental (ω_1) and first (ω_2) harmonic odd partials of same amplitude, $(\omega_2 = 2.01\omega_1)$ 56

Fig. 4.15. Fundamental (ω_1) and first two (ω_2, ω_3) harmonic odd partials of same amplitude, $(\omega_2 = 2.01\omega_1; \omega_3 = 3.02\omega_1)$ 56

Fig. 4.16. Fundamental (ω_1) and first three $(\omega_2, \omega_3, \omega_4)$ harmonic odd partials of same amplitude, $(\omega_2 = 2.01\omega_1; \omega_3 = 3.02\omega_1; \omega_4 = 4.05\omega_1)$ 56

Fig. 4.17. Fundamental (ω_1) and first two (ω_2, ω_3) harmonic odd partials of same amplitude, $(\omega_2 = 3\omega_1; \omega_3 = 5\omega_1)$ 57

Fig. 4.18. Fundamental (ω_1) and first (ω_2) inharmonic odd partials of same amplitude, ($\omega_2 = 2.88\omega_1$) 58

Fig. 4.19. Fundamental (ω_1) and first two (ω_2, ω_3) inharmonic odd partials of same amplitude, ($\omega_2 = 2.88\omega_1; \omega_3 = 4.78\omega_1$) 58

Fig. 4.20. Fundamental (ω_1) and first three ($\omega_2, \omega_3, \omega_4$) inharmonic odd partials of same amplitude, ($\omega_2 = 2.88\omega_1; \omega_3 = 4.78\omega_1; \omega_4 = 6.68\omega_1$) 58

Fig. 5.1. Central difference space-time grid 62

Fig. 5.2. First order central difference scheme 62

Fig. 5.3. Second order central difference scheme 63

Fig. 5.4. Schematic diagram of Courant stable and unstable choices of time and space steps (Δt and Δx) [84] 67

Fig. 5.5. D'Alembert's traveling waves [43] 68

Fig. 5.6. Digital waveguide model of ideal string fixed at both ends [84] 69

Fig. 5.7. Complete lateral motion cycle for a string excited at $\frac{L}{3}$ 71

Fig. 5.8. Combination of lateral motion of an undamped fixed-fixed string 71

Fig. 5.9. Lateral vibration (ideal 1D wave equation) at $\frac{L}{3}$ using $\Delta t = \Delta x / c_T$ as grid..... 73

Fig. 5.10. Lateral vibration (ideal 1D wave equation) at $\frac{L}{3}$ using $\Delta t = \Delta x / c_A$ as grid... 73

Fig. 5.11. Coupled system behavior at $\frac{L}{3}$ 75

Fig. 5.12. Complete lateral motion cycle for a string lifted at one end excited at $\frac{L}{3}$ 77

Fig. 5.13. Combination of lateral motion of an undamped fixed-partially clamped string 77

Fig. 5.14. Rightmost (bottom) and leftmost (top) tilts of fixed-partially clamped string. 78

Fig. 5.15. Oscillation at various position of the string with partially clamped end at $x = L$ 79

Fig. 5.16. Combined FFT of all points on a fixed-partially clamped string 80

Fig. 5.17. Combined FFT of all points on a fixed-fixed string 80

Fig. 6.1. Experiment setup diagram 83
Fig. 6.2. Static load cell SW-500C from Transducer Techniques 83
Fig. 6.3. Digital strain gauge P3500 from Measurement Group 84
Fig. 6.4. Model 912 quartz dynamic load cell from Kistler Instrument 86
Fig. 6.5. Analyzer and oscilloscope 87
Fig. 6.6. Experiment setup 88
Fig. 6.7. Dynamic force sensor signal recorded by oscilloscope for 0.33 mm string 90
Fig. 6.8. FFT of dynamic force sensor signal from the analyzer for 0.33 mm string 91
Fig. 6.9. FFT of sound clip recorded for 0.33 mm string 92
Fig. 6.10. Dynamic force sensor signal recorded by oscilloscope for 0.43 mm string 93
Fig. 6.11. FFT of dynamic force sensor signal from the analyzer for 0.43 mm string 94
Fig. 6.12. FFT of sound clip recorded for 0.43 mm string 95
Fig. 6.13. Dynamic force sensor signal recorded by oscilloscope for 0.66 mm string 96
Fig. 6.14. FFT of dynamic force sensor signal from the analyzer for 0.66 mm string 97
Fig. 6.15. FFT of sound clip recorded for 0.66 mm string 98
Fig. 6.16. Dynamic force sensor signal recorded by oscilloscope for 0.91 mm string 99
Fig. 6.17. FFT of dynamic force sensor signal from the analyzer for 0.91 mm string ... 100
Fig. 6.18. FFT of sound clip recorded for 0.91 mm string 101
Fig. 6.19. Dynamic force sensor signal recorded by oscilloscope for 1.17 mm string ... 102
Fig. 6.20. FFT of dynamic force sensor signal from the analyzer for 1.17 mm string ... 103
Fig. 6.21. FFT of sound clip recorded for 1.17 mm string 104
Fig. 6.22. Dynamic force sensor signal recorded by oscilloscope for 1.42 mm string ... 105
Fig. 6.23. FFT of dynamic force sensor signal from the analyzer for 1.42 mm string ... 106
Fig. 6.24. FFT of sound clip recorded for 1.42 mm string 107
Fig. 6.25. FFT of sound clip recorded for room noise 108
Fig. 6.26. FFT of sounds recorded for each string from a Yamaha guitar 109
Fig. 6.27. Top and bottom (left), and right and left (right) string motions 112

List of Tables

Table 3.1. Fundamental frequency (f_1) with respect to stiffness and string length 31

Table 3.2. First partial frequency (f_2) with respect to stiffness and string length 32

Table 3.3. Second partial frequency (f_3) with respect to stiffness and string length 32

Table 3.4. Third partial frequency (f_4) with respect to stiffness and string length 32

Table 3.5. Fourth partial frequency (f_5) with respect to stiffness and string length 33

Table 3.6. Fifth partial frequency (f_6) with respect to stiffness and string length 33

Table 3.7. Inharmonicity with respect to stiffness and string length 34

Table 6.1. Static load cell SW-500C specifications 84

Table 6.2. Strain gauge P3500 gauge factor setting 85

Table 6.3. Dynamic load cell model 912 specifications 86

Table 6.4. Devices used in current experiment 88

Table 6.5. Guitar string properties 89

Table 6.6. Frequencies table 110

Table 6.7. Inharmonicity table 111

List of Symbols

Notation	Description	Units
A	cross section area	m^2
c_A	axial/longitudinal wave velocity	m/s
c_T	transverse/lateral wave velocity	m/s
d	diameter	m
E	Young's modulus / modulus of elasticity	N/m^2
F	force	N
f	frequency	$1/s$
f_1	fundamental frequency	$1/s$
f_n	n partial frequency	$1/s$
G	amplitude of vibration	m
H	amplitude of vibration	m
J	amplitude of vibration	m
K	amplitude of vibration	m
k	spring constant	N/m

L_A	string length between both fixed ends	m
L_T	string length between both supported points	m
n	partial number	
O	Landau symbol representing the order of the function	
$\vec{r}$	vibrating string length (vector)	m
s	vibrating string length (scalar)	m
T_o	initial tension	N
t	time	s
u	displacement	m
u^x	displacement along x	m
u^y	displacement along y	m
u^z	displacement along z	m
x	axial/longitudinal direction	
y	transverse/lateral direction; excited direction	
z	transverse/lateral direction; $\perp$ to excited direction	
β	inharmonicity coefficient	
Δ	finite difference operator	
ε	strain	
θ	angle	$\circ$
κ	wave number	
λ	wave length	m
ξ	amplification factor	

ρ	mass per length	kg/m
σ	stress	N/m^2
τ	dummy variable	
ω	angular frequency	rad/s
ω_n^x	axial/longitudinal angular frequency in x axis	rad/s
ω_n^y	transverse/lateral angular frequency in y axis	rad/s
ω_n^z	transverse/lateral angular frequency in z axis	rad/s

Chapter 1

Introduction

Strings, ropes and cables are used in many mechanisms, and their applications vary from load carrying, signal/energy transportation to sound generation. Suspension bridges, cable supported elevators, transmission lines and musical strings are few examples among many cable structures. While single thread is flexible yet weak, a strand can be significantly stronger. This principle can be readily verified from textile and fiber reinforced materials. From manufacturing to applications, many industries are closely tied to strings and cables. In many works, strings and cables are simply modeled as fixed at both ends. However, this theoretical boundary condition does not necessary reflect the reality. In electric transmission lines, cables are suspended from the tower supports without clamping them, and in pulley system, cable at one side is always under higher tension than the other. Various supports between the two fixed ends also condition the string behavior such as in bridges and frets in musical instruments. All those examples reflect various boundary conditions that different cable/string systems are subjected to.

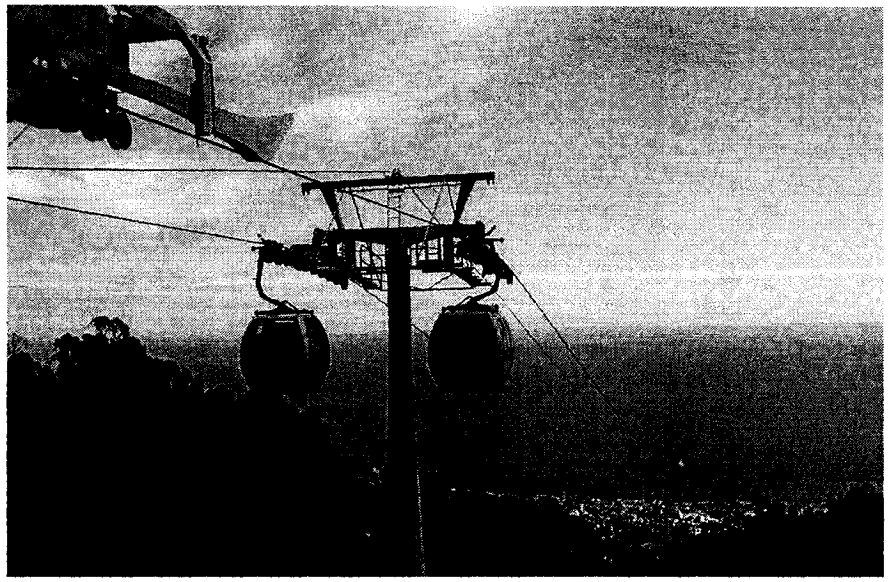

Fig. 1.1. Cable car transportation system

1.1 Types of String Vibration

Vibrating systems can perform either free or forced vibration. In string and cable systems, those that are driven by motors or engines such as elevators and cable cars are undergoing forced vibration since they are continuously under the action of a force input. Naturally, those systems will vibrate at the exciting frequency introduced by the applied force. When an initial input is introduced and the system is left to vibrate freely at its natural frequency, it undergoes free vibration and gets naturally damped out over time. Some of the examples of free vibration include strings in musical instruments excited by plucking, hammering or bowing, and electrical transmission lines and suspension bridges excited by sudden strong wind. In the case of cable cars as shown in Fig. 1.1, besides the applied force from the motor, it is also affected by wind. Irrespective of whether they

undergo forced or free vibration, all the cables exhibit, to a certain degree, three modes of vibrations: transverse, axial and torsional. Acting perpendicular to the string, also known as lateral vibration, the transverse motion is the most predominant behavior in strings and cables. The axial vibration is introduced by string stretching during lateral motion. Also known as longitudinal vibration, the axial motion is often ignored in analyses as its magnitude is considered negligible compared to that of the lateral vibration. Not as common as the two just mentioned, torsional vibration can be observed when strong wind blows on ice accreted transmission line cables with an eccentric ice load. The three types of motions are illustrated in Fig. 1.2.

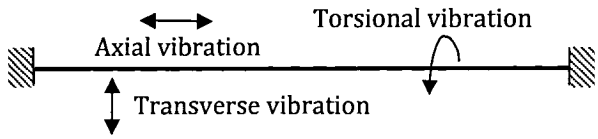

Fig. 1.2. Types of vibration on a fixed-fixed string

1.2 Fundamental and Partials

In vibrating systems, due to boundary conditions, only specific vibration modes are possible. In a string fixed at both ends, the possible vibration modes are shown in Fig. 1.3. The longest wave allowed is called the fundamental, while all others are called harmonics or partials. A harmonic is defined as integer multiples of the fundamental frequency. A vibrating string seldom oscillates at a single frequency but rather as a summation of fundamental and multiple partials where the fundamental is the dominant

frequency. This defines vibrating string pattern as a mixture of waves which typically have whole number ratios between the frequencies. Acoustically, this mathematical relationship between fundamental and partials represents a certain pattern in frequency spectrum which is pleasant to human ears.

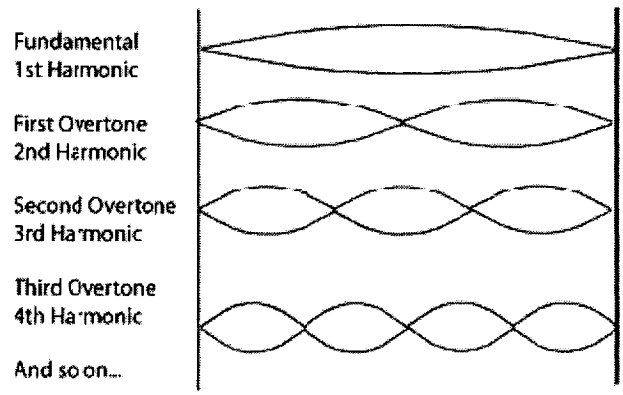

Fig. 1.3. Standing waves between two fixed ends

Theoretically, harmonics or partials are at multiples of the fundamental frequency. However, studies performed by H. Fletcher et al. [33] on piano strings have shown the presence of inharmonicity due to nonlinear behavior of the stretched string due to string stiffness. Inharmonicity is a common term referring to spectra in which one or several partials are shifted slightly away from their harmonic positions. Since the inharmonicity is directly affected by the string stiffness, there will be a higher degree of inharmonicity in soft strings such as optical fiber and textile threads than in larger and stiffer steel cables. According to H. Fletcher et al. [33], inharmonicity is not necessarily unpleasant; and a slight inharmonicity actually adds a certain warmth to the sound. They further point out that a small amount of inharmonicity in synthesized piano tones renders the sound

more natural. Due to inharmonicity, the term partial will be used in this thesis as it is more appropriate than harmonic.

1.3 Literature Review

Since strings are one of the most common structural elements in many mechanical systems, their vibrations have been extensively studied and well documented. However, most of the studies simply consider completely fixed boundary condition which does not always reflect the real situation. There are very few studies exploring the effect of boundary conditions on the string vibration.

1.3.1 Axial-transverse string model

Historically, the vibrating string has sparked interest of several mathematicians namely D'Alembert, Euler, Bernoulli, and Lagrange. While the 1D wave equation has been known for a while, it had to wait until early 20^{th} Century for some basic coupled models to be proposed as in the book written by W. F. Osgood [79]. This initial work was later improved by A. H. Nayfeh [74] with a truly 3D model that included axial and transverse motion. He further proposed different conditions for soft and stiff strings based on the amplitude of axial and lateral motions. However, the stress-strain relation used turns out to be an approximation to Hooke's law. This later misled works done by others such as R. Narashima [73], J. A. Elliott [29, 30], C. E. Gough [42], N. B. Tufillaro [91, 92], H. P. W. Gottlieb [41], A. Watzky [99], etc. The correct model was proposed by E.

V. Kurmyshev [58] using the exact Hooke's equation for elastic string with large amplitude of oscillation. However, his attempt at solving the equations mathematically could only include the fundamental mode.

1.3.2 Transmission line cable

In electricity transmission, huge columns are used to support the long overhead transmission lines at various points. The cables are connected to the columns by insulators which do not firmly clamp the cables to the supports as shown in Fig. 1.4. Such cables are subject to a certain sag which allows wind induced oscillations. The cable motion is generally classified into three types, namely, galloping, aeolian and wake induced vibrations. Among those, the low frequency large amplitude galloping oscillation is the most important to be considered. J. P. den Hartog [28] presented one of the first models for galloping vibration on an iced transmission line cable considering the aerodynamic properties of the ice profile. Later, T. Ohkuma et al. [77, 78] did significant works investigating factors that initiate and cause of the galloping leading to the consideration of parameters such as the initial angle of wind attack, the initial icing angle and the wind speed. A full multi span 3D model was proposed by J. Wang and J. L. Lilien [97], which can predict the galloping behavior of the iced transmission lines within an acceptable accuracy. However, among all the works, only aerodynamic aspects are focused while neglecting the effect of boundary condition on the cable behavior.

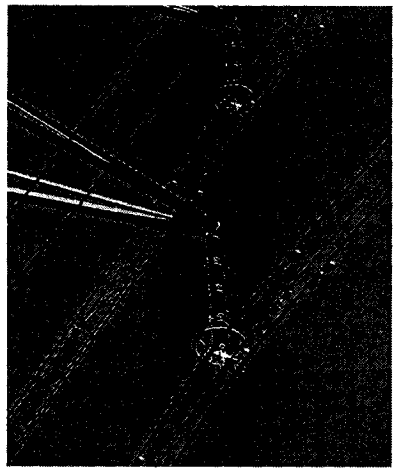

Fig. 1.4. Transmission line cables

1.3.3 Suspension bridge

Developed in the early 19th Century, the modern suspension bridge has gained wide popularity due to its long span capacity. However, with the collapse of the Tacoma Narrows Bridge (see Fig. 1.5) in 1940 due to wind induced vibration, studies have mainly focused on aerodynamic instability as reported by F. Bleich et al. [12]. Numerous studies have also been carried out by several authors on particular bridges. However, all those studies uniquely focused on the effect of wind and the aerodynamic force on the complete bridge. C. Su et al. [89] have done investigations on a suspension bridge at various stages of erection, however, the effect of various boundary conditions that the cables experienced during construction was not discussed.

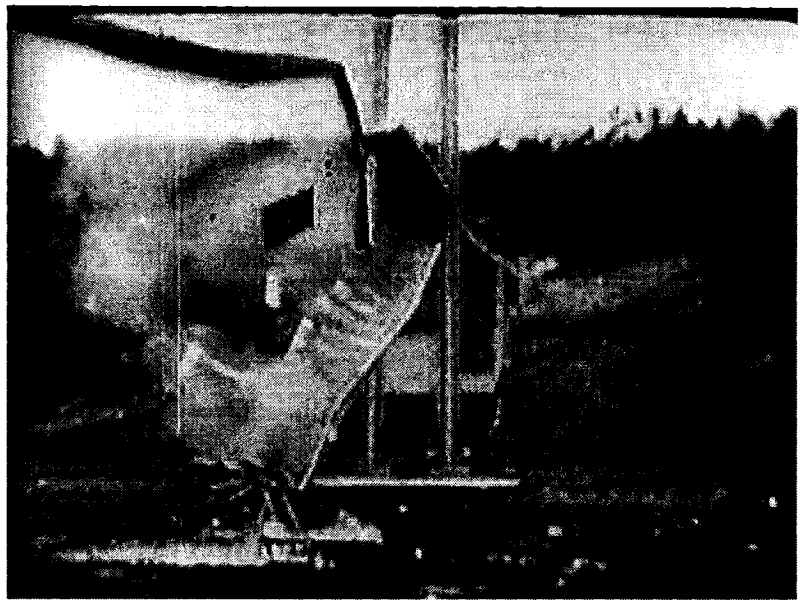

Fig. 1.5. Collapse of Tacoma Narrows Bridge

L. Caracoglia and N. P. Jones [16, 17] have studied the dynamic behavior of a simplified cable network, composed of a set of interconnected truss elements. The transverse cables, defined as cross-ties, were used to counteract the undesired oscillations induced by wind-rain combination. C. Lemaitre and al. [61] have modeled the rainwater rivulets on a cable subjected to wind action by proposing special criterion for the appearance and position of rivulets. D. Q. Cao [15] et al. further investigated the effect of moving rivulets on the cable dynamics while a complete model including the rivulet position and its movement has been proposed by L. Wang and Y. L. Xu [98]. J. Kim and S. P. Chang [54] have investigated the effect of an inclined cable with displaceable boundaries and derived the dynamic stiffness for each degree of freedom. The boundary condition has finally gained attention with works from M. A. Zarubinskaya, and W. T. van Horssen [105, 106] investigating the effect of boundary conditions on the bridge by considering a rectangular

plate with two opposites sides simply supported and the other sides attached to linear springs.

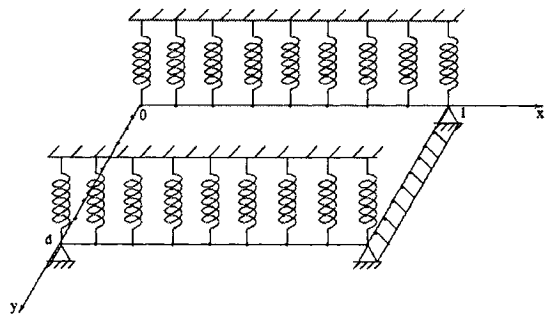

Fig. 1.6. Zarubinskaya and van Horssen's suspension bridge modeled [105, 106]

1.3.4 Pulley, conveyor and winding systems

Belt drivers are used for transferring energy while pulley mechanisms are used for winding fibers. In all cases, a circular disk, cylinder or cone is mounted on a shaft. Rotating at a constant or variable speed, they are driving, driven or winding belts, cables, or strings which are subjected to vibration due to mass unbalances. L. J. Cveticanin [26, 27] has reported several studies on textile machine rotors used for thread winding. His main work deals with the rotor unbalanced due to the nonlinear thread tension. By comparing analytical and numerical results, L. J. Cveticanin concluded that the amplitude of vibration has tendency to decrease with time, and it will decrease faster if the angular velocity is larger. However, only the first layer of winding was analyzed. C. N. Bapat [6] investigated the effect of variation in mass density and tension of a string by using a multi sections method where each section has different mass density and tension. The

transverse vibration of an axially accelerating string was studied by M. Pakdemirli et al. [82] performing stability analysis using an eight-term series solution. The results showed that the instability occurs at much higher amplitudes and frequencies than typical devices such as tape machines and band saws. Furthermore, based on work done by R. B. Bhat et al. [11], a belt moving on an elastic foundation is unstable for any velocity larger than the wave velocity in the belt material. L. Zhang and J. W. Zu [107, 108] have investigated the non-linear vibration of moving belt considering the effects of elastic and viscoelastic parameters, axial moving speed and the geometric nonlinearity.

1.4 Objectives and Scope of Thesis

The survey of work done has shown extensive vibration studies on various string and cable systems found on suspension bridges, trolley cars, elevator cables, electric transmission line cables, musical stringed instruments, and textile bobbins. However, in most of the works, the boundary condition analysis has been widely neglected and they considered the string and cables as completely fixed at both ends. The aim of the present study is to explore the effect of boundary condition on string vibrating with two case studies. The first case verifies the effect of a partially clamped end on the behavior of the string vibration. This investigation explores what has been neglected in many cases by simply considered the string to be completely fixed. The second case considers a string fixed at both ends and supported at two points making the lateral vibration to take place between the supports while the axial vibration induced by lateral motion occurs between the two fixed ends. This is one of the first and few studies of coupled model where the

boundary position for axial and transverse vibrations of a coupled system is different. For the simulation, the numerical method is used to obtain the string behavior without solving the wave equations analytically. An experimental setup is built to compare simulation data with actual results for the fixed string with supported section. For the partially fixed model, only simulation results are presented.

1.5 Thesis Organization

After the brief introduction in Chapter 1 about the type of string vibrations and the literature review, Chapter 2 covers the transverse and axial string vibrations with classical boundary condition. In Chapter 3, boundary conditioning of string vibration is analyzed with a partially clamped string and an axial-transverse coupled case where the transverse vibration only occurs in a section of the string length while the axial vibration covers the complete string. Caused by the uneven reflection of the travelling waves, the boundary conditioning is directly the cause of beat phenomenon. Covered in Chapter 4, beat phenomenon is the interference between two or more vibrations with closely spaced frequencies. Chapter 5 deals with the simulation of equations derived in Chapter 3. Besides simulation results, methods such as finite difference and digital waveguide in string simulation are also presented. In Chapter 6, the experiment and the collected data are discussed and compared with the simulation results from previous chapter. Finally, Chapter 7 concludes this thesis by summarizing the work done and outlines recommendations for future research directions.

Chapter 2

Strings with Classical Boundary Condition

After the brief literature review in Chapter 1, the classical case study of vibrating string will be reviewed in this chapter. As one of the fundamental vibration system studies, the oscillating string offers the advantage of mathematical simplicity while still providing on understanding toward more complex systems, such as the vibrating membrane which is merely a 2D combination of vibrating string models. In addition, the knowledge of string vibration can be extended to include beam vibration, which can be viewed as axial string vibration if the beam is replaced by a slender cylindrical rod. In this chapter, the transverse and axial vibrations are studied individually with classical boundary condition that considers both ends of the string to be completely fixed.

2.1 1D Transverse Vibration

From transmission line cable to clothes line, the freely vibrating stretched string is commonplace in daily life. In all the cases, transverse vibrations are possible in two

perpendicular planes. In this thesis, the plane of excitation is always defined as y, while z is perpendicular to the $x-y$ plane. By considering only a single plane as shown in Fig. 2.1, it is possible to derive a wave equation from the forces acting on the string where it is distributed from the equilibrium position after plucking. The free vibrating string is assumed to be of negligible stiffness, uniform linear density, and stretched to a tension T_o. For small transverse displacement (u^y), the tension is assumed to be constant throughout the string. Also dissipative force (damping) is not considered in this analysis.

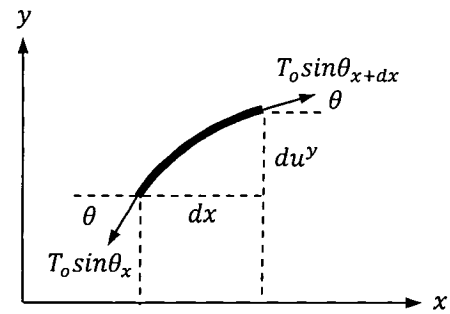

Fig. 2.1. Transverse vibration string segment

Let the x coordinate of a point on the string represent its horizontal distance measured along the string from the left-hand support, and its y coordinate the transverse displacement measured from the equilibrium position. Consider a segment of the string of infinitesimal length as indicated in Fig. 2.1. It is reasonable to assume $\cos\theta \approx 1$ and $\sin\theta \approx \tan\theta$ for small transverse displacement. Then the difference between the x components of the tension at the two ends of the element ds cancel out each other. For transverse motion, the y components are given by

$$\rho dx \frac{\partial^2 u^y}{\partial t^2} = (T_o \sin\theta)_{x+\partial x} - (T_o \sin\theta)_x \tag{2.1}$$

where ρdx is the mass of the element of the string. Considering only the first two terms of Taylor's series expansion:

$$f(x+dx) = f(x) + \frac{\partial f(x)}{\partial x} dx \tag{2.2}$$

the Eq.(2.1) can be expressed as

$$\rho dx \frac{\partial^2 u^y}{\partial t^2} = (T_o \sin\theta)_x + \frac{\partial (T_o \sin\theta)}{\partial x} dx - (T_o \sin\theta)_x = \frac{\partial (T_o \sin\theta)}{\partial x} dx \tag{2.3}$$

Since the transverse displacement of the string is considered small, and correspondingly that the angle θ is small, $\sin\theta$ is approximated as $\tan\theta$ which is equal to $\frac{\partial u^y}{\partial x}$. The equation obtained is the well known wave equation

$$c_T^2 \frac{\partial^2 u^y}{\partial x^2} = \frac{\partial^2 u^y}{\partial t^2} \tag{2.4}$$

where $c_T = \sqrt{\frac{T_o}{\rho}}$ is the velocity of wave propagation in transverse direction expressed as a relation between the tension applied to tighten the string and the string mass per unit length. The wave equation can be solved mathematically by separation of variables and the solution takes the form of $u^y(x,t) = X(x)T(t)$ where $X(x)$ and $T(t)$ are the space and time portions of motion. Substituting into Eq. (2.4) and separating the variables gives

$$\frac{X''}{X} = \frac{1}{c_T^2}\frac{\ddot{T}}{T} \tag{2.5}$$

This leads to the following expressions

$$X'' + \tau^2 X = 0 \tag{2.6a}$$

$$\ddot{T} + \tau^2 c_T^2 T = 0 \tag{2.6b}$$

where $-\tau^2$ is an arbitrary constant. The general solution of the above two differential equations are

$$X(x) = G\cos(\tau x) + H\sin(\tau x) \tag{2.7a}$$

$$T(t) = J\cos(c_T \tau t) + K\sin(c_T \tau t) \tag{2.7b}$$

Since the boundary condition is assumed to be fixed at both ends (let $x = 0$ for the position of string at left end and $x = L_T$ for the one at right end), the boundary condition commands the amplitude of motion to be zero at both supports and the solution of Eq. (2.7a) becomes

$$G = 0 \tag{2.8a}$$

$$H \sin(\tau L_T) = 0 \tag{2.8b}$$

Considering the non-trivial solution, $\sin(\tau L_T) = 0$, which provides the value of the arbitrary constant τ as,

$$\tau = \frac{n\pi}{L_T} \tag{2.9}$$

The corresponding string motion is given by

$$u^y(x,t) = \sum_{n=1}^{\infty} \sin\left(\frac{n\pi x}{L_T}\right)\left[J^* \cos\left(\frac{n\pi c_T t}{L_T}\right) + K^* \sin\left(\frac{n\pi c_T t}{L_T}\right)\right] \tag{2.10}$$

where $J^* = HJ$ and $K^* = HK$ are arbitrary constants that are determined from the initial conditions. For a string excited at the midpoint with an impulse of H, the equation of motion without damping is

$$u^y(x,t) = \frac{8H}{\pi^2}\sum_{n=1}^{\infty}\frac{1}{n^2}\sin\left(\frac{n\pi}{2}\right)\sin\left(\frac{n\pi x}{L_T}\right)\cos\left(\frac{n\pi c_T t}{L_T}\right) \tag{2.11}$$

The string motion described by Eq. (2.11) is shown in Fig. 2.2 where the string is bouncing back and forth between the maximum upward position representing the initial condition (Fig. 2.2a) and the maximum downward position (Fig. 2.2g) formed by reflected waves from fixed boundary condition at both ends.

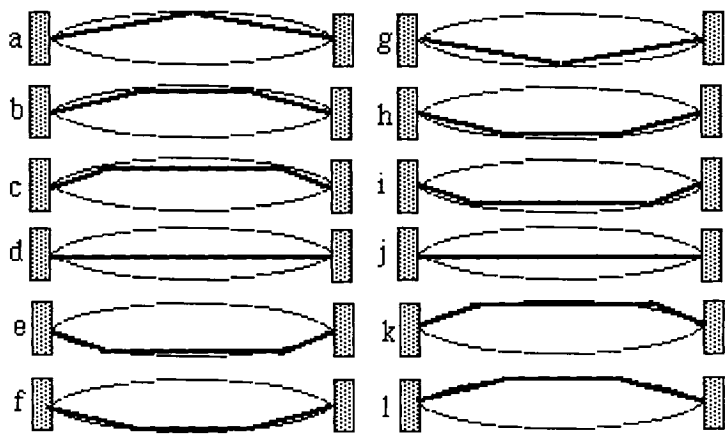

Fig. 2.2. Motion of a single oscillation cycle of string with an initial impulse displacement at center

Clearly, from Eq. (2.11), the natural frequencies of transverse oscillation are

$$f_n^y = f_n^z = \frac{\omega_n^y}{2\pi} = \frac{\omega_n^z}{2\pi} = \frac{n}{2L_T}\sqrt{\frac{T_o}{\rho}} \tag{2.12}$$

From the above equation, it can be seen that the frequency of the string can be modified by choosing the value of mass and length of the string as well the tension applied. In musical stringed instruments, where a wide range of frequencies is desired, the player is constantly varying the resonance frequency by holding at various locations of the strings such as in the case of guitar and violin. Mass also has a significant role to determine the string natural frequency. The best example is again found in musical instruments where some strings with thin core are covered with one or several layers of windings (see Fig. 2.3). This approach directly increases the mass without affecting too much the stiffness and tension applied, thus producing significantly lower frequencies without lowering the tension and making the string too slack to play.

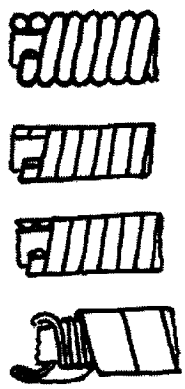

Fig. 2.3. Different types of string winding

2.2 2D Transverse Vibration

During vibration, it is easily observable that strings have tendency to follow an orbital motion rather than simply oscillate on a fixed plane corresponding to the initial

impulse excitation direction. The phenomenon was first observed by Hunton as reported by H. Harrison [45]. The reference to other subsequent experiments can be found in the book by A. H. Nayfeh and D. T. Mook [74]. It is observed that the whirling motion, sometimes also referred to as ballooning or tubular motion occurs when the amplitude and frequency of a plane excitation and the phase difference between the response and the excitation exceeds certain critical values. An experimental study by T. C. Molteno and N. B. Tufillaro [68, 69] suggests that the string does the following bifurcation sequence: periodic → quasi-periodic → chaotic → quasi-periodic → periodic. W. T. van Horssen et al. [94, 95] have since studied extensively the stability problem of the string and have proposed equations for various whirling orbits where some are shown in Fig. 2.4. Since it is not germane to the current studies, the stability analysis will not be covered in this thesis. However, it is important to point out that it has been long appreciated that the two perpendicular transverse modes decay at different rates, since the coupling to the soundboard via the bridge is different for the two planes.

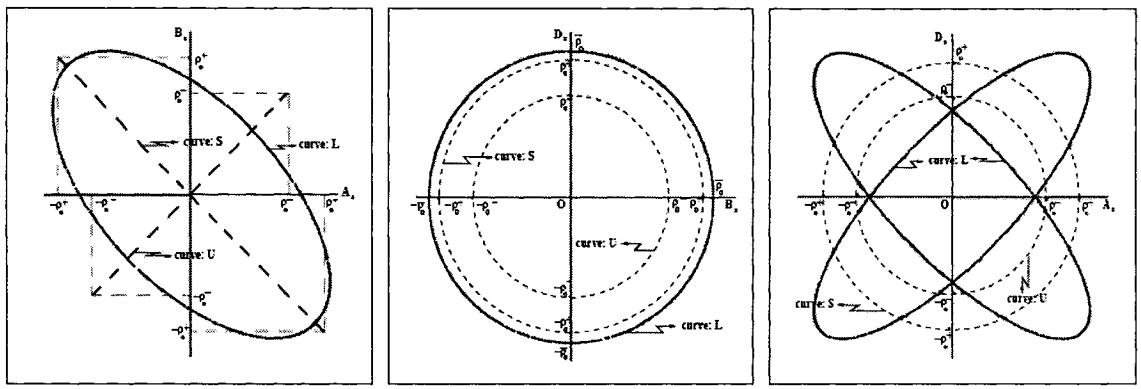

Fig. 2.4. Various whirling orbits [94]

Despite the absence of proven theory for the exact cause of the whirling motion from original excitation direction, it is clear that the motion between the two transverse vibrations is merely a phase shift of 90 degree with a certain difference in amplitude. Similar to the motion described by Eq. (2.11) for y plane, the z plane equation is obtained by replacing $\cos\left(\frac{n\pi c_T t}{L_T}\right)$ by $\sin\left(\frac{n\pi c_T t}{L_T}\right)$ considering no amplitude change.

$$u^z(x,t) = \frac{8A}{\pi^2}\sum_{n=1}^{\infty}\frac{1}{n^2}\sin\left(\frac{n\pi}{2}\right)\sin\left(\frac{n\pi x}{L_T}\right)\sin\left(\frac{n\pi c_T t}{L_T}\right) \tag{2.13}$$

2.3 Axial Vibration

Besides transverse vibration, another important type of wave motion is the propagation of longitudinal waves in the string. Also known as axial vibration, it is perhaps the type of vibration the most common in daily life. In fact, sound is defined as a longitudinal vibration of particles of the medium through which the sound travels. The axial vibration of a string is derived similar to that of the vibration of a bar. While the string is executing lateral vibrations, the transverse amplitude is small compared to the string length, and thus the string can be assumed to be straight in the axial direction.

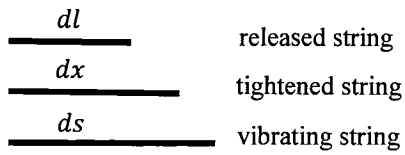

Fig. 2.5. String at different states

From Fig. 2.5, the strain equation is defined as

$$\varepsilon = \frac{ds - dl}{dl} = \frac{ds - dx}{dl} + \frac{dx - dl}{dl} \tag{2.14}$$

The stress is defined as

$$\sigma = \frac{F_x}{A} \tag{2.15}$$

When the stress is divided by strain, it gives the Young's modulus, E as

$$E = \frac{\sigma}{\varepsilon} = \frac{F_x / A}{\varepsilon} \tag{2.16}$$

where A is the cross sectional area of the string. After rearranging, the force applied in axial direction is expressed as

$$F_x = AE\left(\frac{ds-dx}{dl}+\frac{dx-dl}{dl}\right) \tag{2.17}$$

Since $T_o = AE\left(\frac{dx-dl}{dl}\right)$ is the initial tension applied to tighten the string, which can be rewritten as $dl = \frac{dx}{\left(\frac{T_0}{AE}+1\right)}$, Eq. (2.17) can be expressed as:

$$F_x(x) = (AE+T_o)\left(\frac{ds-dx}{dx}\right)+T_o \tag{2.18}$$

Let $u^x = ds - dx$, which is the axial displacement of the string during longitudinal vibration, Eq. (2.18) becomes:

$$F_x(x) = (AE+T_o)\frac{\partial u^x}{\partial x}+T_o \tag{2.19}$$

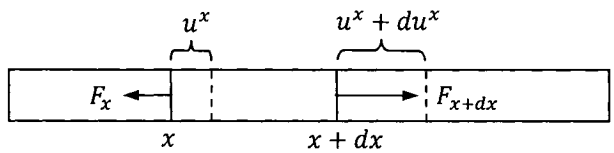

Fig. 2.6. Axial vibration string segment

The net force applied on an infinitesimal element is expressed as the difference between the forces exerted at position x and $x+dx$.

$$\rho dx \frac{\partial^2 u^x}{\partial t^2} = F_{x+dx} - F_x \tag{2.20}$$

where ρdx is the mass of the element of the string. Again Eq. (2.20) can be approximated using the first two terms of Taylor's series expansion as in Eq. (2.2), and substituting Eq. (2.19) into Eq. (2.20) gives

$$c_A^2 \frac{\partial^2 u^x}{\partial x^2} = \frac{\partial^2 u^x}{\partial t^2} \tag{2.21}$$

where $c_A = \sqrt{\frac{AE + T_o}{\rho}}$ is the velocity of wave propagation in axial direction and it is expressed as a relation between the initial tension applied and three properties of the string: its cross section area, modulus of elasticity and density. Note that in many string analyses, the initial tension T_o is not considered as the strain equation used doesn't consider the initial tension. Like transverse motion, the solution to Eq. (2.21) is obtained by the method of separation of variables discussed previously and a similar solution is obtained as

$$u^x(x,t) = \sum_{n=1}^{\infty} \sin\left(\frac{n\pi x}{L_A}\right)\left[J^* \cos\left(\frac{n\pi c_A t}{L_A}\right) + K^* \left(\frac{n\pi c_A t}{L_A}\right)\right] \tag{2.22}$$

where again J^* and K^* are arbitrary constants that are determined from the initial conditions. The string length subject to axial vibration is represented by L_A. The natural frequency is now expressed as

$$f_n^x = \frac{\omega_n^x}{2\pi} = \frac{n}{2L_A}\sqrt{\frac{AE + T_o}{\rho}} \tag{2.23}$$

It is seen from the above equation that the axial natural frequency is controlled by similar parameters as in lateral vibrations except that it also depends on the string cross sectional area and Young's modulus of string's material. In axial vibration applications such as the elevator cables, the length of cable holding the elevator is constantly varying as the elevator moves up and down as well as the tension applied due to the change in total mass of passengers. It therefore offers a wide range of natural frequencies when operating.

2.4 Summary

In this chapter, axial and lateral motions have been studied individually with classical boundary conditions represented by a fully clamped string at both ends. From the equations obtained, both transverse and axial vibration natural frequencies are very similar where they vary with respect to string length, initial tension and string density. In addition, the axial vibration is submitted to the influence of further parameters namely the cross section area and the Young's modulus of string material. The coupling between

transverse motions is briefly presented where they are considered to be separated by a phase difference of 90 degrees while the transient motion is ignored. In the next chapter, the effect of boundary conditions on string behavior will be studied.

Chapter 3

Boundary Conditioning

In string vibration analysis, most of the works simply consider the string to be firmly fixed at both ends. However, cables and strings sometimes are actually exposed to various boundary situations which differ from the fully clamped boundary conditions. In the previous chapter, the individual axial and transverse vibrations were presented with the classical fixed-fixed boundary condition at both ends of the string. In this chapter, two case studies are used to explore the effect of different boundary conditions on the string motion. The first case attacks the situation where one end is subject to a partial clamped condition. Since the reflected wave from partially clamped and fully clamped ends do not necessarily match each other, the standing wave pattern (see Chapter 4) is expected to vary with time. The second case seeks the coupled motion between axial vibration in the complete string and the lateral vibration in a portion of the cable. This situation exists when, fixed at both ends, the string is supported at two intermediate points between which the lateral vibration takes place. Since the two supports allow the string to slide, the longitudinal vibration induced by lateral motion occurs along the complete length of

the string. This special case investigates the effect of boundary conditions located at different positions for a coupled system.

3.1 Effect of Partial Clamping

In this section, the effect of partial clamping at one end of the string is analyzed. This represents a more realistic boundary condition in several string/cable systems where the end is not completely fixed as in transmission lines and pulley systems. The model is illustrated in Fig. 3.1. The slider allows deflections along a transverse direction while preventing the displacements of the string end along the string.

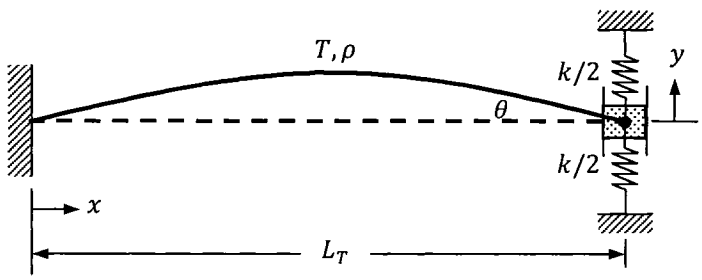

Fig. 3.1. String with partial clamped end

The equation of lateral motion is again the wave equation presented in Eq. (2.4), but with slightly different boundary conditions:

$$u^{y}_{x=0} = 0 \tag{3.1a}$$

$$T\sin\theta = -ku^{y}_{x=L_T} \tag{3.1b}$$

Considering small transverse displacement for metallic string, the tension is assumed to be uniform throughout the string. In addition, with small angle θ, it is possible to replace $\sin\theta$ with $\tan\theta$ which is equal to $\frac{\partial u^y}{\partial x}$. The boundary condition in Eq. (3.1b) becomes

$$T_o \frac{\partial u^y}{\partial x} = -k u^y_{x=L_T} \tag{3.1c}$$

Applied to the wave equation, the above boundary conditions will govern or condition the behavior of the string. The wave equation can be solved using the method of separation of variables as a combination of Eqs. (2.7a) and (2.7b).

$$u^y(x,t) = \left(G\cos(\tau x) + H\sin(\tau x)\right)\left(J\cos(c_T \tau t) + K\sin(c_T \tau t)\right) \tag{3.2}$$

With the boundary conditions from Eqs. (3.1a) and (3.1c), the following equation is obtained

$$G = 0 \tag{3.3a}$$

$$-k\sin(\tau L_T) = T_o \tau \cos(\tau L_T) \tag{3.3b}$$

After rearranging,

$$\tan(\tau L_T) = -\frac{T_o \tau}{k} \tag{3.4}$$

The above equation is a transcendental equation whose roots (τ) can be found graphically as the points of intersection of the right hand and left hand sides of Eq. (3.4) (see Fig. 3.2) [63].

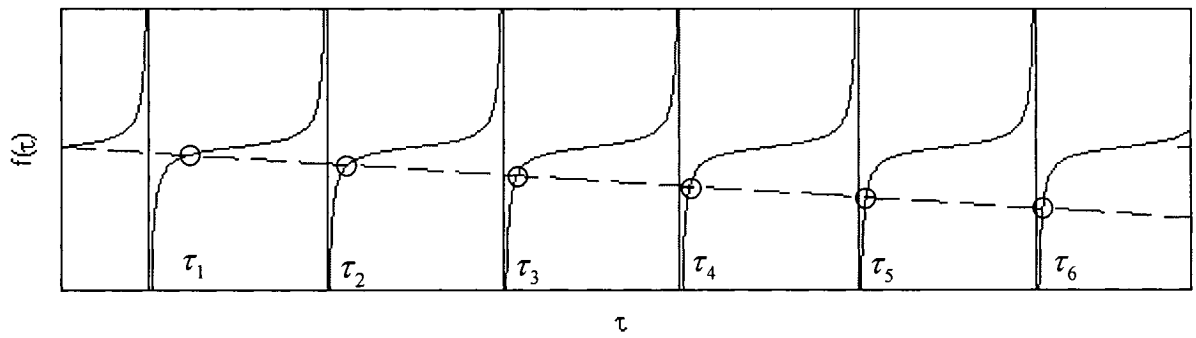

Fig. 3.2 Graphical solution of transcendental equation

From Eq. (3.4), the string length directly influences the period of tangent curve, and therefore the approximate range of fundamental and the partials. The straight line formed by right hand side of Eq. (3.4) will vary if the stiffness at the end of string changes, thus intercepting the tangent curve at different positions giving different values of τ. The natural frequencies are represented by:

$$f_n = \frac{\omega_n}{2\pi} = \frac{c_T \tau_n}{2\pi} = \sqrt{\frac{T_o}{\rho}} \frac{\tau_n}{2\pi} \tag{3.5}$$

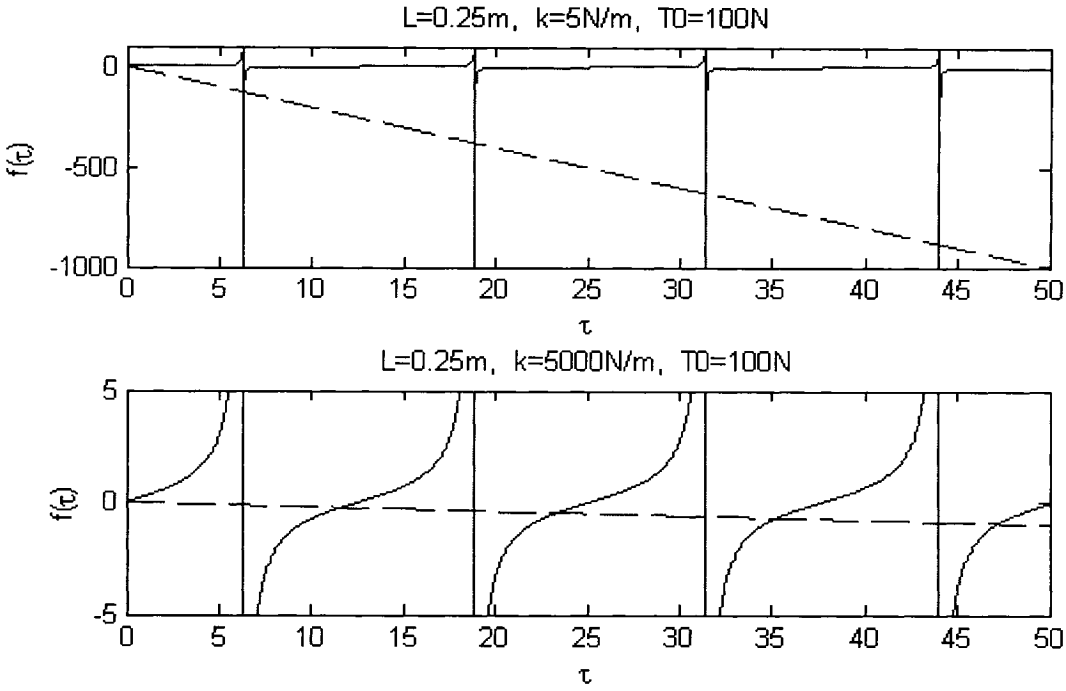

Fig. 3.3. Graphical solution of Eq. (3.4) with $L = 0.25m$

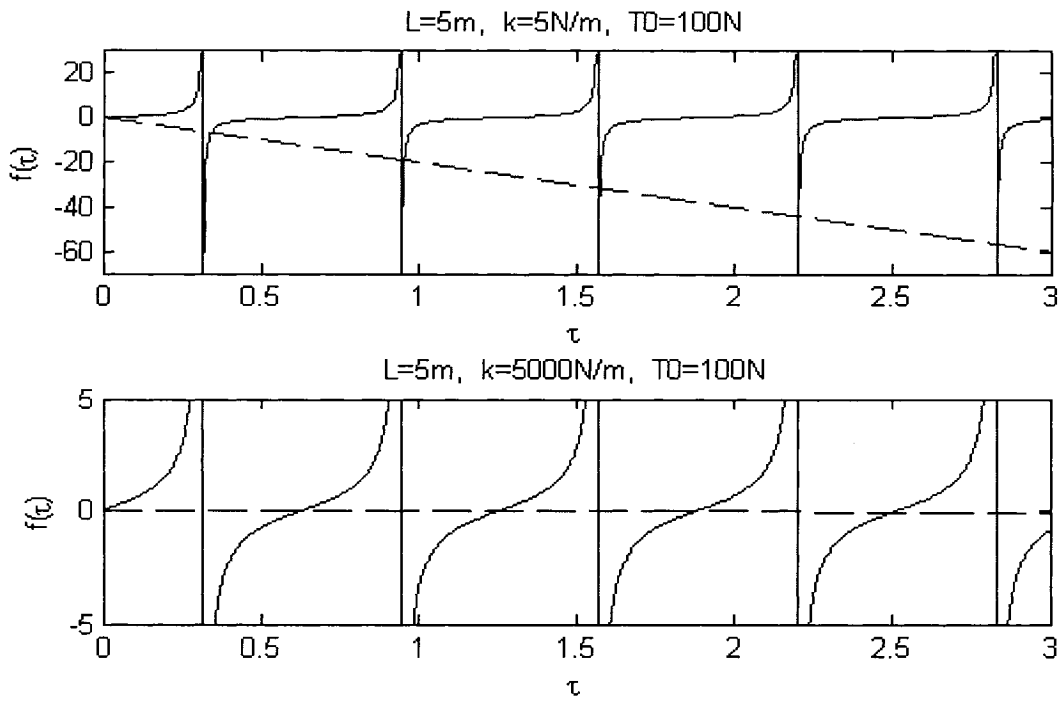

Fig. 3.4. Graphical solution of Eq. (3.4) with $L = 5.00m$

From Fig. 3.2, it is clear that the straight line does not cut the periodic tangent curve at the exact same position for each repetition. This suggests the presence of inharmonicity due to the partially clamped end condition of the string. Inharmonicity is defined as partials slightly shifted away from their harmonic positions. In Figs. 3.3 and 3.4, cases of variation in string length and stiffness are shown. While string length and tangent line's period are inversely proportional, it is clear that a smaller period leads to a smaller variation in inharmonicity between partials while larger period causes bigger variation. Since at higher partials, the straight line is more and more intercepting the vertical portion of the tangent line, This suggests that higher partials are more and more harmonic between them. Ultimately, inharmonicity will stabilized with a constant difference between consecutive partials. It is also interesting to point out that at low stiffness, partials are only at odd multiples of fundamental only (i.e.: $f_2 = 3f_1$, $f_3 = 5f_1$, $f_4 = 7f_1$, etc.). Natural frequencies for various stiffnesses for and different string lengths have been tabulated in Tables 3.1 to 3.3.

Table 3.1. Fundamental frequency (f_1) with respect to stiffness and string length

Stiffness (k)	String length (L_T)			
	0.25 m	0.50 m	1.00 m	5.00 m
5 N/m	$1.006\,c_T$ Hz	$0.505\,c_T$ Hz	$0.255\,c_T$ Hz	$0.054\,c_T$ Hz
50 N/m	$1.049\,c_T$ Hz	$0.546\,c_T$ Hz	$0.294\,c_T$ Hz	$0.076\,c_T$ Hz
500 N/m	$1.345\,c_T$ Hz	$0.758\,c_T$ Hz	$0.420\,c_T$ Hz	$0.095\,c_T$ Hz
5000 N/m	$1.857\,c_T$ Hz	$0.961\,c_T$ Hz	$0.492\,c_T$ Hz	$0.099\,c_T$ Hz
∞ N/m	$2.000\,c_T$ Hz	$1.000\,c_T$ Hz	$0.500\,c_T$ Hz	$0.100\,c_T$ Hz

Tension applied (T_o) = 100 N

Table 3.2. First partial frequency (f_2) with respect to stiffness and string length

Stiffness (k)	String length (L_T)			
	0.25 m	0.50 m	1.00 m	5.00 m
5 N/m	$3.002\,c_T$ Hz	$1.502\,c_T$ Hz	$0.753\,c_T$ Hz	$0.151\,c_T$ Hz
50 N/m	$3.018\,c_T$ Hz	$1.517\,c_T$ Hz	$0.767\,c_T$ Hz	$0.164\,c_T$ Hz
500 N/m	$3.158\,c_T$ Hz	$1.644\,c_T$ Hz	$0.867\,c_T$ Hz	$0.193\,c_T$ Hz
5000 N/m	$3.723\,c_T$ Hz	$1.924\,c_T$ Hz	$0.980\,c_T$ Hz	$0.199\,c_T$ Hz
∞ N/m	$4.000\,c_T$ Hz	$2.000\,c_T$ Hz	$1.000\,c_T$ Hz	$0.200\,c_T$ Hz

Tension applied (T_o) = 100 N

Table 3.3. Second partial frequency (f_3) with respect to stiffness and string length

Stiffness (k)	String length (L_T)			
	0.25 m	0.50 m	1.00 m	5.00 m
5 N/m	$5.002\,c_T$ Hz	$2.502\,c_T$ Hz	$1.251\,c_T$ Hz	$0.251\,c_T$ Hz
50 N/m	$5.010\,c_T$ Hz	$2.510\,c_T$ Hz	$1.261\,c_T$ Hz	$0.259\,c_T$ Hz
500 N/m	$5.097\,c_T$ Hz	$2.594\,c_T$ Hz	$1.335\,c_T$ Hz	$0.290\,c_T$ Hz
5000 N/m	$5.610\,c_T$ Hz	$2.889\,c_T$ Hz	$1.471\,c_T$ Hz	$0.299\,c_T$ Hz
∞ N/m	$6.000\,c_T$ Hz	$3.000\,c_T$ Hz	$1.500\,c_T$ Hz	$0.300\,c_T$ Hz

Tension applied (T_o) = 100 N

Table 3.4. Third partial frequency (f_4) with respect to stiffness and string length

Stiffness (k)	String length (L_T)			
	0.25 m	0.50 m	1.00 m	5.00 m
5 N/m	$7.001\,c_T$ Hz	$3.501\,c_T$ Hz	$1.751\,c_T$ Hz	$0.351\,c_T$ Hz
50 N/m	$7.007\,c_T$ Hz	$3.507\,c_T$ Hz	$1.757\,c_T$ Hz	$0.357\,c_T$ Hz
500 N/m	$7.071\,c_T$ Hz	$3.570\,c_T$ Hz	$1.816\,c_T$ Hz	$0.386\,c_T$ Hz
5000 N/m	$7.518\,c_T$ Hz	$3.856\,c_T$ Hz	$1.962\,c_T$ Hz	$0.398\,c_T$ Hz
∞ N/m	$8.000\,c_T$ Hz	$4.000\,c_T$ Hz	$2.000\,c_T$ Hz	$0.400\,c_T$ Hz

Tension applied (T_o) = 100 N

Table 3.5. Fourth partial frequency (f_5) with respect to stiffness and string length

Stiffness (k)	String length (L_T)			
	0.25 m	0.50 m	1.00 m	5.00 m
5 N/m	$9.001\,c_T$ Hz	$4.501\,c_T$ Hz	$2.251\,c_T$ Hz	$0.451\,c_T$ Hz
50 N/m	$9.006\,c_T$ Hz	$4.506\,c_T$ Hz	$2.256\,c_T$ Hz	$0.456\,c_T$ Hz
500 N/m	$9.056\,c_T$ Hz	$4.555\,c_T$ Hz	$2.303\,c_T$ Hz	$0.483\,c_T$ Hz
5000 N/m	$9.446\,c_T$ Hz	$4.827\,c_T$ Hz	$2.452\,c_T$ Hz	$0.483\,c_T$ Hz
∞ N/m	$10.000\,c_T$ Hz	$5.000\,c_T$ Hz	$2.500\,c_T$ Hz	$0.500\,c_T$ Hz

Tension applied (T_o) = 100 N

Table 3.6. Fifth partial frequency (f_6) with respect to stiffness and string length

Stiffness (k)	String length (L_T)			
	0.25 m	0.50 m	1.00 m	5.00 m
5 N/m	$11.001\,c_T$ Hz	$5.501\,c_T$ Hz	$2.751\,c_T$ Hz	$0.551\,c_T$ Hz
50 N/m	$11.007\,c_T$ Hz	$5.505\,c_T$ Hz	$2.755\,c_T$ Hz	$0.555\,c_T$ Hz
500 N/m	$11.046\,c_T$ Hz	$5.545\,c_T$ Hz	$2.794\,c_T$ Hz	$0.580\,c_T$ Hz
5000 N/m	$11.388\,c_T$ Hz	$5.800\,c_T$ Hz	$2.944\,c_T$ Hz	$0.598\,c_T$ Hz
∞ N/m	$12.000\,c_T$ Hz	$6.000\,c_T$ Hz	$3.000\,c_T$ Hz	$0.600\,c_T$ Hz

Tension applied (T_o) = 100 N

From the data in Tables 3.1 to 3.6, the comparison between the partials and the fundamental has been tabulated below (see Table 3.7). Notice that at low stiffness, partials are almost at odd multiples of fundamental frequency. In general speaking, decrease in stiffness and string length leads to greater inharmonicity.

Table 3.7. Inharmonicity with respect to stiffness and string length

Stiffness (k)	Ratio	String length (L_T)			
		0.25 m	0.50 m	1.00 m	5.00 m
5 N/m	f_2/f_1	2.984	2.974	2.953	2.796
	f_3/f_1	4.972	4.954	4.906	4.648
	f_4/f_1	6.959	6.933	6.867	6.500
	f_5/f_1	8.947	8.913	8.827	8.352
	f_6/f_1	10.935	10.893	10.788	10.204
50 N/m	f_2/f_1	2.877	2.778	2.609	2.158
	f_3/f_1	4.776	4.597	4.289	3.408
	f_4/f_1	6.680	6.423	5.976	4.697
	f_5/f_1	8.585	8.253	7.673	6.000
	f_6/f_1	10.493	10.082	9.371	7.303
500 N/m	f_2/f_1	2.348	2.169	2.064	2.032
	f_3/f_1	3.790	3.422	3.179	3.053
	f_4/f_1	5.257	4.710	4.324	4.063
	f_5/f_1	6.733	6.009	5.483	5.084
	f_6/f_1	8.213	7.315	6.652	6.105
5000 N/m	f_2/f_1	2.005	2.002	1.992	2.010
	f_3/f_1	3.021	3.006	2.990	3.020
	f_4/f_1	4.048	4.012	3.988	4.020
	f_5/f_1	5.087	5.023	4.984	4.949
	f_6/f_1	6.132	6.035	5.984	6.040
∞ N/m	f_2/f_1	2.000	2.000	2.000	2.000
	f_3/f_1	3.000	3.000	3.000	3.000
	f_4/f_1	4.000	4.000	4.000	4.000
	f_5/f_1	5.000	5.000	5.000	5.000
	f_6/f_1	6.000	6.000	6.000	6.000

Tension applied (T_o) = 100 N

3.2 3D Coupled String Model

In the previous chapter, the transverse and axial vibrations have been presented separately. For a string excited laterally, axial vibration also takes place since it is induced by lateral motion. In this section equations of coupled axial and lateral motions will be considered. The nonlinearity of the tension due to large lateral oscillations of the string will also be considered in the coupled model. For the coupled model, the variation of boundary condition between axial and transverse motions will be explored with the case of a fixed-fixed string with two supporting points, A and B as shown in Fig. 3.5. As illustrated, the transverse vibration will only occur inside this section (L_T) while the axial vibration takes place along the complete length of the string $(L_A = L_T + L_1 + L_2)$.

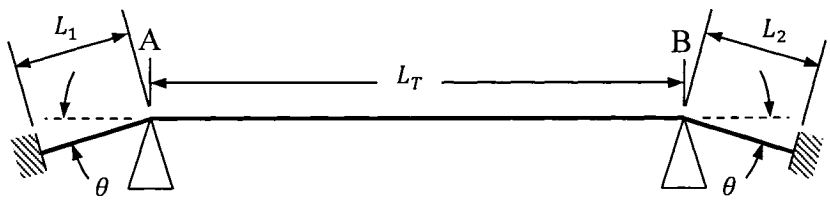

Fig. 3.5. String model

Since early work by W. F. Osgood [79] almost a century ago, several models have been proposed, including E. V. Kurmyshev's [58] model derived from A. H. Nafey's [74] work which is by far the most accurate. However, modification is required to convert E. V. Kurmyshev's soft string model to apply on metallic strings. The derivation first starts by considering an element of the string as shown in Fig. 3.6.

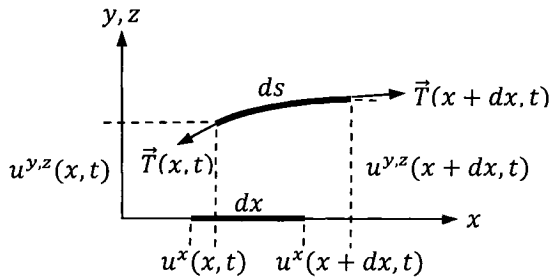

Fig. 3.6. String segment

Considering the equilibrium of the element,

$$\rho dx \frac{\partial^2 \vec{u}}{\partial t^2} = d\vec{T} \tag{3.6}$$

where $\vec{u}(x,t)$ is the displacement vector written as $u^x\hat{i} + u^y\hat{j} + u^z\hat{k}$. The tension vector is defined from Hooke's stress-strain relation

$$\vec{T} = AE\left(\frac{L_f - L_i}{L_i}\right)\frac{d\vec{r}}{ds} = \left[AE\left(\frac{\partial s}{\partial x} - 1\right) + T_o\frac{\partial s}{\partial x}\right]\frac{d\vec{r}}{ds} \tag{3.7}$$

where $\frac{d\vec{r}}{ds}$ is the unit vector. The vector between the two ends of the string segment of Fig. 3.6 is expressed as

$$d\vec{r} = (dx + du^x)\hat{i} + du^y\hat{j} + du^z\hat{k} = \left[\left(1 + \frac{\partial u^x}{\partial x}\right)\hat{i} + \frac{\partial u^y}{\partial x}\hat{j} + \frac{\partial u^z}{\partial x}\hat{k}\right]dx \tag{3.8}$$

and its magnitude is expressed as

$$ds = \left[\left(1 + \frac{\partial u^x}{\partial x}\right)^2 + \left(\frac{\partial u^y}{\partial x}\right)^2 + \left(\frac{\partial u^z}{\partial x}\right)^2\right]^{1/2} dx \tag{3.9}$$

The value of $\frac{\partial s}{\partial x}$ and $\frac{d\vec{r}}{ds}$ in Eq. (3.7) is derived using Eqs. (3.8) and (3.9) by expanding to the second order using Taylor series. Depending on whether the amplitude of string oscillation is large or not, two cases are stated as following:

$$O\left(\frac{\partial u^x}{\partial x}\right) = O\left(\left(\frac{\partial u^y}{\partial x}\right)^2\right) = O\left(\left(\frac{\partial u^z}{\partial x}\right)^2\right) \tag{3.10a}$$

$$O\left(\frac{\partial u^x}{\partial x}\right) = O\left(\frac{\partial u^y}{\partial x}\right) = O\left(\frac{\partial u^z}{\partial x}\right) \tag{3.10b}$$

where O is the Landau notation for the order of the function and it is used to characterize the relationship between the displacement in the three axis. For highly flexible strings, E. V. Kurmyshev considers that the axial and transverse vibrations are having similar amplitudes by using condition stated in Eq. (3.10b). In the case of metallic strings and cables, it is more suitable to use the case expressed by Eq. (3.10a). Note that the two

cases are not distinguished in many works even though they lead to different equations of motion as shown in A. Watzky's [99] work. Expanding Eq. (3.9) with respect to Eq. (3.10a) to second order gives

$$\frac{\partial s}{\partial x} = 1 + \frac{\partial u^x}{\partial x} + \frac{1}{2}\left[\left(\frac{\partial u^y}{\partial x}\right)^2 + \left(\frac{\partial u^z}{\partial x}\right)^2\right] \tag{3.11}$$

Similarly,

$$\begin{aligned}\frac{dx}{ds} = 1 - \frac{\partial u^x}{dx} + \left(\frac{\partial u^x}{\partial x}\right)^2 + \left(\frac{\partial u^y}{\partial x}\right)^2\left[-\frac{1}{2} + \frac{3}{2}\frac{\partial u^x}{\partial x} + \frac{3}{8}\left(\frac{\partial u^y}{\partial x}\right)^2\right] \\ + \left(\frac{\partial u^z}{\partial x}\right)^2\left[-\frac{1}{2} + \frac{3}{2}\frac{\partial u^x}{\partial x} + \frac{3}{8}\left(\frac{\partial u^z}{\partial x}\right)^2\right]\end{aligned} \tag{3.12}$$

Put Eq. (3.12) into Eq. (3.8) by keeping up to first and second orders for axial and lateral motions, respectively, to obtain

$$\frac{d\vec{r}}{ds} = \frac{d\vec{r}}{dx}\frac{dx}{ds} = \left[1 - \frac{1}{2}\left(\left(\frac{\partial u^y}{\partial x}\right)^2 + \left(\frac{\partial u^z}{\partial x}\right)^2\right)\right]\hat{i} + \frac{\partial u^y}{\partial x}\hat{j} + \frac{\partial u^z}{\partial x}\hat{k} \tag{3.13}$$

With Eqs. (3.11) and (3.13) back into tension vector equation, it gives

$$\vec{T} = \left[T_o + (T_o + AE)\frac{\partial u^x}{\partial x} + \frac{AE}{2}\left(\left(\frac{\partial u^y}{\partial x}\right)^2 + \left(\frac{\partial u^z}{\partial x}\right)^2\right)\right]\hat{i} + T_o\frac{\partial u^y}{\partial x}\hat{j} + T_o\frac{\partial u^z}{\partial x}\hat{k} \quad (3.14)$$

Knowing the tension vector, Eq. (3.6) is then expressed as

$$\frac{\partial^2 u^x}{\partial t^2} = \frac{\partial}{\partial x}\left[\frac{(T_o + AE)}{\rho}\frac{\partial u^x}{\partial x} + \frac{AE}{2\rho}\left(\left(\frac{\partial u^y}{\partial x}\right)^2 + \left(\frac{\partial u^z}{\partial x}\right)^2\right)\right] \quad (3.15a)$$

$$\frac{\partial^2 u^y}{\partial t^2} = \frac{T_o}{\rho}\frac{\partial}{\partial x}\left[\frac{\partial u^y}{\partial x}\right] \quad (3.15b)$$

$$\frac{\partial^2 u^z}{\partial t^2} = \frac{T_o}{\rho}\frac{\partial}{\partial x}\left[\frac{\partial u^z}{\partial x}\right] \quad (3.15c)$$

Comparing the above equations with individual equation of motion from lateral, Eq. (2.4), and axial vibration, Eq. (2.21), it clearly indicates that the axial vibration is under the influence of the two lateral motions. Considering the mathematical challenge the additional terms bring in the axial vibration and the need to simulate all the partials, it will be simpler to solve the above set of equations by using a numerical method. Although the wave equations are identical for both lateral motions, Eqs. (3.15b) and (3.15c), there is actually a phase difference between the two in view of the orbital motion. Since the above equations are solved using numerical method, the analyze will be presented in Chapter 5 with the complete simulation results.

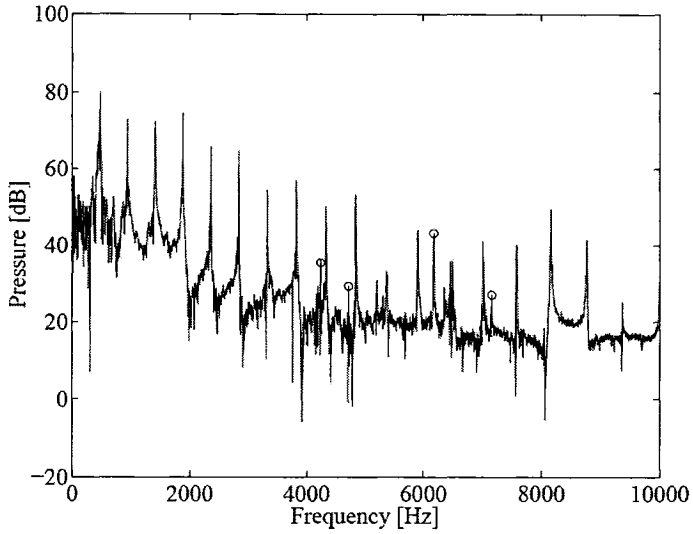

Fig. 3.7. Spectrum of a piano note with phantom partials marked by circles [3]

It is worth mentioning that in the acoustic analysis of a piano frequency spectrum, studies have suggested that the longitudinal vibration is considered to be the source of phantom partials (see Fig. 3.7). First pointed out by I. Nakamura and D. Naganuma [72], they have found a series of partials having one-fourth of inharmonicity compared to the main partials from fundamental. J. Woodhouse [101] later stated that the amplitude of those partials seems to be modulated according to the longitudinal modal frequencies. Works done by J. Bensa [9] and B. Bank [1, 2, 3, 4, 5] further implemented the phantom partials into their piano sound synthesis to obtain more realistic sounds.

3.3 Summary

In this chapter, two cases of boundary study has been investigated analytically. In the first case representing a partially fixed string, inharmonicity was observed which may

lead to beat phenomenon in the string motion. The inharmonicity increases with decrease in string length and stiffness. At extreme case, the partials will be shifted in such way that they are near to odd multiples of fundamental frequency. In Chapter 4, the beat phenomenon between closely spaced frequencies and between fundamental and inharmonic partial(s) are investigated. The second case was a axial-transverse coupled model. The particularity of this model is that the position of boundary for transverse and axial vibrations are at different location. From the derived equations, the transverse motion is influencing axial vibration while the transverse motion remains unaffected by axial vibration. For the two case studies, it is possible to obtain simulation of the string motion with the wave equation and the boundary conditions. In Chapter 5, finite element method is presented as it allows modeling of complete behavior of string motion without dealing individually with each mode.

Chapter 4

Beat Phenomenon

As mentioned earlier, the partially clamped string produces inharmonicity while the 3D coupled vibration that occurs on different string lengths may also present inharmonicity between axial and transverse vibrations. In this chapter, a very interesting phenomenon that occurs when two vibrations of slightly different frequencies interfere together will be discussed. This is the well known beat phenomenon, where the amplitude builds up and then diminishes in a regular pattern as shown in Fig. 4.1. The beat phenomenon is very common in mechanical applications where two mechanisms are operating at approximately, but not exactly, the same speed. Because of the high loads induced during the amplitude increase which may cause large stresses beyond designed safety limits, the beat phenomenon is a very important design consideration. Beyond mechanical, it is also well known in acoustical and electrical fields. In musical instruments, it may affect greatly the quality of the music while the properties of beat phenomenon are used to transmit signals through amplitude modulation techniques. Since the variation of the boundary condition in strings and cables will introduce closely spaced

natural frequencies, beat phenomenon can occur and it is important to study this phenomenon. Furthermore, beat phenomena between the fundamental and the slightly inharmonic partials are quite interesting.

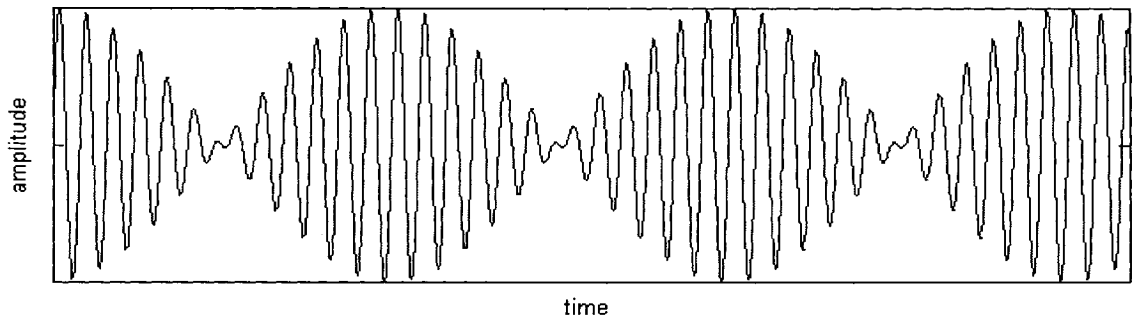

Fig. 4.1. Two vibrations of same amplitude and close frequencies ($\omega_1 \approx \omega_2$)

4.1 Introduction

A good example of a system exhibiting the beat phenomenon is when two or more pumps are connected to the same pipe, and the rotating speeds of each pump are not exactly the same due to slightly different slip speeds of their drive motors. The pulsating vibration or beat becomes noticeable in the system and its amplitude may go beyond what is acceptable, even though the vibration level of each pump is within acceptable limits. Similarly, beat can also occur in pulley/belt systems. For instance, a drive and driven pulley of the same nominal diameter are capable of producing beats if belt slippage occurs causing both to run at slightly different speeds. It can also form with vibration originating from a single source. This happens when the forcing frequency is close to the natural/resonant frequency of the system. While vibrating at its own frequency close to

system's natural frequency, the vibrating source excites the responding member causing it to oscillate at its resonant frequency which in turn produces beating in the system with the input frequency. Acoustically, a beat can be described as a distinct fluctuation in volume which has a wobbling sound. When playing two same notes, if the pitch (frequency) of one of the notes is slightly raised or lowered, a beat begins to appear. The same analogy applies to noise generated by moving mechanisms. The larger the discrepancy between the two frequencies, the faster is the beat. This will be explained mathematically in the following section.

4.2 Beat Equation

Mathematically speaking, a beat is simply two vibrations with closely spaced frequencies interfering with each other. It is represented by the summation of the respective sinusoidal expression of two vibrations as in Eq. (4.1).

$$u(t) = G\sin(\omega_1 t) + H\sin(\omega_2 t) \tag{4.1}$$

From the above equation, it is hard to get a feeling of the actual behavior of beat phenomenon. This equation can be rewritten in a form of amplitude modulated sinusoidal process. By assuming $\varpi_1 = \left(\frac{\omega_1 + \omega_2}{2}\right)$ and $\varpi_2 = \left(\frac{\omega_1 - \omega_2}{2}\right)$, Eq. (4.1) can be written as:

$$u(t) = G\sin\left((\varpi_1 + \varpi_2)t\right) + H\sin\left((\varpi_1 - \varpi_2)t\right) \tag{4.2}$$

Using the trigonometry identity of

$$\sin(\varpi_1 \pm \varpi_2) = \sin \varpi_1 \cos \varpi_2 \pm \cos \varpi_1 \sin \varpi_2 \tag{4.3}$$

and rearranging, the final equation is obtained as

$$\begin{aligned} u(t) = (G+H)\sin\left(\frac{\omega_1+\omega_2}{2}t\right)\cos\left(\frac{\omega_1-\omega_2}{2}t\right) \\ +(G-H)\sin\left(\frac{\omega_1-\omega_2}{2}t\right)\cos\left(\frac{\omega_1+\omega_2}{2}t\right) \end{aligned} \tag{4.4}$$

A beat phenomenon also appears between sine and cosine oscillations. It results with a beat that has a phase shift compared to two sine oscillations together. From Eq. (4.4), for positive amplitude, the first portion clearly will have significant effect since its coefficient is the sum of the amplitudes. The second portion has smaller influence, especially when the two amplitudes are close to each other. The graphical representation of Eq. (4.4) is shown in Fig. 4.2 where each of the two portions of Eq. (4.4) is an individual beat of different amplitude range with a phase shift of 90° between them. The addition of the second portion of Eq. (4.4) smoothes out the fluctuation of the beat presented by first portion. In the case where the amplitude difference is large, the beat will eventually be harder to notice as the amplitude modulation decreases. Therefore, considering positive G and H, the first portion of Eq. (4.4) can be considered as the one creating beat while the second portion is reducing the beat phenomenon.

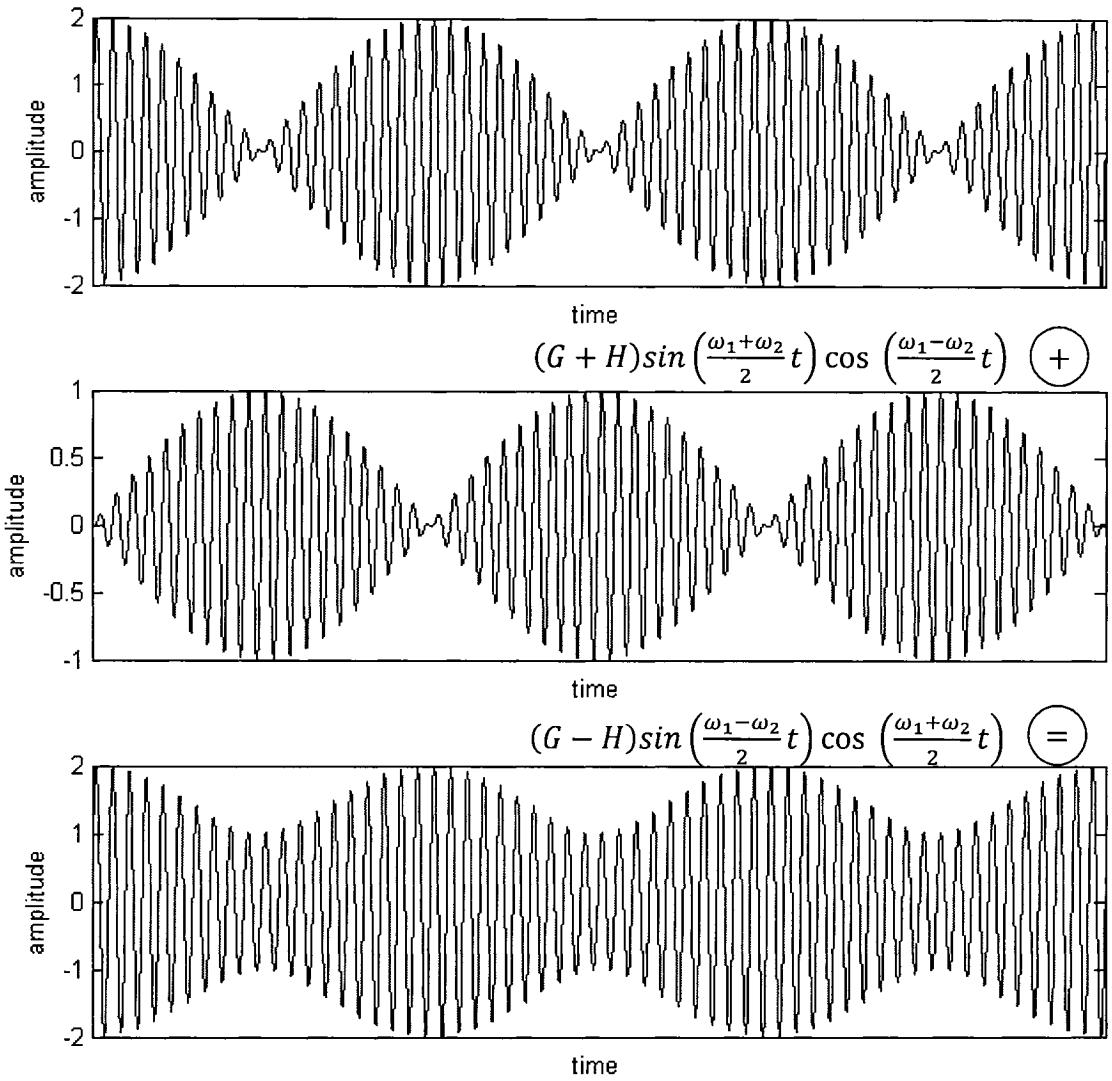

Fig. 4.2. Two vibrations of different amplitudes $(G = 1.5, H = 0.5)$ and close frequencies $(\omega_1 \approx \omega_2)$

For two vibrations of same amplitudes $(G = H)$, the Eq. (4.4) is simplified to:

$$u(t) = 2H\sin\left(\frac{\omega_2+\omega_2}{2}t\right)\cos\left(\frac{\omega_1-\omega_2}{2}t\right) \tag{4.5}$$

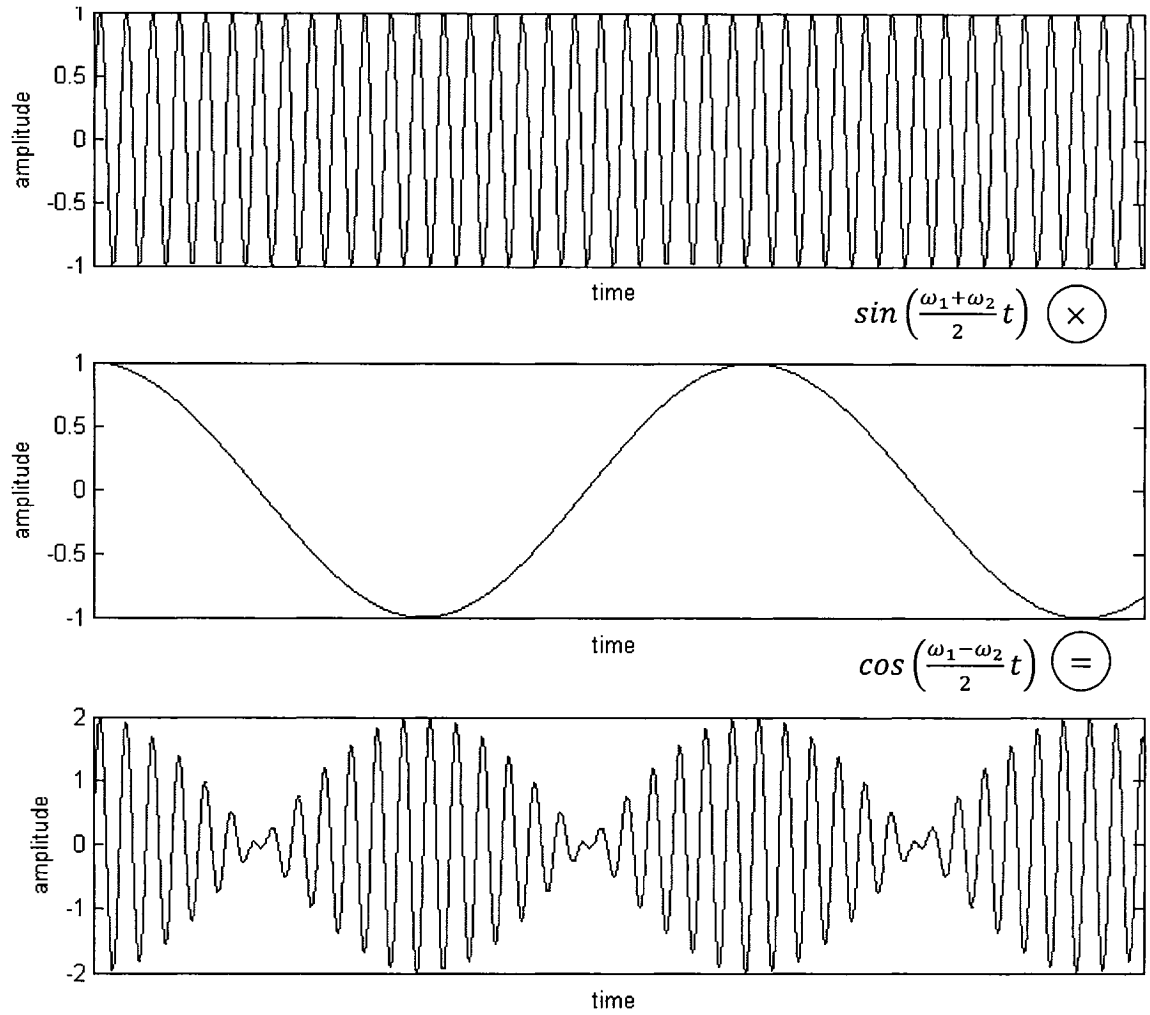

Fig. 4.3. Graphic representation of beat equation (Eq. (4.5))

The behavior of Eq. (4.5) is depicted in Fig. 4.1 and the graphical representation is shown in Fig. 4.3. The beat frequency refers to the rate at which the amplitude modulation occurs which is the envelope of the signal (second graph of Eq.(4.3)). It is equal to the simple arithmetic difference between the two interfering frequencies, and bigger is the difference, higher will be the beat frequency thus faster will be the beat. From Eq. (4.5), one can view $\cos\left(\frac{\omega_1-\omega_2}{2}t\right)$ as the beat envelope, while $\sin\left(\frac{\omega_1+\omega_2}{2}t\right)$ being the

vibration inside the envelope. The graphical representation of Eq. (4.5) is shown in Fig. 4.3.

4.3 Beat Frequency

In many applications, the beat frequency phenomenon is employed as the fundamental principle of operation. In the case of a sensitive Doppler pulse probe used to detect the movement of the blood through an artery, the frequency of the reflected sound can be mixed with the source frequency to produce a beat frequency. Any artery constriction or obstruction can be detected by an increase in the blood speed in the artery as a change in beat frequency. Similarly, radar speed detectors operate under the same principle where a wave is transmitted to the moving vehicle. The transmitted wave is bounced back with a shift in frequency caused by Doppler effect. The device then detects the beat frequency between the directed and reflected waves to provide a measure of the vehicle speed. As illustrated in Fig. 4.3, beat phenomenon is produced when a given frequency is modulated by another. This led to the first method used to broadcast commercial radio known as amplitude modulation (AM) where a modulating signal (first graph of Fig. 4.3) is multiplied with a carrier wave (second graph of Fig. 4.3) using a frequency mixer. The output of this process (third graph of Fig. 4.3) is a signal with the same frequency as the carrier but with peaks and troughs that vary in proportion to the strength of the modulating signal. Besides amplitude modulation (AM), there are other forms of wave modulations such as frequency modulation (FM) and phase modulation (PM). It is

important to mention that both FM and PM in telecommunication are actually angle modulation and represented by the following equations:

$$u_{FM}(t) = \sin(\omega t + \sin(\omega t)) \tag{4.6a}$$

$$u_{PM}(t) = \sin(\omega t + \cos(\omega t)) \tag{4.6b}$$

A real frequency modulation equation should be of the following form:

$$u_{\omega M}(t) = \sin((\omega + \sin(\omega t))t) \tag{4.7}$$

Comparing to FM band, which is also widely used in commercial radio applications, AM has a narrow bandwidth which limits the quality of sound that is received. Besides limited fidelity, the adjacent radio stations transmitted by AM tend to interfere with each other. Since the 1970's wideband FM has been preferred for musical broadcasts due to its higher audio fidelity and noise-suppression characteristics.

4.4 Wave Interference

Beat phenomenon is simply a specific case of wave interference. Any oscillation interacting with another in the same medium is wave interference. Depending on how they interact, the perception of the vibration varies. Two types of wave interference can occur: constructive when they are in phase resulting in the addition of both amplitudes,

and destructive interference when they are out of phase and subtract each other as shown in Fig. 4.5. The wave interference of traveling waves is the concept behind the digital waveguide modeling method discussed further in Chapter 5.

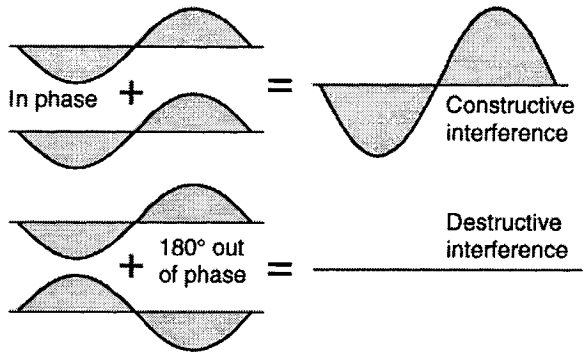

Fig. 4.4. Wave interference and phase

The modes of vibration associated with resonance in extended objects such as strings and beams have characteristic patterns called standing waves. A standing wave pattern is a vibration pattern created within a medium when the vibration frequency of the source causes reflected waves from one end of the medium to interfere constructively with incident waves from the source such that specific points along the medium appear to be standing still. It can be seen as interference of two waves of the same amplitude and frequency (and therefore same wavelength) travelling in opposite directions. With variation of boundary condition, the reflected wave is therefore expected to differ slightly to disturb the standing wave pattern.

4.5 Inharmonicity

As defined earlier, inharmonicity is a common term referring to spectra in which one or several partials are shifted slightly away from their harmonic positions. Since beat phenomenon appears between two close frequencies, this leads to the investigation of the effect of inharmonic partials. Graphically, the summation of fundamental and its first harmonic partial of same amplitude is as shown in Fig. 4.6 resulting in amplitude addition, while the vibration repeats itself at the fundamental frequency. In comparison, the effect of inharmonicity from the partial is illustrated in Figs. 4.7 and 4.8. At first sight, it seems like a beating phenomenon, but upon a closer look, the mean value varies in a harmonic fashion while the absolute amplitude of the envelope remains constant instead of increasing and decreasing as shown previously. It is interesting to note that the vibration of the fundamental (ω_1) and the first inharmonic partial (ω_2) repeats itself at the frequency of $|\omega_2 - 2\omega_1|$ instead of $|\omega_2 - \omega_1|$ as suggested by the beat equation. There is also a phase shift if the partial is slightly higher or lower than twice the fundamental frequency.

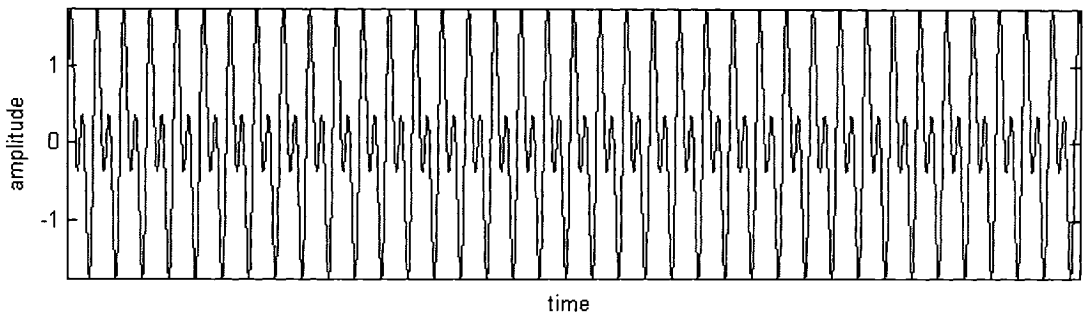

Fig. 4.6. Fundamental (ω_1) and first harmonic partial (ω_2) of same amplitude, $(\omega_2 = 2\omega_1)$

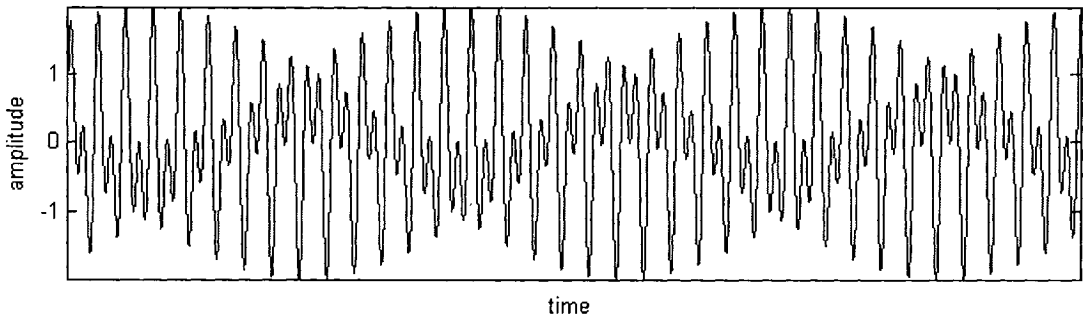

Fig. 4.7. Fundamental (ω_1) and first inharmonic partial (ω_2) of same amplitude, $(\omega_2 \approx 2\omega_1 \,\&\, \omega_2 < 2\omega_1)$

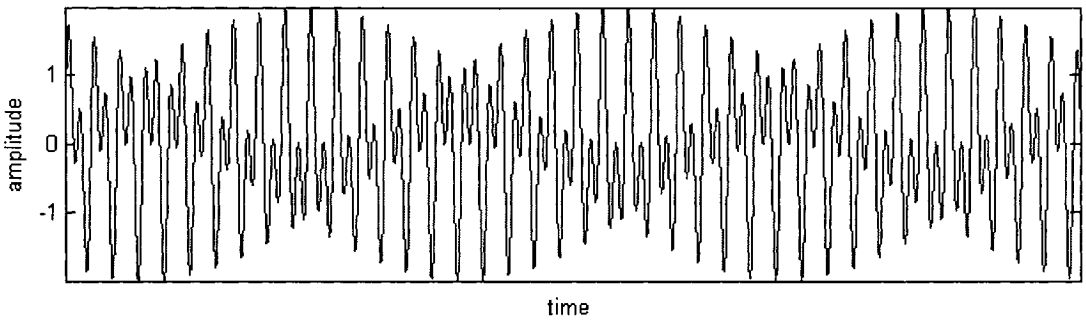

Fig. 4.8. Fundamental (ω_1) and first inharmonic partial (ω_2) of same amplitude, $(\omega_2 \approx 2\omega_1 \,\&\, \omega_2 > 2\omega_1)$

When multiple partials are considered, the way the inharmonicity varies will greatly affect the behavior of the signal. For fundamental and first and second harmonic partials, the behavior is shown in Fig. 4.9 which is quite similar to that shown in Fig. 4.6. With inharmonicity, if all the partials decrease or increase in frequency from their harmonic positions, the outcome in Figs. 4.10 and 4.11 shows similarities with those in Figs. 4.7 and 4.8 where the mean varies harmonically with the amplitude of the envelop remains almost constant. However, from the sound generated, beating is audible which is caused by the inner and denser section (Figs. 4.7 and 4.8).

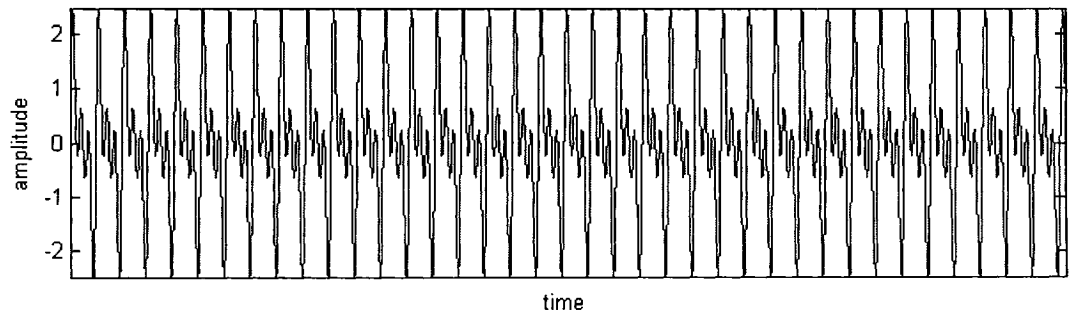

Fig. 4.9. Fundamental (ω_1) and first two (ω_2, ω_3) harmonic partials of same amplitude,

$$(\omega_2 = 2\omega_1; \omega_3 = 3\omega_1)$$

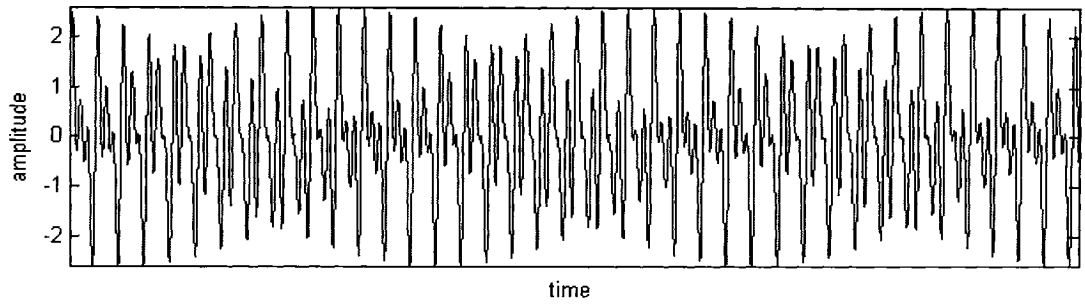

Fig. 4.10. Fundamental (ω_1) and first two (ω_2, ω_3) inharmonic partials of same amplitude, $(\omega_2 \approx 2\omega_1 \,\&\, \omega_2 > 2\omega_1; \omega_3 \approx 3\omega_1 \,\&\, \omega_3 > 3\omega_1)$

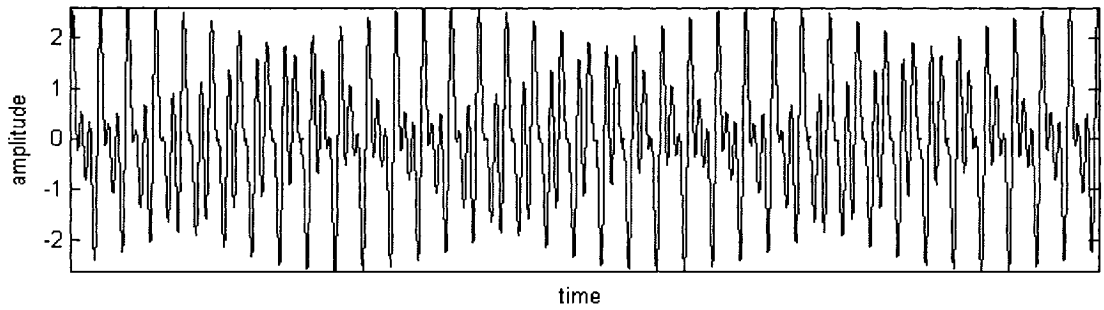

Fig. 4.11. Fundamental (ω_1) and first two (ω_2, ω_3) inharmonic partials of same amplitude, $(\omega_2 \approx 2\omega_1 \,\&\, \omega_2 < 2\omega_1; \omega_3 \approx 3\omega_1 \,\&\, \omega_3 < 3\omega_1)$

In the case where a partial is slightly at higher frequency while another is slightly lower, the vibration patterns in Figs. 4.12 and 4.13 show no sign of clear beat phenomenon. However, from audio clips generated, the inner denser section seems to cause beat phenomenon which is at higher beat frequency than in Figs. 4.10 and 4.11. From Table 3.7, inharmonic partials often all shift at higher or lower frequencies. Mix cases like in Figs. 4.12 and 4.13 are very rare.

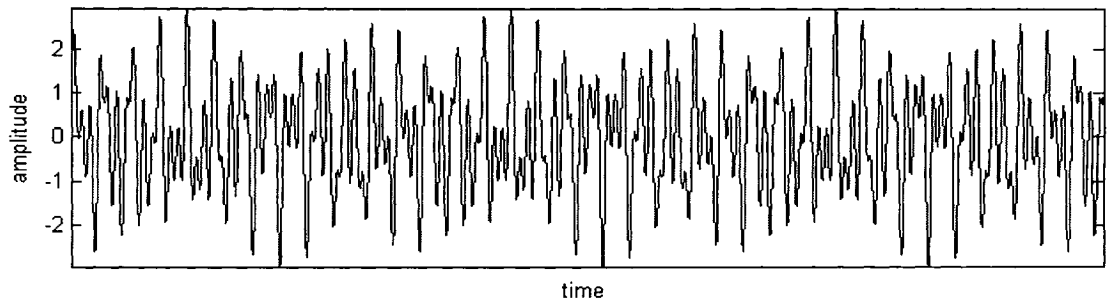

Fig. 4.12. Fundamental (ω_1) and first two (ω_2, ω_3) inharmonic partials, of same amplitude, $(\omega_2 \approx 2\omega_1 \,\&\, \omega_2 < 2\omega_1; \omega_3 \approx 3\omega_1 \,\&\, \omega_3 > 3\omega_1)$

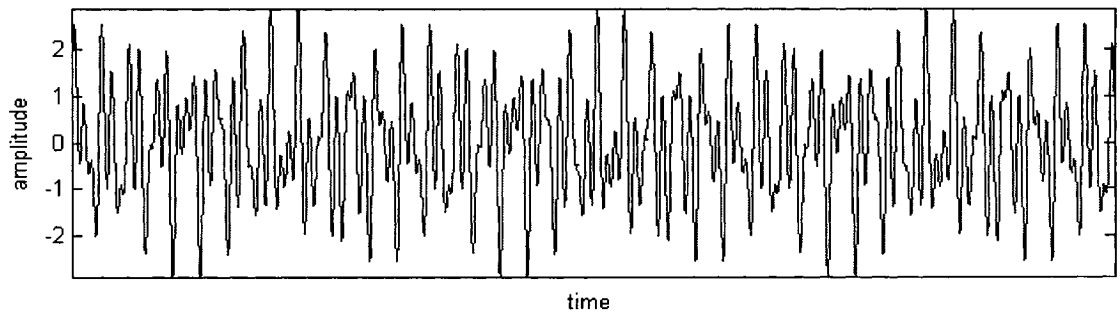

Fig. 4.13. Fundamental (ω_1) and first two (ω_2, ω_3) inharmonic partials of same amplitude, $(\omega_2 \approx 2\omega_1 \,\&\, \omega_2 > 2\omega_1; \omega_3 \approx 3\omega_1 \,\&\, \omega_3 < 3\omega_1)$

In the case of partially fixed string with high stiffness, Figs. 4.14 to 4.16 have been obtained from data for $k = 5000\,\text{N/m}$ and $L_T = 0.25\,\text{m}$ from Table 3.7. The inharmonic partials in this case are all shifted at higher frequencies. They clearly show that any additional inharmonic partials will modify the signal waveform, and influences the beat phenomenon formed in the inner darker section.

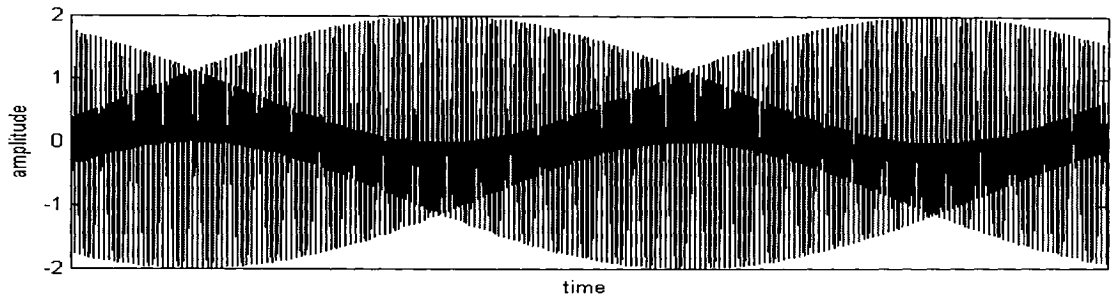

Fig. 4.14. Fundamental (ω_1) and first (ω_2) harmonic odd partials of same amplitude, $(\omega_2 = 2.01\omega_1)$

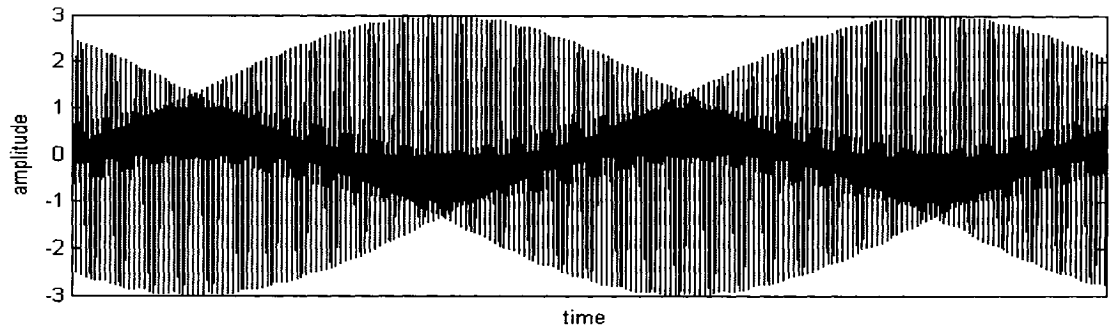

Fig. 4.15. Fundamental (ω_1) and first two (ω_2, ω_3) harmonic odd partials of same amplitude, $(\omega_2 = 2.01\omega_1; \omega_3 = 3.02\omega_1)$

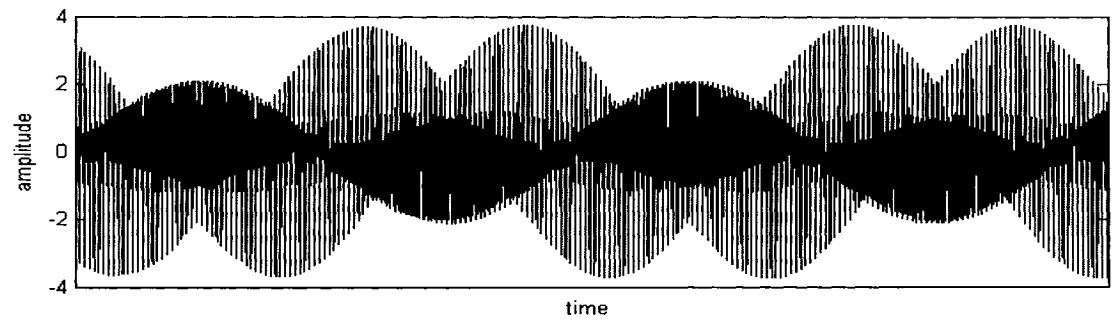

Fig. 4.16. Fundamental (ω_1) and first three $(\omega_2, \omega_3, \omega_4)$ harmonic odd partials of same amplitude, $(\omega_2 = 2.01\omega_1; \omega_3 = 3.02\omega_1; \omega_4 = 4.05\omega_1)$

For the partially fixed string with low stiffness, it has been shown in previous chapter that partials are inharmonic at close to odd multiples of fundamental frequencies. The combination of fundamental and its first two harmonic odd partials of same amplitude is as shown in Fig. 4.17. Any addition of higher odd harmonic partials will simply increase the amplitude while the signal form remains unchanged.

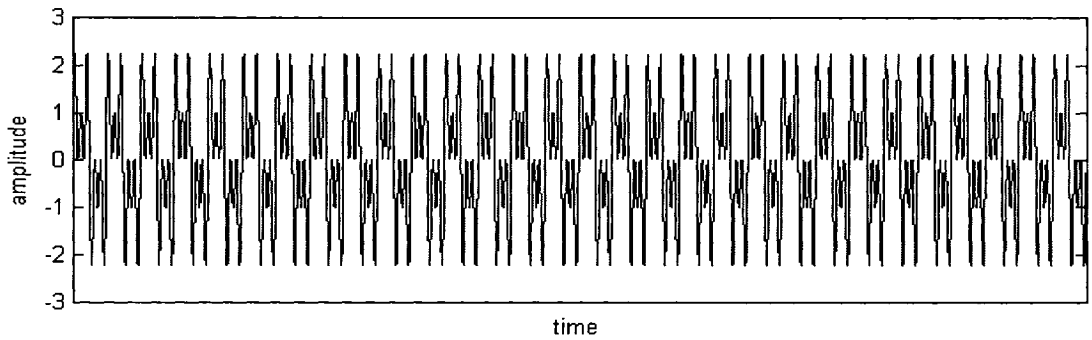

Fig. 4.17. Fundamental (ω_1) and first two (ω_2, ω_3) harmonic odd partials of same amplitude, $(\omega_2 = 3\omega_1; \omega_3 = 5\omega_1)$

For inharmonic odd partials, Figs. 4.18 to 4.20 have been obtained from data for $k = 50$ N/m and $L_T = 0.25$ m from Table 3.7. Again, any additional of inharmonic partials, despite odd multiples only, will form beat phenomenon from the inner denser sections. As a simple rule, any additional inharmonic partials will intensify a beat like denser section at center of the signal.

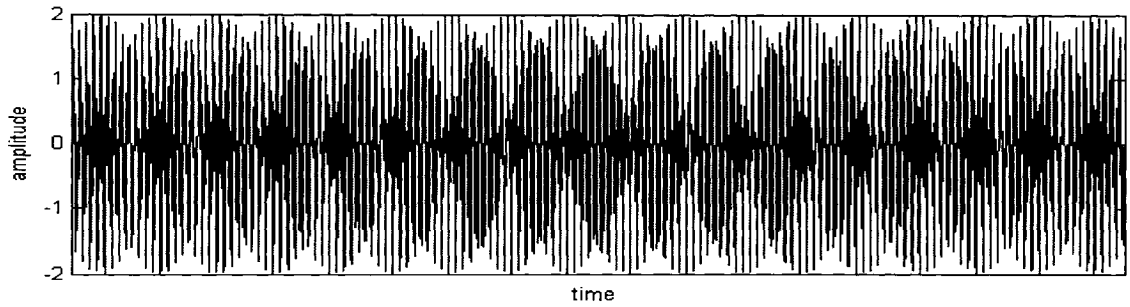

Fig. 4.18. Fundamental (ω_1) and first (ω_2) inharmonic odd partials of same amplitude, $(\omega_2 = 2.88\omega_1)$

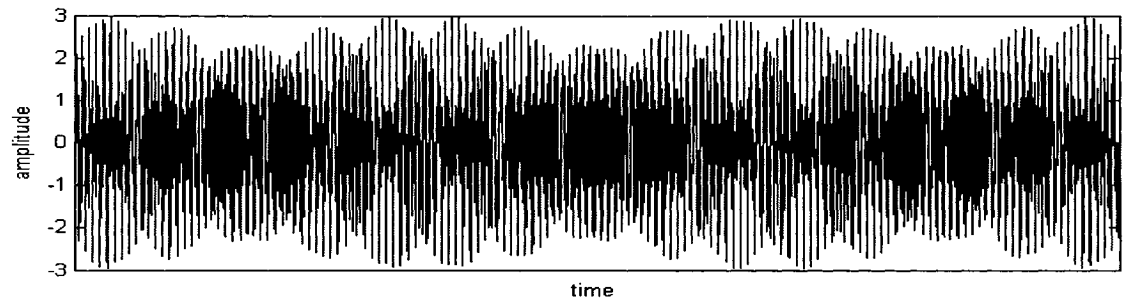

Fig. 4.19. Fundamental (ω_1) and first two (ω_2, ω_3) inharmonic odd partials of same amplitude, $(\omega_2 = 2.88\omega_1; \omega_3 = 4.78\omega_1)$

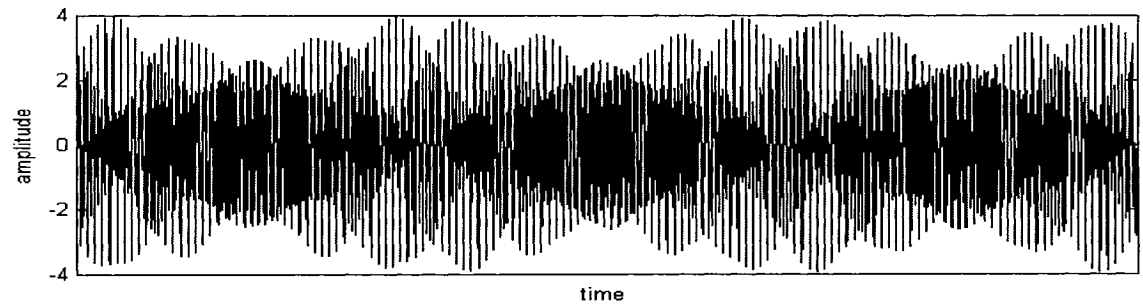

Fig. 4.20. Fundamental (ω_1) and first three $(\omega_2, \omega_3, \omega_4)$ inharmonic odd partials of same amplitude, $(\omega_2 = 2.88\omega_1; \omega_3 = 4.78\omega_1; \omega_4 = 6.68\omega_1)$

4.6 Summary

In this chapter, the wave interference between two closely spaced frequencies and between fundamental and inharmonic partials was presented. From the graphs obtained, the beat phenomenon clearly occurs between two closely spaced frequencies. In the case of fundamental and inharmonic partials, beat phenomenon is observed to take place inside the signal formed by a denser section. The graphical representation of various beat phenomena is important since they will help in recognition of beating from the simulation and experiment string motions observed. They will be covered in Chapter 5 and 6, respectively.

Chapter 5

Simulation

In Chapter 3, equations representing 3D coupled vibration were presented. Often, the exact solution is hard to obtain from partial differential equations. Simpler methods have been developed to bypass the mathematical challenge. After studying beat phenomena due to inharmonicity in Chapter 4, it will be interesting to see how the complete string will behave with a certain degree of inharmonicity. For the wave equation, the two most popular modeling techniques are finite difference and digital waveguide approaches. The finite difference method is the direct numerical solution of the equation, and the digital waveguide is the discretization of the traveling wave solutions of the wave equation. The digital waveguide has enjoyed a huge popularity in synthesized music due to its fairly accurate sound reproduction. For string motion however, the finite-difference method provides better results as the simulation is not divided into traveling waves, thus representing the actual standing wave of the string motion. The finite difference is also easy to use in 2D and 3D structures. In this thesis, only the finite difference method is used and the explanation will be focused on this

approach to provide background to the simulation obtained from the equations derived previously. In this chapter, the fundamental concept of the finite difference method will be presented and a brief presentation of the digital waveguide is followed, since it is related to finite difference method. Finally, string motions will be presented in the later sections of current chapter.

5.1 Finite Difference Method

Finite difference string model has gained wide popularity since it is directly connected to the wave equation and is straightforward to use for single as well as multiple dimensional structures. Moreover, connecting different structures together is relatively simple. However, its application has been limited by some serious drawbacks such as the stability concern and the numerical dispersion. The latter means a slight shift in the modal frequencies from the continuous system (real solution), which can, in some cases, limit the accuracy of the model using this method. However, the difference is negligible for low frequency vibration in strings and cables.

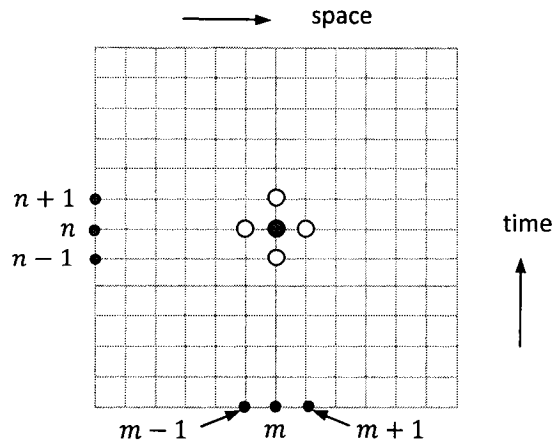

Fig. 5.1. Central difference space-time grid

In finite difference modeling, the solution of a partial differential equation is computed by replacing derivatives by finite differences. Either forward, backward or central difference schemes are used, but due to stability concern, the central difference scheme is preferred. Discrete time modeling of spatially continuous vibrating system such as a string involves discretization of both space and time on a grid of $x_m = m\Delta x$ and $t_n = n\Delta t$ as shown in Fig. 5.1.

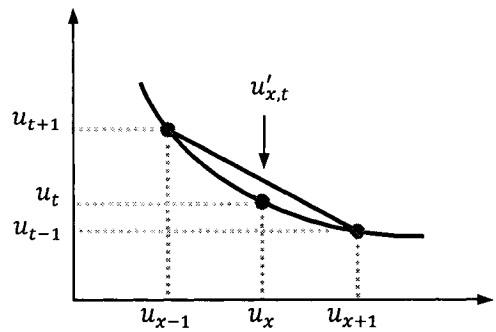

Fig. 5.2. First order central difference scheme

The central difference is a two-point scheme that uses the neighboring points (either left and right, or top and bottom) to obtain the derivative using the average value of the two points and the known grid size. Considering the grid shown in Fig. 5.2, the derivative with respect to space is represented by the following central difference scheme:

$$u'(x,t) = \frac{du_{x,t}}{dx} \approx \frac{u_{x+1,t} - u_{x-1,t}}{2dx} \tag{5.1}$$

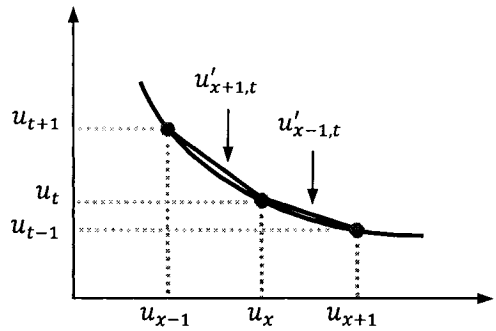

Fig. 5.3. Second order central difference scheme

As for the second order derivative, it can be expressed as a central difference between two first order derivatives.

$$u''(x,t) = \frac{d^2u_{x,t}}{dx^2} \approx \frac{\frac{du_{x+0.5,t}}{\Delta x} - \frac{du_{x-0.5,t}}{\Delta x}}{\Delta x} \tag{5.2a}$$

$$\frac{d^2u_{x,t}}{dx^2} \approx \frac{\frac{u_{x+1,t} - u_{x,t}}{\Delta x} - \frac{u_{x,t} - u_{x-1,t}}{\Delta x}}{\Delta x} \tag{5.2b}$$

$$\frac{d^2u_{x,t}}{dx^2} \approx \frac{u_{x+1,t} - 2u_{x,t} + u_{x-1,t}}{\Delta x^2} \tag{5.2c}$$

Similarly, the second order central difference on time grid is expressed as

$$\frac{d^2u_{x,t}}{dt^2} \approx \frac{u_{x,t+1} - 2u_{x,t} + u_{x,t-1}}{\Delta t^2} \tag{5.3}$$

The combination of Eq. (5.2c) and (5.3) is the finite difference form of the ideal wave equation (Eq. (2.4)) using central difference scheme. After rearranging, the ideal wave equation becomes:

$$u^y_{x,t+1} = \left(\frac{c_T \Delta t}{\Delta x}\right)^2 (u^y_{x+1,t} - 2u^y_{x,t} + u^y_{x-1,t}) + 2u^y_{x,t} - u^y_{x,t-1} \tag{5.4}$$

With known initial impulse amplitude and boundary condition at both ends, the finite difference method automatically computes the next value of the element at position x from the past state of the string including neighboring positions data, without solving the wave equation analytically. In addition, unlike the close-form solution, the numerical method automatically considers all the partials in the simulation. The finite difference scheme has proven so far to be easy to derive, takes little storage and executes quickly. Unfortunately, the finite difference method is not always stable and it may be useless in cases such as the forward time centered space difference scheme. To find out if a given

numerical scheme is stable or not, the von Neumann stability analysis is a fine tool that can give a first simple validation. [84]

The von Neumann stability procedure, in principle, performs a spatial Fourier transform along all spatial dimensions reducing the finite difference scheme to a time recursion in terms of the spatial Fourier transform of the system. It is important to underline that the von Neumann stability analysis a) does not take into account the boundary effects; b) assumes that the coefficients of the finite difference equations are sufficiently slowly varying to be considered constant in time and space. Under these assumptions, the solution can be seen as a sum of eigenmodes which at each grid point has the form of [84, 86, 87]

$$u(x,t) = u_{x,t} = u_{m,n} = \xi^n e^{i\kappa mx} \tag{5.5}$$

where $\kappa = \frac{2\pi}{\lambda}$ denotes the wave number (which can have any value) where λ is the wavelength, and $\xi = \xi(x)$ is a complex number called amplification factor that depends on κ. The criterion for stability is defined as the value of κ that keeps the amplification factor less than 1 as stated below:

$$|\xi|^2 = \xi\xi^* \leq 1 \tag{5.6}$$

The amplification factor, $\xi(\kappa)$, is found by applying Eq. (5.5) in Eq. (5.4)

$$\xi = \left(\frac{c_T \Delta t}{\Delta x}\right)^2 (2\cos(\kappa x)) + 2\left(1 - \left(\frac{c_T \Delta t}{\Delta x}\right)^2\right) - \frac{1}{\xi} \tag{5.7}$$

whose solution is [79, 81]

$$\xi = 1 + \left(\frac{c_T \Delta t}{\Delta x}\right)^2 (\cos(\kappa x) - 1) \pm \frac{c_T \Delta t}{\Delta x} \sqrt{\left(\frac{c_T \Delta t}{\Delta x}\right)^2 (\cos(\kappa x) - 1)^2 + 2(\cos(\kappa x) - 1)} \tag{5.8}$$

By applying Eq. (5.8) into the condition represented by Eq. (5.6), it gives $|\xi|^2 = 1$. This means that there is no amplitude dissipation in the presented finite difference scheme. Actually, for all central difference schemes, the von Neumann stability condition is always satisfied. In some other schemes, it is only satisfied with certain conditions leading to specific requirement concerning the value of Δx and Δt. Unfortunately, for methods such as forward time central space, the condition can not be met and thus they are unconditionally unstable. [84]

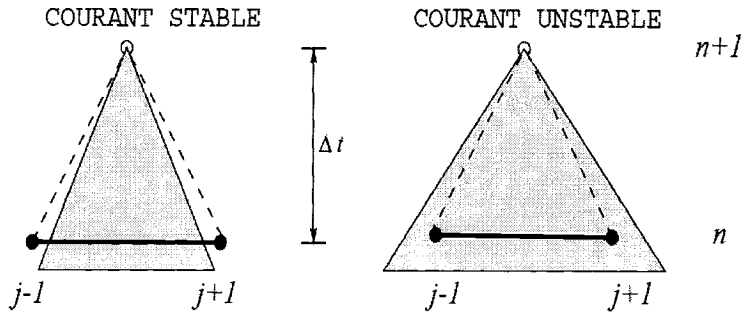

Fig. 5.4. Schematic diagram of Courant stable and unstable choices of time and space steps (Δt and Δx) [84]

If the von Neumann condition is satisfied without any requirement, the Courant-Friedrichs-Lewy stability criterion is used to determine the grid size. Often called simply the Courant condition, it states that the system is numerically stable for [84]

$$\left(\frac{c_T \Delta t}{\Delta x}\right)^2 \geq 1 \quad \Rightarrow \quad \Delta x \geq c_T \Delta t \tag{5.9}$$

In the MATLAB simulation of the ideal wave equation developed for the present thesis, the grid is chosen to fit $\Delta t = \frac{\Delta x}{c_T}$, where the value of Δx used is always 1 cm, and the velocity of wave propagation is defined by the tension and mass per length of the string as in $c_T = \sqrt{\frac{T_o}{\rho}}$. Similarly, for axial vibration, the grid is selected following $\Delta t = \frac{\Delta x}{c_A}$, where $c_A = \sqrt{\frac{AE + T_o}{\rho}}$. The above procedure has been applied to all finite difference models presented in this study.

5.2 Digital Waveguide Method

Interestingly enough, the above Courant condition is the connecting bridge between finite difference and digital waveguide methods. First introduced by J. O. Smith [86, 87] in 1983, the digital waveguide modeling technique is based on D'Alembert's traveling wave solution for the ideal wave equation. This method is especially well suited for simulation of 1D resonators such as vibrating string, acoustic tube and thin bar. Considering its easy to use, low computation cost and fairly accurate sound synthesis, the digital waveguide method has enjoyed a great amount of popularity in the computer music field. Developed from D'Alembert's traveling wave solutions, the two traveling waves are discretized to form a set of bidirectional delay lines. Filters are added to simulate environment changes to the traveling waves, and the whole is presented as a feedback loop model (see Fig. 5.6).

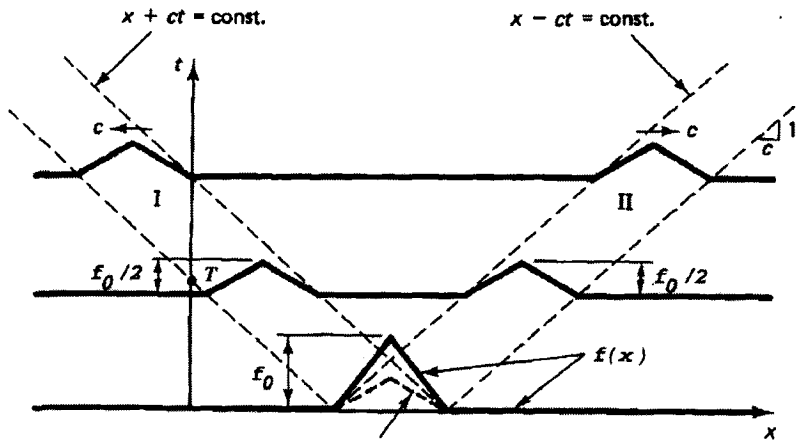

Fig. 5.5. D'Alembert's traveling waves [43]

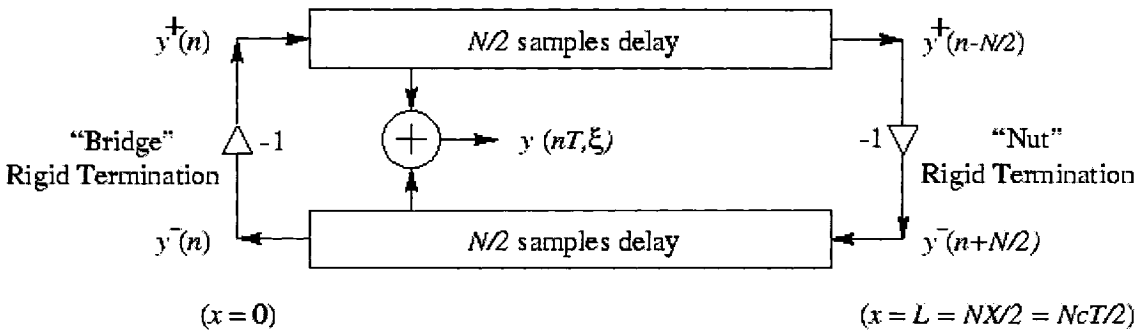

Fig. 5.6. Digital waveguide model of ideal string fixed at both ends [84]

Consider the grid size to follow $c_T = \dfrac{\Delta x}{\Delta t}$ as stated earlier, Eq. (5.4) is then simplified into

$$u^y_{x,t+1} = u^y_{x+1,t} + u^y_{x-1,t} - u^y_{x,t-1} \tag{5.10}$$

Consider the D'Alembert's traveling wave solution to the wave equation as

$$u(x,t) = u_{x,t} = u(x - ct) + u(x + ct) \tag{5.11}$$

Its discretized version then takes the following form

$$u_{x,t} = u(m\Delta x - cn\Delta t) + u(m\Delta x + cn\Delta t) \tag{5.12}$$

Applying Eq. (5.12) to Eq. (5.10) gives

$$\begin{aligned} & u(m\Delta x - c(n+1)\Delta t) + u(m\Delta x + c(n+1)\Delta t) \\ & = u((m+1)\Delta x + cn\Delta t) + u((m-1)\Delta x - cn\Delta t) \end{aligned} \tag{5.13}$$

The above relationship is only valid if and only if $c_T = \frac{\Delta x}{\Delta t}$, which is the assumed speed of traveling waves in the digital waveguide method. Therefore the finite difference and digital waveguide are equivalent if and only if the specific case of Courant condition of $c_T = \frac{\Delta x}{\Delta t}$ is applied in finite difference scheme.

5.3 Simulation Results

In the previous chapter, various equations of string motion were derived. In the present work, all simulations are performed using MATLAB 7.0 with the numerical method previously described. First, considering the string's lateral motion, it is possible to obtain the motion of the string after being excited to validate the simulation's accuracy with known results. According to Fig. 2.2, any excited string with an impulse displacement should bounce back and forth between the imaginary boundaries drawn by the maximum upward and downward lateral displacements. For the simulation, the string is considered to be excited at one third of its length, and the motion is presented in Fig. 5.7. Drawing all lines together gives a boundary defined in Fig. 5.8. As expected, all curves lie inside the maximum displacement curve toward the top and bottom. This validates the modeling technique with known results from Fig. 2.2 for an undamped string.

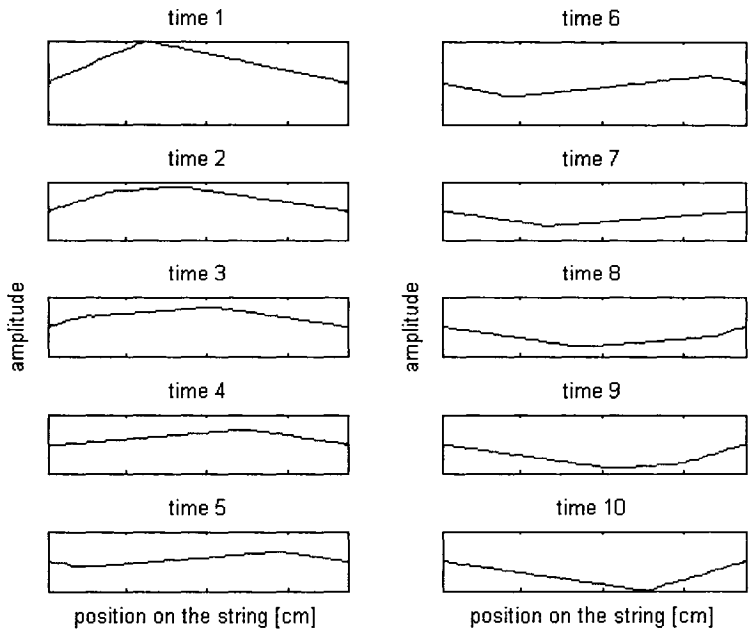

Fig. 5.7. Complete lateral motion cycle for a string excited at $\frac{L}{3}$

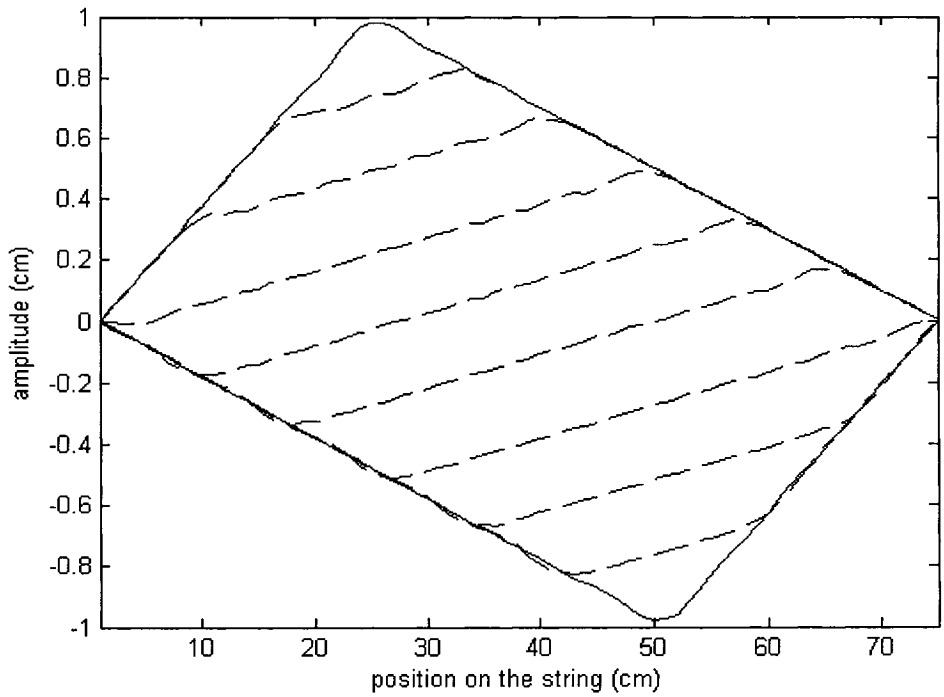

Fig. 5.8. Combination of lateral motion of an undamped fixed-fixed string

For the 1D numerical method model, the individual motion of each point on the string is oscillating between the top and bottom boundaries shown in Fig. 5.8. The axial-transverse coupling is much more complicated. When applying uncoupled longitudinal and lateral equations into von Neumann and Courant stability criterion, they give different space-time grids which make the coupling impossible unless we adopt one of the two grids. Note that in both ideal transverse and axial wave equations, there is no amplitude addition or dissipation as $|\xi|^2 = 1$ for both cases. From Courant stability condition (Fig. 5.4), the axial vibration will be unstable using larger lateral grid since $\frac{\Delta x}{c_T} >> \frac{\Delta x}{c_A}$. However, the lateral vibration is stable with smaller axial grid but results in slightly downward shift of the curves as shown in Fig. 5.10 compared to Fig. 5.9. Despite the small inaccuracy, the difference remains small after one second, thus validating the application of axial grid size in lateral vibration simulation.

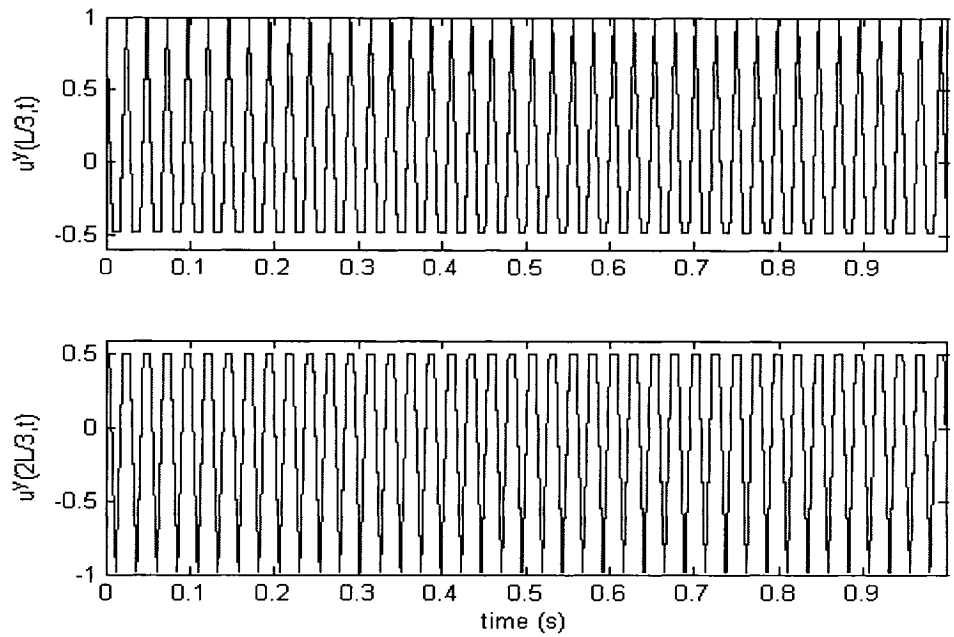

Fig. 5.9. Lateral vibration (ideal 1D wave equation) at $\frac{L}{3}$ using $\Delta t = \Delta x / c_T$ as grid

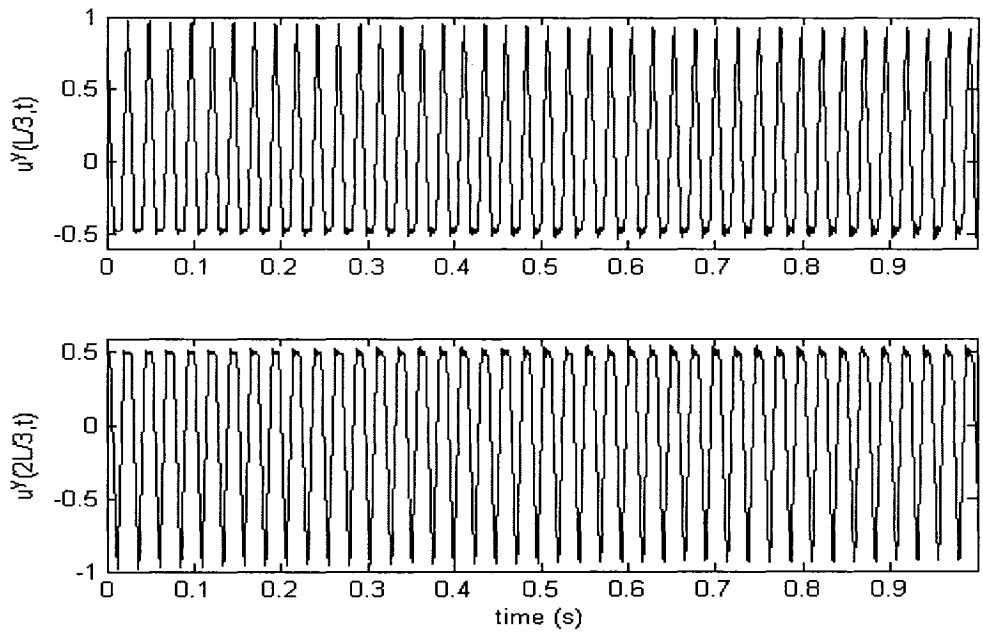

Fig. 5.10. Lateral vibration (ideal 1D wave equation) at $\frac{L}{3}$ using $\Delta t = \Delta x / c_A$ as grid

For a coupled system, considering the coupled equations rewritten below, it is impossible to apply the von Neumann stability criteria on Eq. (5.14a) due to the multiplication of partial differential terms at right hand side of the equation.

$$\frac{\partial^2 u^x}{\partial t^2} = \frac{(T_o + AE)}{\rho}\frac{\partial^2 u^x}{\partial x^2} + \frac{AE}{\rho}\left(\frac{\partial u^y}{\partial x}\frac{\partial^2 u^y}{\partial x^2} + \frac{\partial u^z}{\partial x}\frac{\partial^2 u^z}{\partial x^2}\right) \tag{5.14a}$$

$$\frac{\partial^2 u^y}{\partial t^2} = \frac{T_o}{\rho}\frac{\partial^2 u^y}{\partial x^2} \tag{5.14b}$$

$$\frac{\partial^2 u^z}{\partial t^2} = \frac{T_o}{\rho}\frac{\partial^2 u^z}{\partial x^2} \tag{5.14c}$$

The simulation of the coupled system is illustrated in Fig. 5.11 using axial grid resulting in slightly amplitude downward shift for lateral motion as explained earlier. The axial displacement is considered to be initiated by lateral motion and its behavior depicts strange beat phenomenon mixing long and short beats.

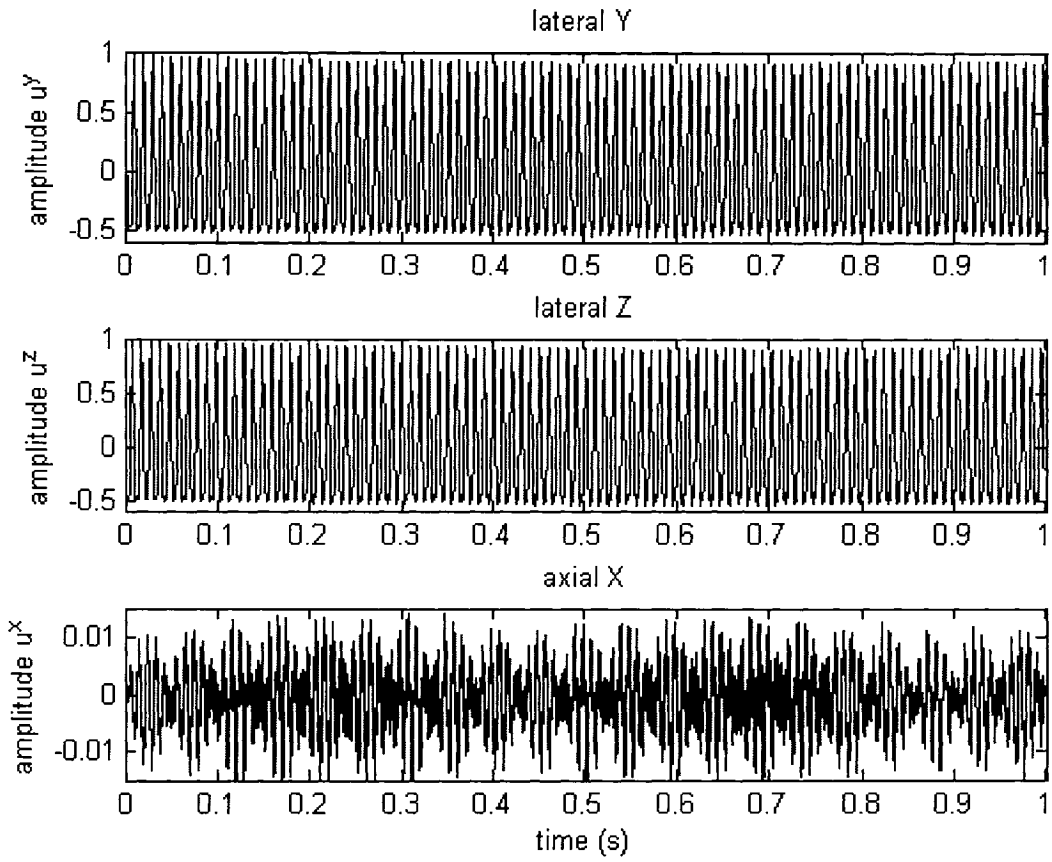

Fig. 5.11. Coupled system behavior at $\frac{L}{3}$

For the string with a partially clamped end, the lateral motion simulation illustrated in Fig. 5.12 shows very little difference with the fixed-fixed version portrayed in Fig. 5.7. However, once plotted together in Fig. 5.13, the string motion is not bound exactly inside the area formed by the two maximum downward and upward displacements. If the two maximum displacements are observed closely, it is clear that they are slightly different from each other. This suggests that the string motion may vary in the long term and no longer follows the boundary shapes after one cycle.

Effectively, due to variations of the reflected wave from partially clamped and fixed ends, there is a small phase shift between the two. This signifies that the long term string motion is no longer bound between the limit drawn in Fig. 5.13. After a few early cyclic motions, the string is bouncing like the top illustration of Fig. 5.14. The string motion keeps changing and finally completely switches sides to tilt toward right side as shown in the bottom illustration of Fig. 5.14 before slowly bouncing back to tilt toward left side after several cycles. This oscillatory motion between tilting toward right and left sides repeats itself since there is no damping in the simulation. It is worth mentioning that the effect of tilting in the opposite direction tends to decrease with an increase in string stiffness of the twisted thread material used to lift the string. A slightly more exaggerated stiffness value was used in Fig. 5.14 to better emphasize the observation regarding the continuous shifting in tilt direction.

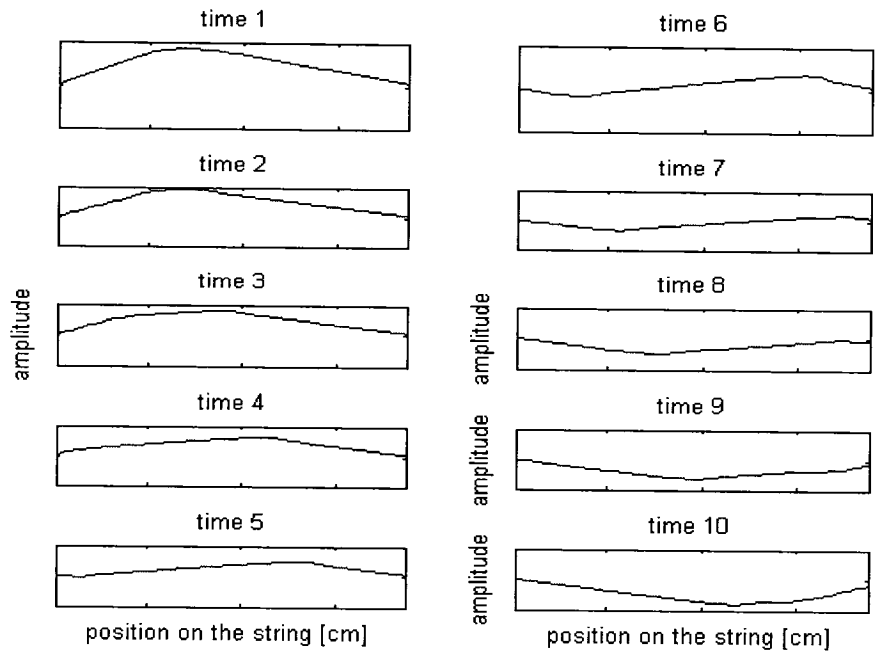

Fig. 5.12. Complete lateral motion cycle for a string lifted at one end excited at $\frac{L}{3}$

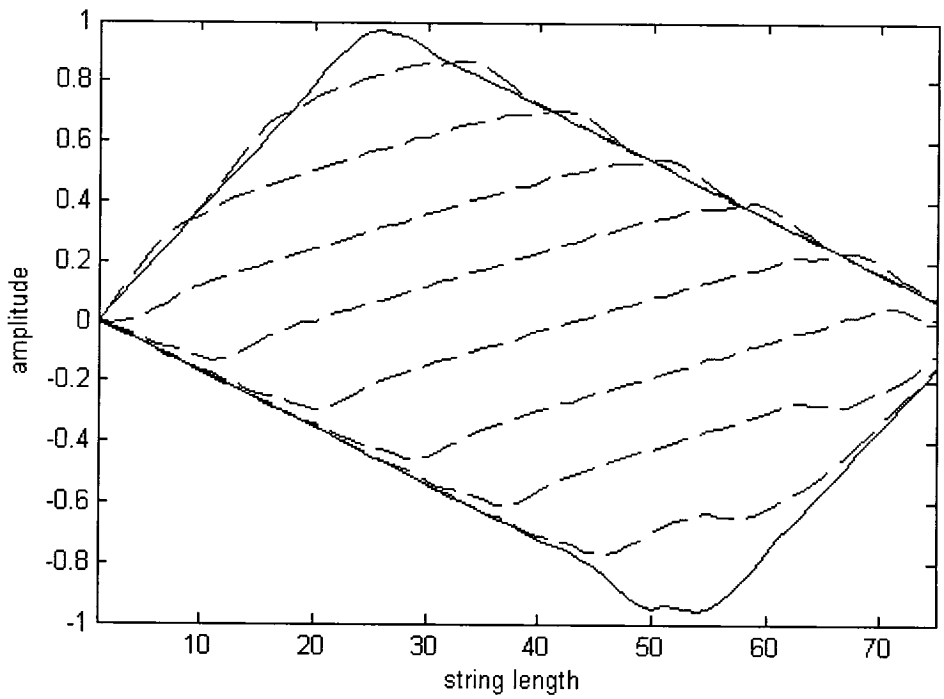

Fig. 5.13. Combination of lateral motion of an undamped fixed-partially clamped string

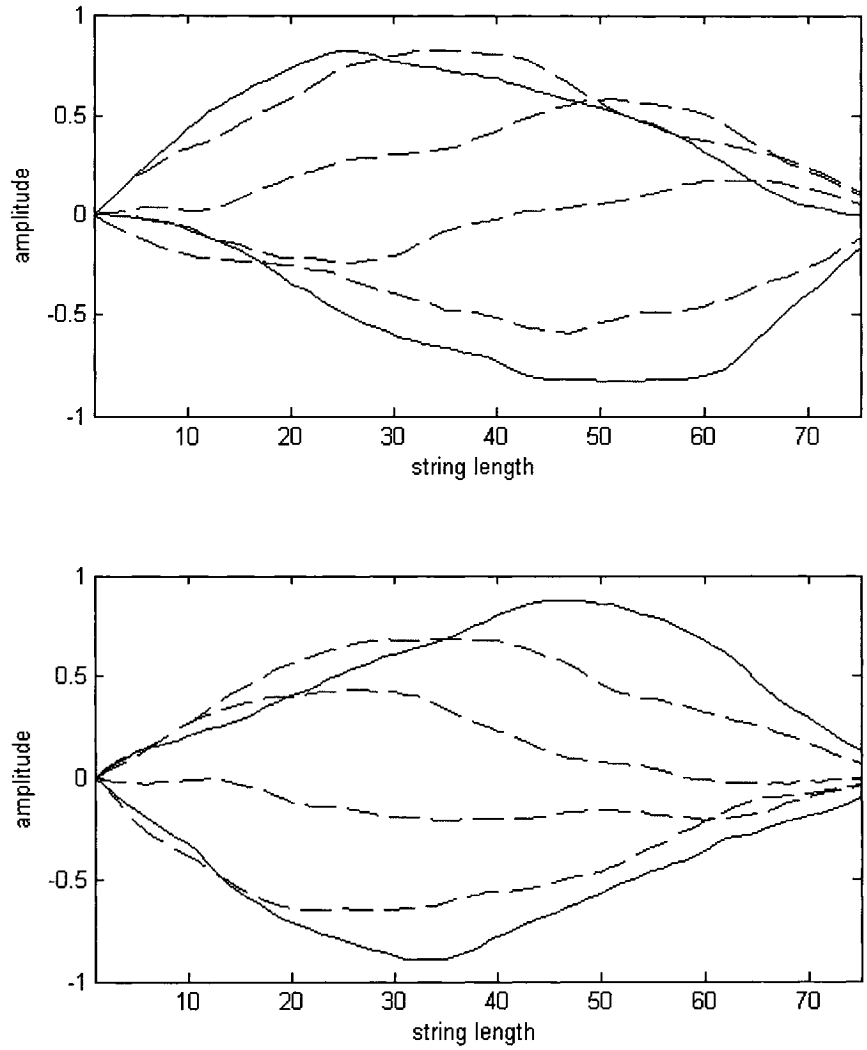

Fig. 5.14. Rightmost (bottom) and leftmost (top) tilts of fixed-partially clamped string

When plotting the motion of various points on the string as portrayed in Fig. 5.15, the presence of a beat is obvious. Finally, a very curious behavior of the string with one end lifted is shown in Fig. 5.16 where the frequency amplitude curve finishes abruptly at the lifted end instead of finishing smoothly like in the case of string without lifting.

Depending on the stiffness of the supporting material, the softer the stiffness, the more abrupt will be the amplitude curve finish at the lifted end.

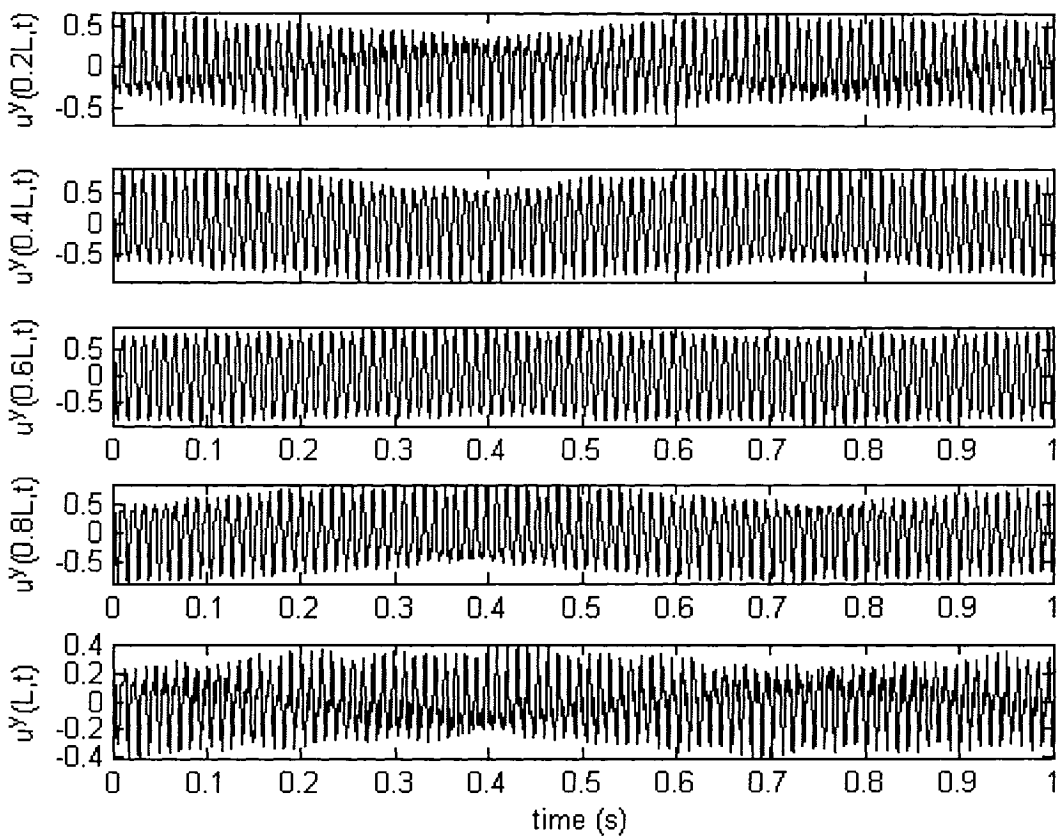

Fig. 5.15. Oscillation at various position of the string with partially clamped end at $x = L$

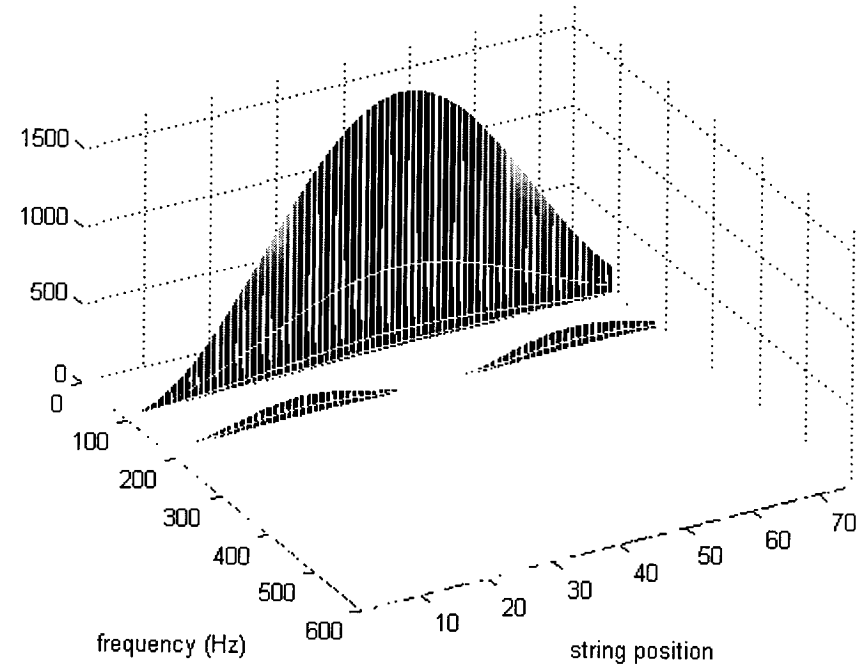

Fig. 5.16. Combined FFT of all points on a fixed-partially clamped string

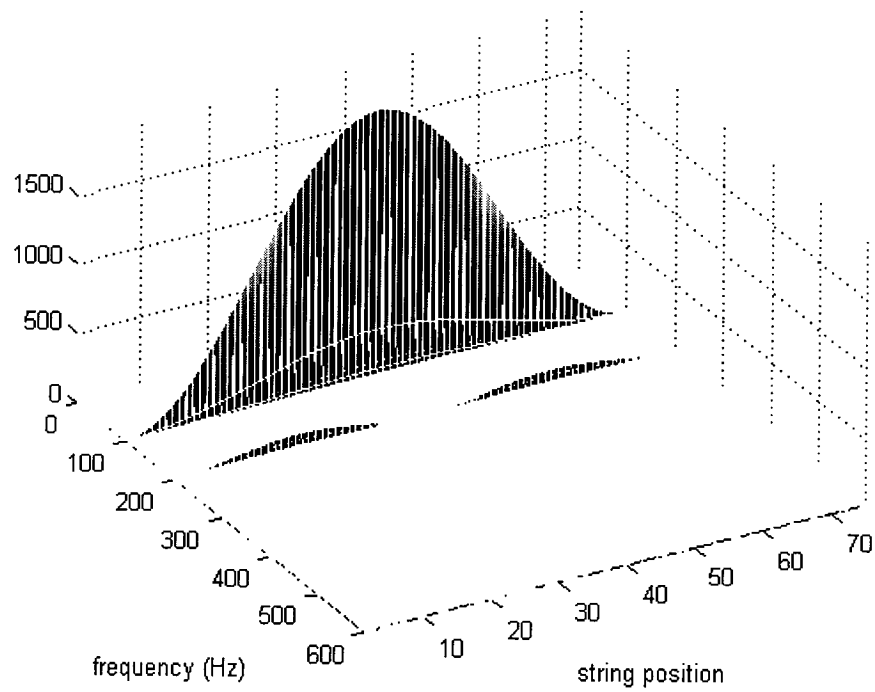

Fig. 5.17. Combined FFT of all points on a fixed-fixed string

5.4 Summary

In this chapter, the finite difference method has been presented with basic stability analysis. As a special type of finite difference scheme, the digital waveguide is briefly discussed. The behavior of the coupled system is modeled using an axial grid since it allows both axial and lateral motion to be stable. The obtained results are quite surprising as the axial motion is showing beat phenomena, resulting from interference between fundamental and inharmonic partials. For a string with a partially clamped end, the simulation shows a phase shift in the reflected wave from the partially clamped end resulting in a beat phenomenon. In Chapter 6, the simulation results will be validated with those obtained from experiment.

Chapter 6

Experiments

In previous chapters, theoretical studies and a computer simulation were presented. However, any theoretical analysis needs to be validated with actual results. In this chapter, experiments are carried out to verify the case of coupled motion of fixed-fixed string with supported points. The experiment is first described and the actual output is compared to the string model derived in the previous chapter. It is important to mention that guitar strings were used in current experiment due to their ready availability in wound and unwound forms, and good quality-price ratio. They are therefore a test bench to other type of strings and cables. The scheme of the experiment setup is shown in Fig. 6.1, and it is designed to enable monitoring the tension and sound pressure variation as well as the orbital motion of an excited string.

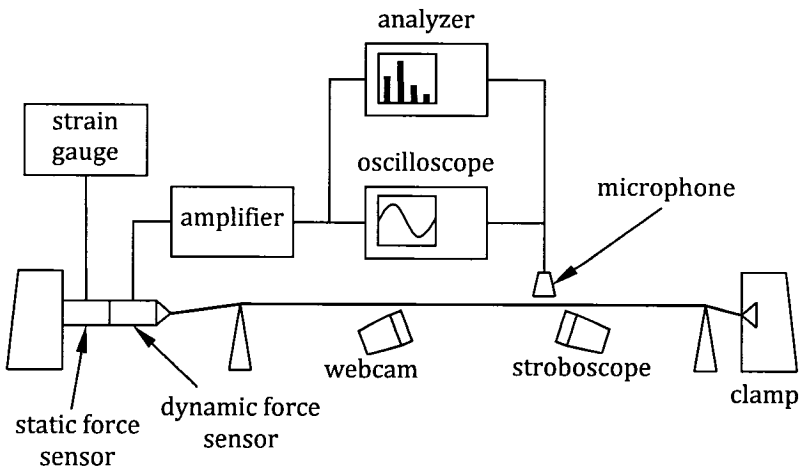

Fig. 6.1. Experiment setup diagram

6.1 Experiment Apparatus and Setup

The setup is fairly simple where the string is fixed at one end by a clamp playing the role of a fixed support. The other end is attached to a turning knuckle allowing various tensions to be applied by tightening the string. The knuckle is mounted to a fixed support via a set of dynamic and static force sensors. Two supports then lift the string at specific positions simulating the transverse vibration boundary conditions.

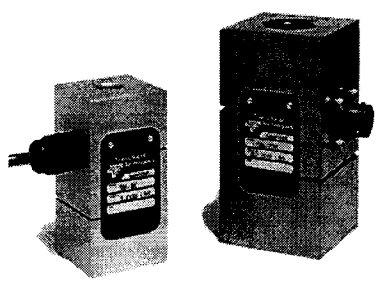

Fig. 6.2. Static load cell SW-500C from Transducer Techniques

Table 6.1. Static load cell SW-500C specifications

Rated output (R.O.)	2 mV/V nominal
Nonlinearity	0.1% of R.O.
Hysteresis	0.1% of R.O.
Nonrepeatability	0.05% of R.O.
Zero Balance	1.0% of R.O.
Compensated Temp. Range	60° to 160°F
Safe Temp. Range	-65° to 200°F
Temp. Effect on Output	0.005% of Load/°F
Temp. Effect on Zero	0.005% of R.O./ °F
Terminal Resistance	350 ohms nominal
Excitation Voltage	10 VDC
Safe Overload	150% of R.O.
Calibration Included	Compression
Optional Calibration	Tension

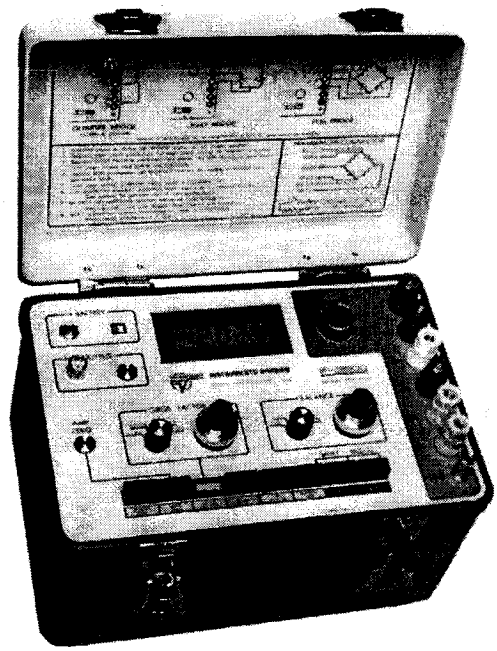

Fig. 6.3. Digital strain gauge P3500 from Measurement Group

Connected to a digital strain indicator, the static force sensor SW-500C indicates the tension applied to tighten the string. With a rated output of 2 mV/V and a load capacity of 500 lbs force, the sensor can be set to various gauge factors. From Table 6.2, a gauge factor of 0.400 will give a full scale count of 20 000 for 500 lbs force, which means a precision of 0.025 lb force. In order to facilitate the reading, the gauge factor of 1.600 has been chosen to have 5 000 counts for the 500 lbs force allowing an accuracy of 0.1 lb force. With the current setting, it will be possible to tighten the string accurately at any desired tension by turning the rotating knuckle with the feedback displayed on the digital strain gauge from the static force sensor.

Table 6.2. Strain gauge P3500 gauge factor setting

FULL SCALE COUNTS	G.F. SETTING		
	TRANSDUCER SENSITIVITY IN mV/V		
	1.5 mV/V	2.0 mV/V	3.0 mV/V
1000	6.000	8.000	12.000
1200	5.000	6.667	10.000
1500	4.000	5.333	8.000
2000	3.000	4.000	6.000
2500	2.400	3.200	4.800
3000	2.000	2.667	4.000
4000	1.500	2.000	3.000
5000	1.200	1.600	2.400
6000	1.000	1.333	2.000
7000	0.857	1.143	1.714
8000	0.750	1.000	1.500
9000	0.667	0.889	1.333
10 000	0.600	0.800	1.200
12 000	0.500	0.667	1.000
15 000	0.400	0.533	0.800
20 000	0.300	0.400	0.600

$$FS = \frac{4000 \times \frac{mV}{V}}{GF} \qquad GF = \frac{4000 \times \frac{mV}{V}}{FS}$$

Since the nonlinearity of the tension during string vibration is considered in the analytical model, the dynamic force sensor is used to monitor the behavior of tension variation after plucking. To minimize error induced by the force sensors, special care has been taken in selecting appropriate devices with high rigidity. The dynamic load cell is capable of supporting tension up to 100 lbs (444.82 N), which exceeds the needs of the current experiment.

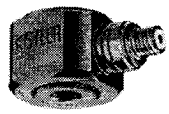

Fig. 6.4. Model 912 quartz dynamic load cell from Kistler Instrument

Table 6.3. Dynamic load cell model 912 specifications

Range: Compression	To 5 000 lbs
Range: Tension	To 100 lbs
Resolution	0.002 lb
Overload	20 percent
Sensitivity (nominal)	50 picocoulombs/lb.
Resonant frequency (nominal) (no load)	60 000 Hz
Rigidity	20×10^{-8} in./lb.
Rise Time	10 microseconds
Linearity (zero based best straight line)	±1 percent
Capacitance (nominal)	58 picofarads
Insulation resistance (min.)	10^{13} ohms
Temperature sensitivity	0.01 percent/°F
Temperature range	-400 to +300 °F
Side force (max.)	100 lbs
Shock and vibration	10 000 g's

Due to the rigidity of the sensor, a signal conditioner is used to amplify the voltage produced by the quartz dynamic load cell. This same signal is then input into the

oscilloscope and the analyzer along with sound pressure from the tip clip microphone in order to obtain data in both time and frequency domains. Both machines are set so that the recording is triggered by the signal coming from the dynamic force sensor.

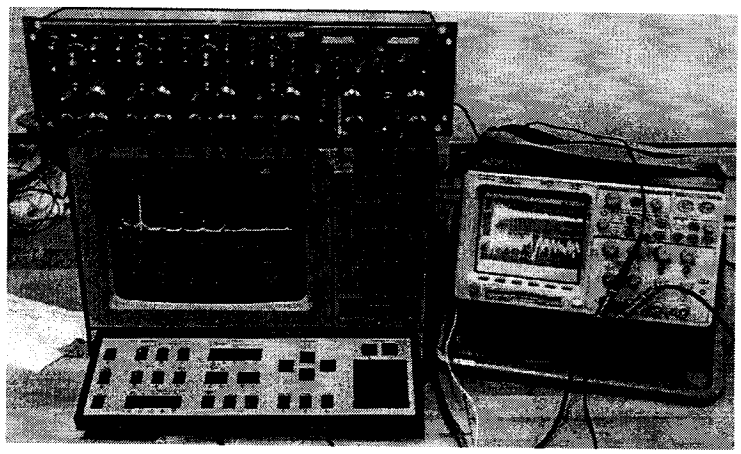

Fig. 6.5. Analyzer and oscilloscope

Besides the microphone, a webcam is positioned close to the string to record the sound into a laptop. Since the sampling rate from webcam can reach 44,000 Hz (44,000 recording per second), the data from webcam will be analyzed where microphone is only used to verified the initial setting since oscilloscope only records 1,000 points. The sound clips obtained are later on analyzed in MATLAB to perform a Fast Fourier Transform (FFT) on specific sound segments. In addition, a stroboscope is used to capture the orbital motion of the string while resonating. Basically, the stroboscope is set to be a bit off from the natural frequency of the string to capture the orbital motion (if it is set at the same frequency, the string will always appear stationary). In summary, devices used in current experiment are listed below in Table 6.4.

Table 6.4. Devices used in current experiment

Device	Company	Model
Signal analyzer	Brüel & Kjær	2035
Oscilloscope	Agilent	54624A
Amplifier/signal conditioner	Unholtz-Dickie	D22PSOX
Strain indicator	Measurements Group	P3500
Stroboscope	General Radio	Strobotac 1531-AB
Omnidireactional tie clip microphone	Nexxtech	3303013
Webcam	Logitech	Messenger
Dynamic load cell	Kistler	920
Static load cell	Transducer Techniques	SW-500C

Fig. 6.6. Experiment setup

6.2 Experimental Results

For the experiment, a set of PhosBronze Acoustic series guitar string from Dean Markley Strings Inc. is used. Guitar strings are simply a test bench for current study. The selection is basically made due to its low price, availability, high quality, various sizes and presence of wound and unwound strings. As the name indicates, the winding is made

of phosphorous bronze and the core is made of steel. The properties of each string are shown below in Table 6.5.

Table 6.5. Guitar string properties

String gauge/ Total ∅ (mm)	Core ∅ (mm)	Mass per length ($\times 10^{-3}$ Kg/m)	Tension (N)	Frequency (Hz)
0.33	0.33	0.7	127	329.63
0.43	0.43	1.2	125	246.94
0.66	0.38	2.7	173	196.00
0.91	0.42	4.9	168	146.83
1.17	0.46	8.2	168	110.00
1.42	0.50	12.3	144	82.41

Once attached, the string is tuned using an electronic tuner and the analyzer to obtain the desired frequency. The tightening tension recorded from the strain gauge will be used for simulation. Arbitrary plucks are applied upward to initiate the recording which is triggered by the dynamic force sensor for both analyzer and oscilloscope. For each string, FFT from both webcam and dynamic force sensor are presented as well as the tension variation with time recorded by dynamic force sensor (see Fig. 6.7 to 6.23). The experiment is performed four times for each string.

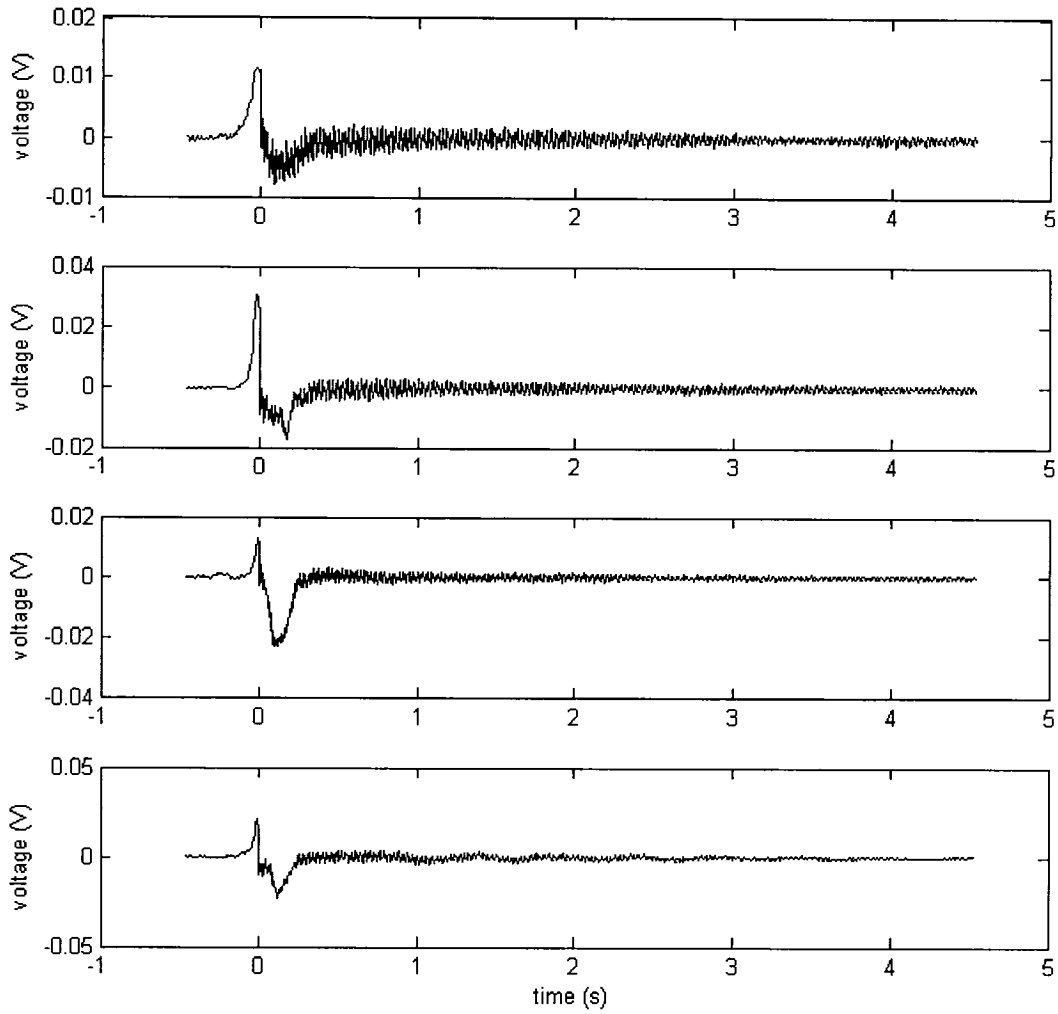

Fig. 6.7. Dynamic force sensor signal recorded by oscilloscope for 0.33 mm string

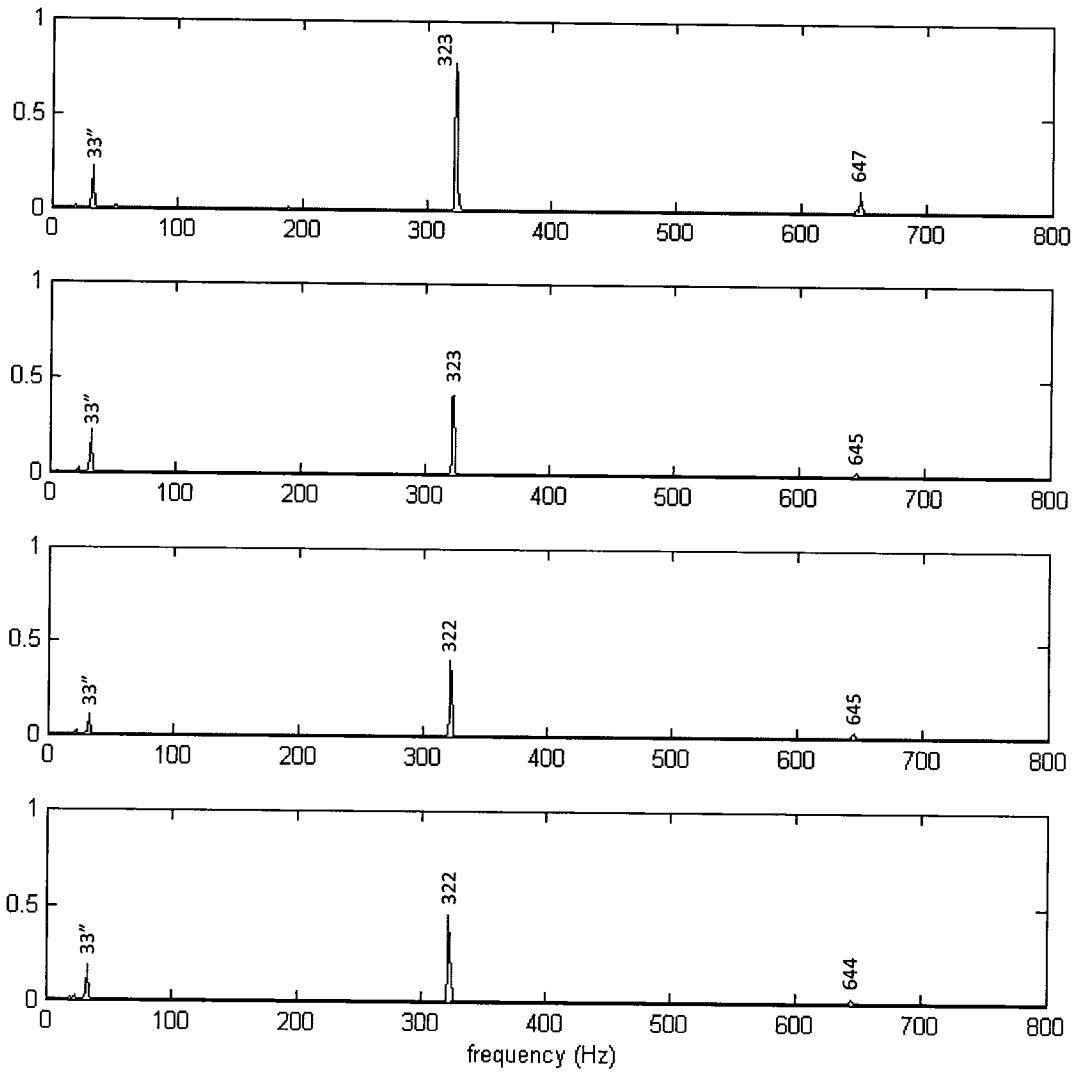

Fig. 6.8. FFT of dynamic force sensor signal from the analyzer for 0.33 mm string

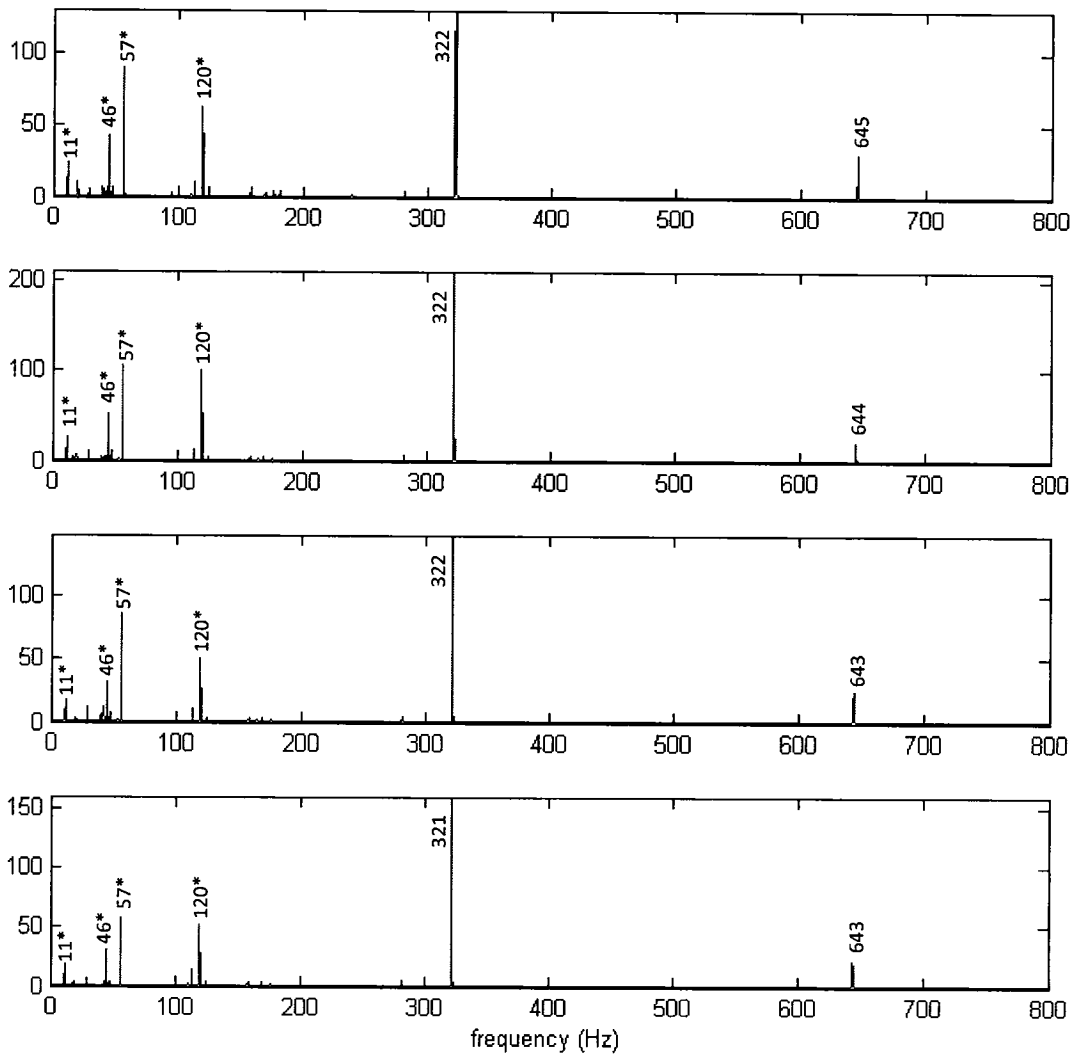

Fig. 6.9. FFT of sound clip recorded for 0.33 mm string

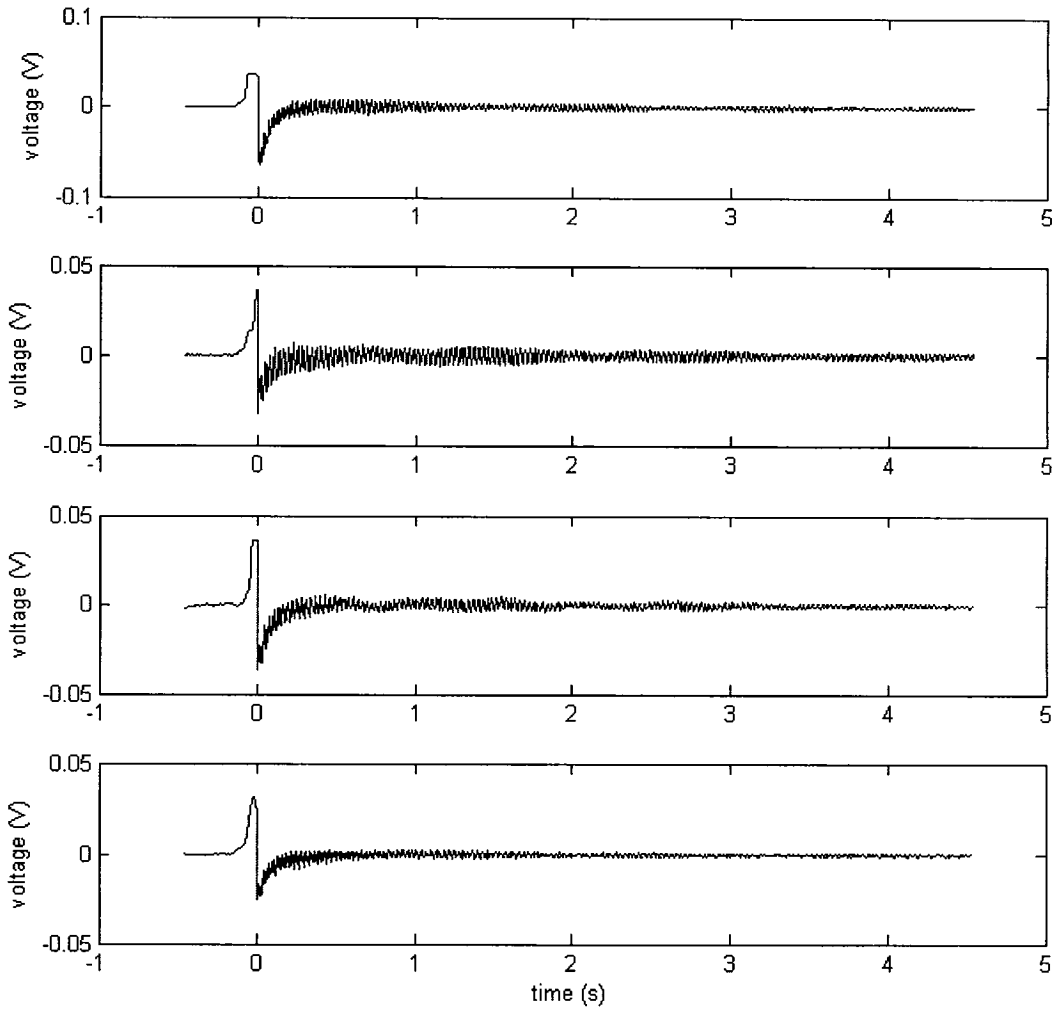

Fig. 6.10. Dynamic force sensor signal recorded by oscilloscope for 0.43 mm string

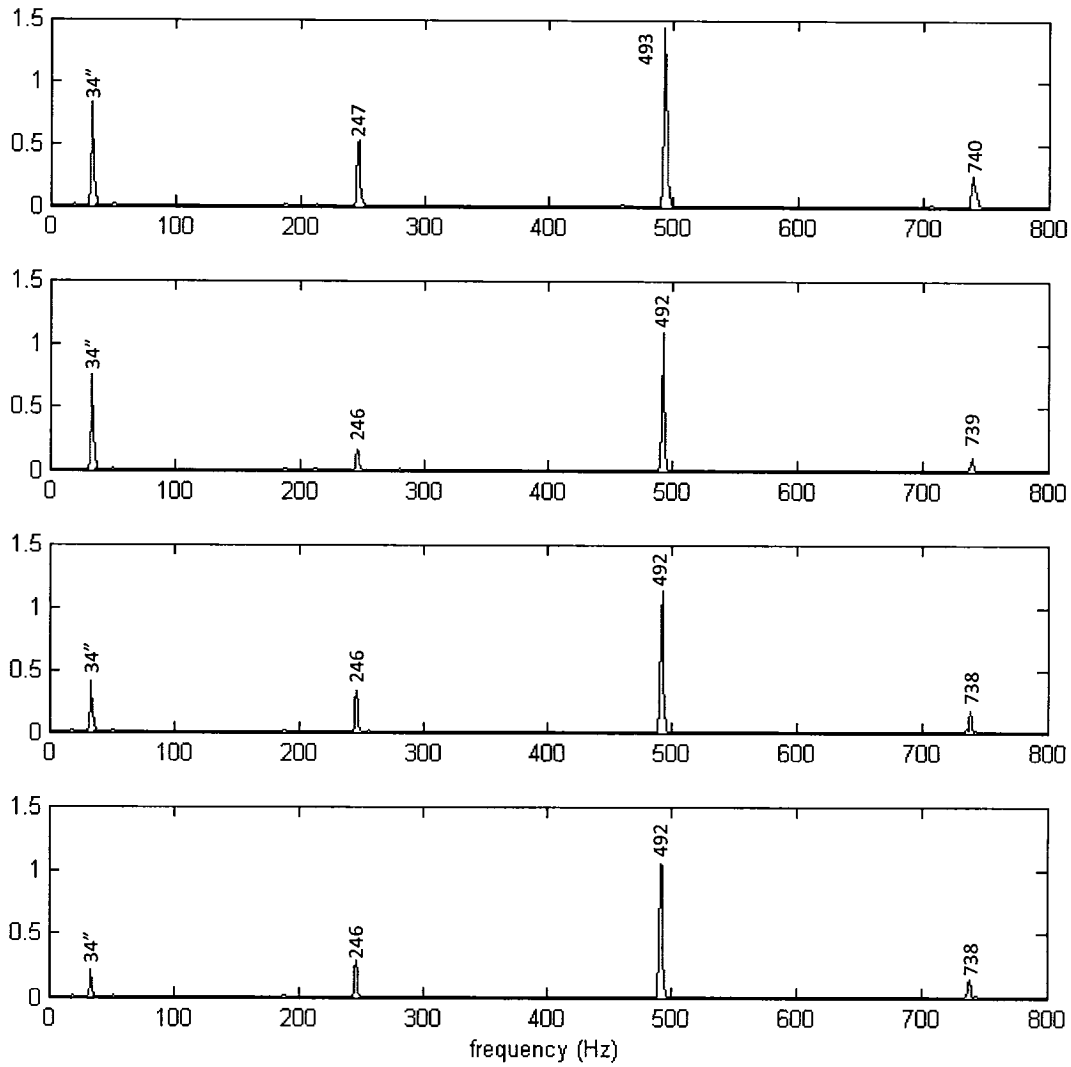

Fig. 6.11. FFT of dynamic force sensor signal from the analyzer for 0.43 mm string

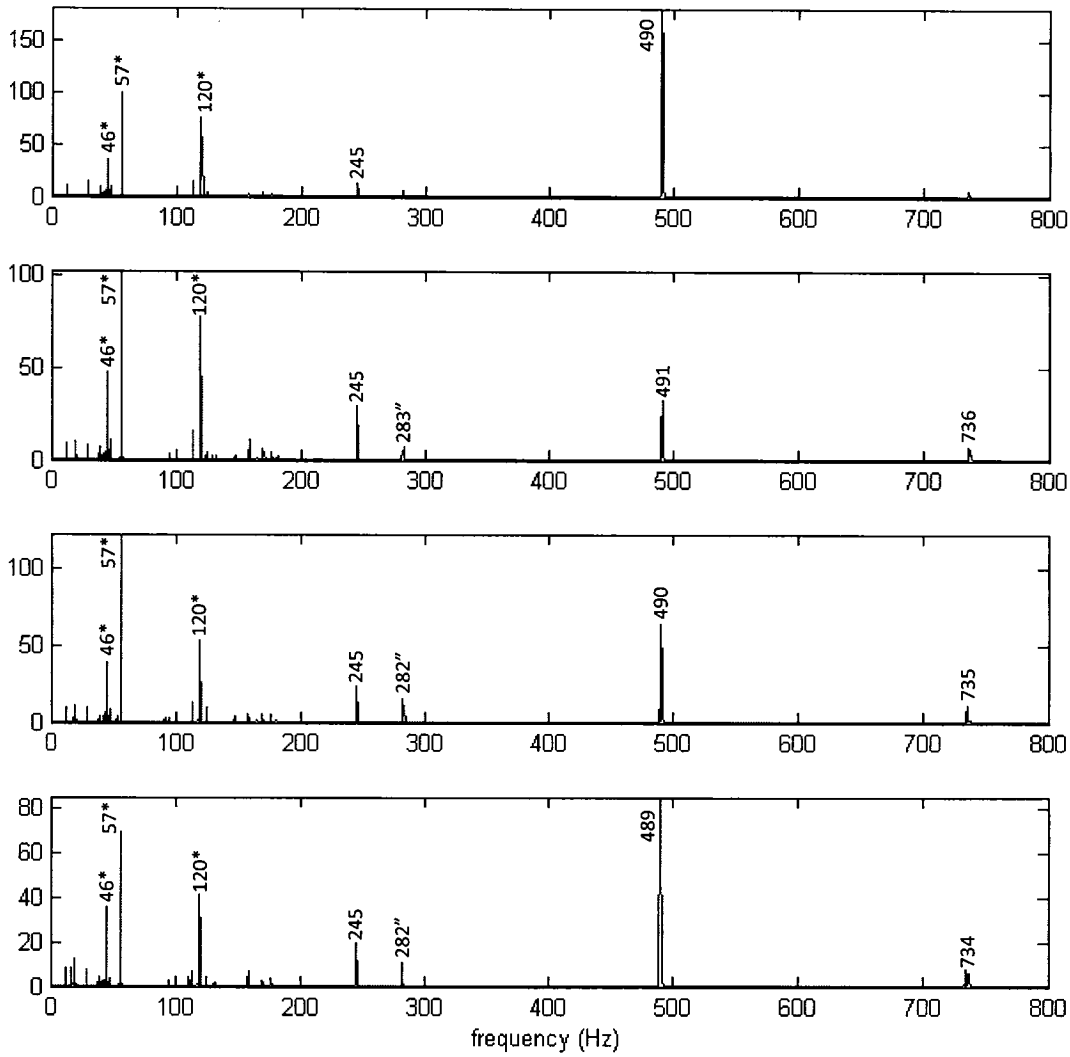

Fig. 6.12. FFT of sound clip recorded for 0.43 mm string

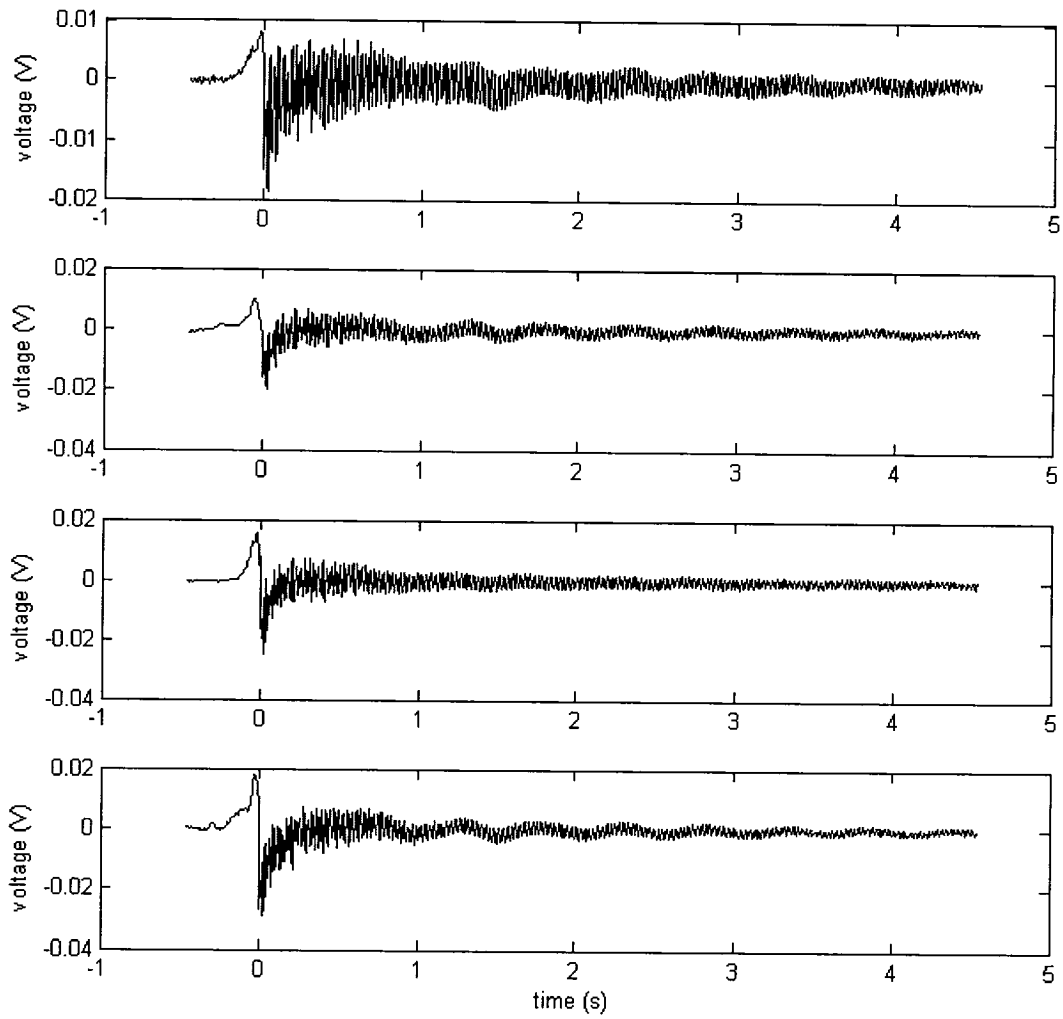

Fig. 6.13. Dynamic force sensor signal recorded by oscilloscope for 0.66 mm string

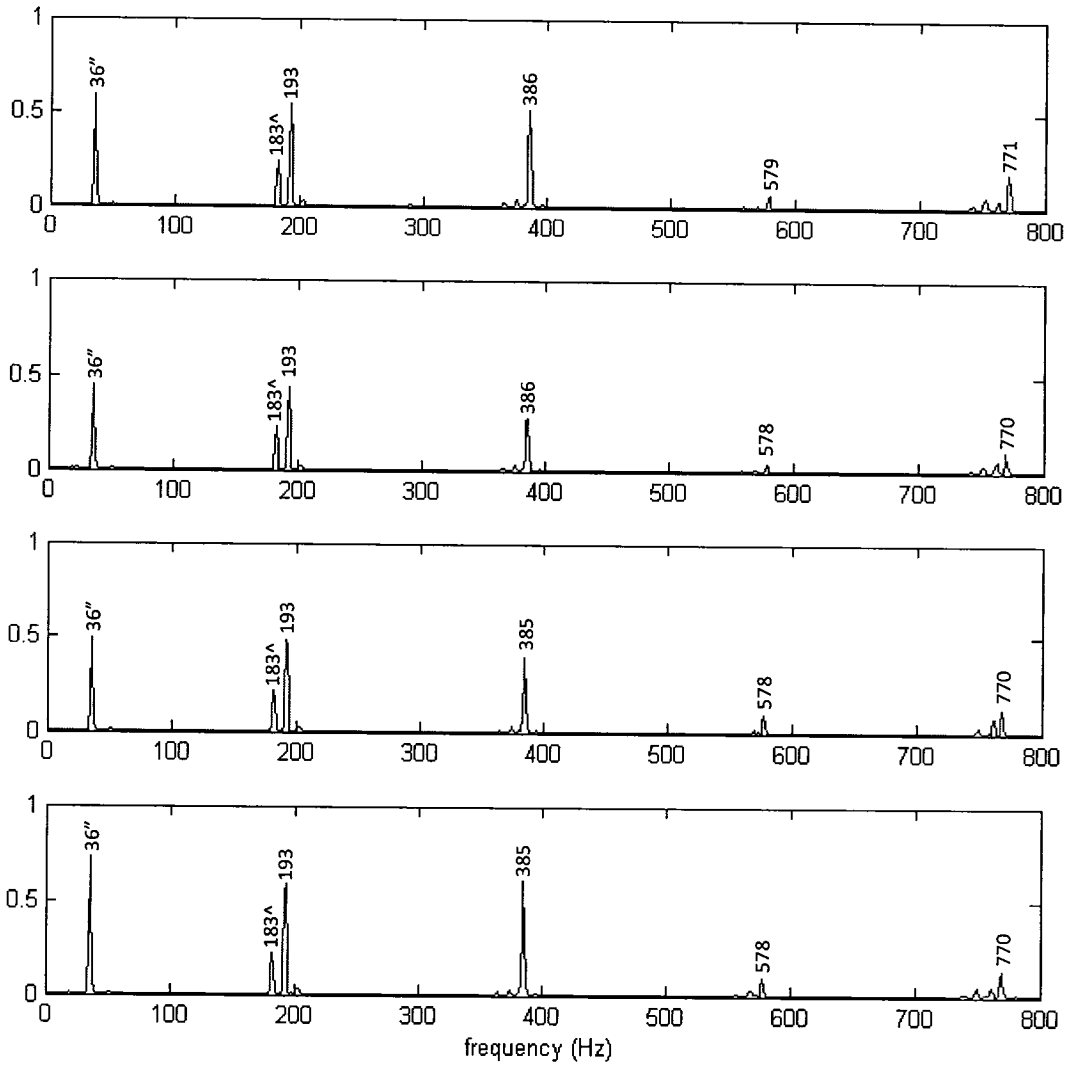

Fig. 6.14. FFT of dynamic force sensor signal from the analyzer for 0.66 mm string

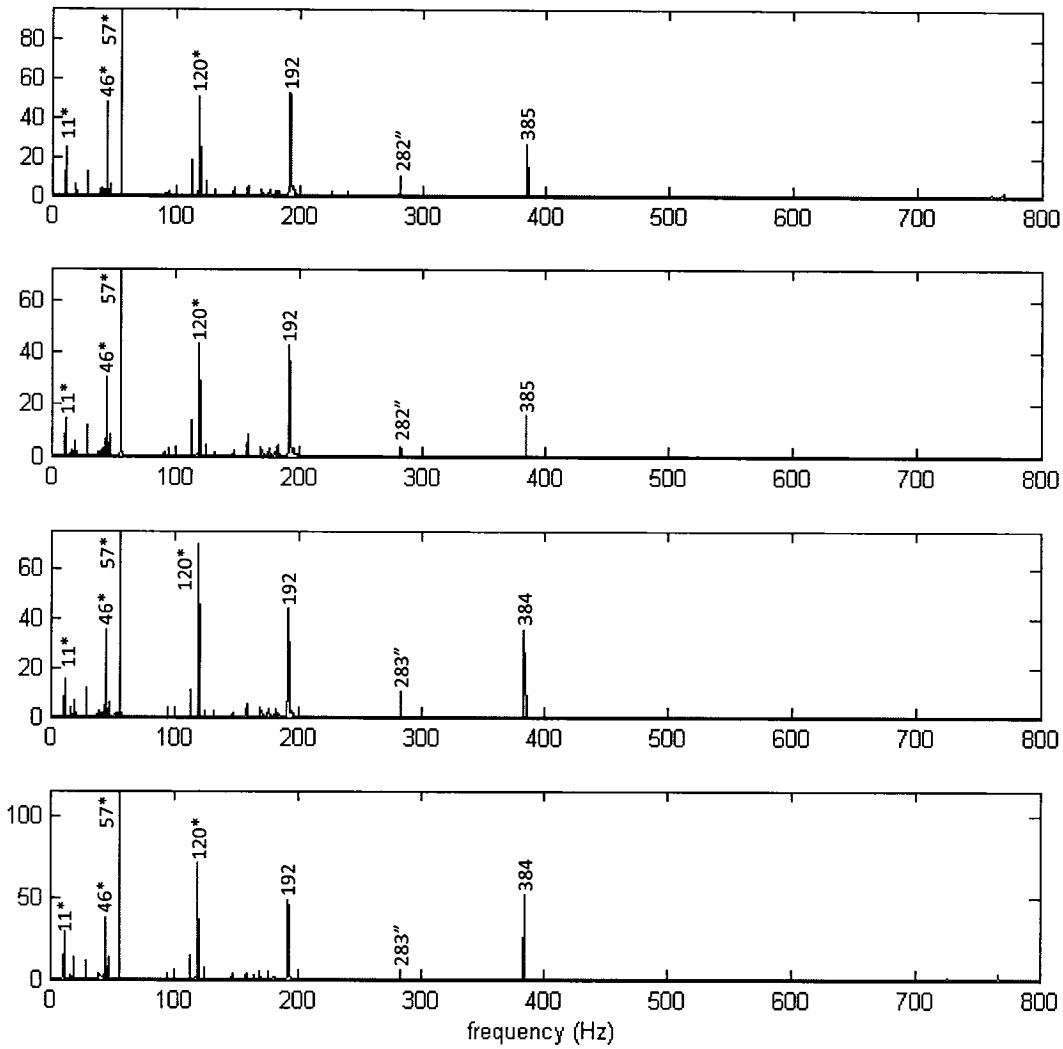

Fig. 6.15. FFT of sound clip recorded for 0.66 mm string

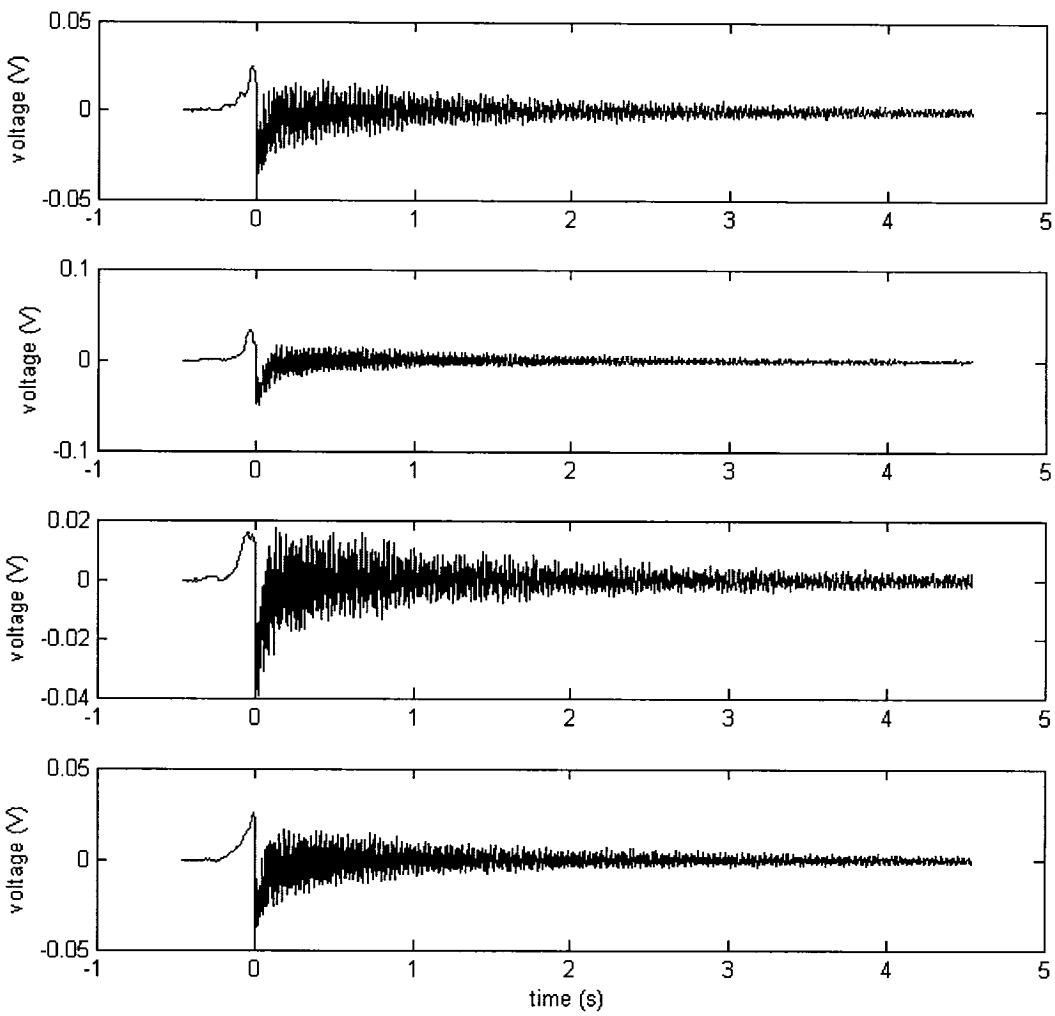

Fig. 6.16. Dynamic force sensor signal recorded by oscilloscope for 0.91 mm string

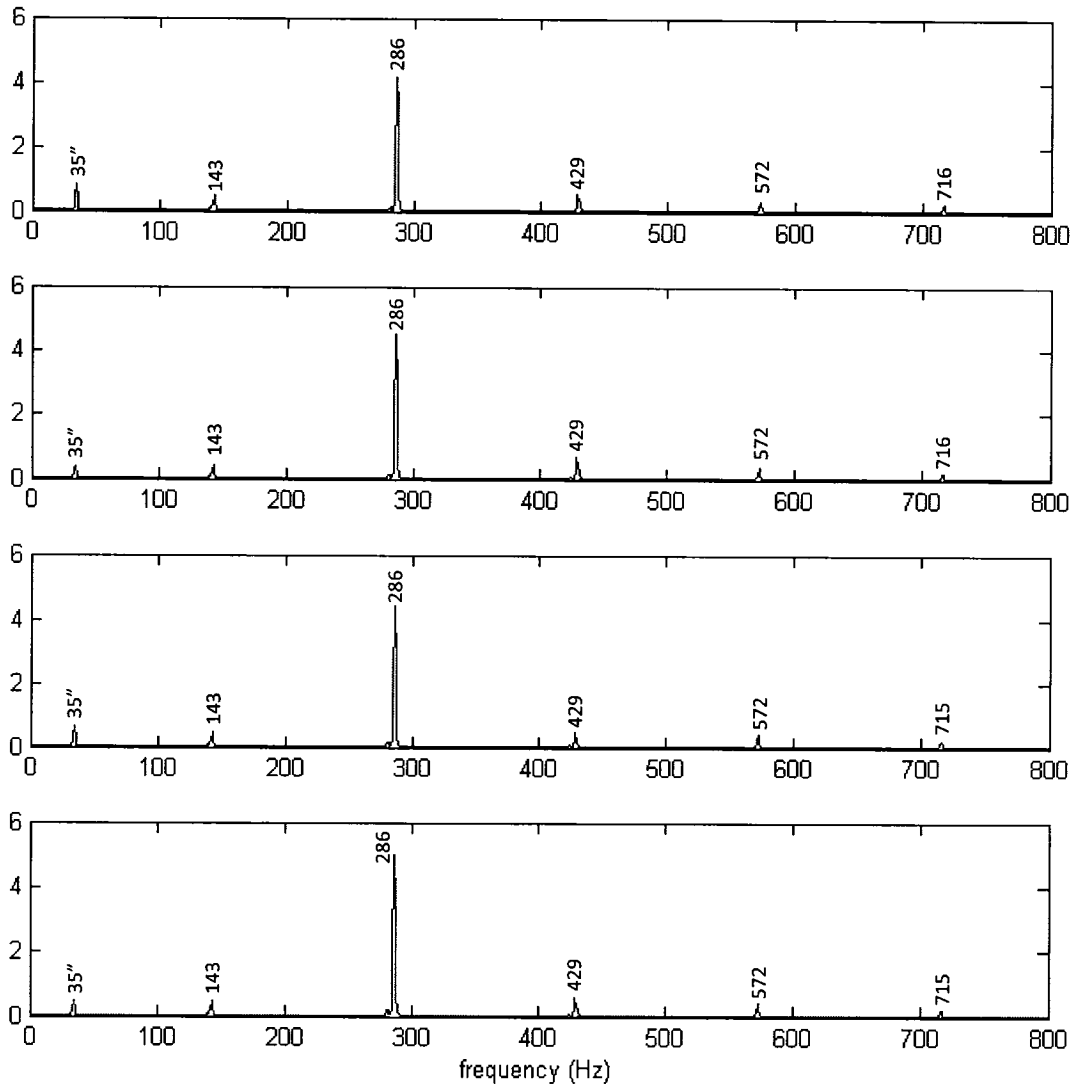

Fig. 6.17. FFT of dynamic force sensor signal from the analyzer for 0.91 mm string

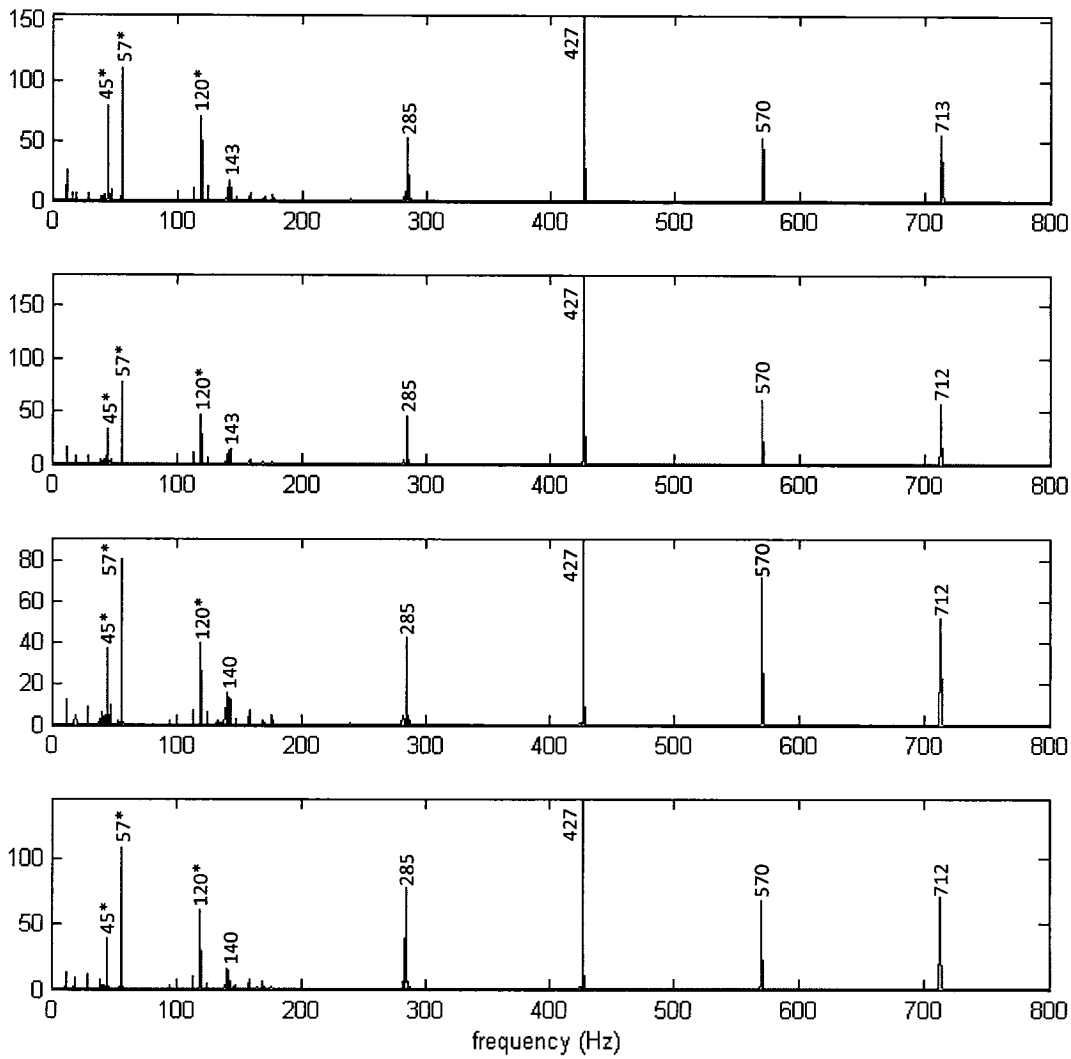

Fig. 6.18. FFT of sound clip recorded for 0.91 mm string

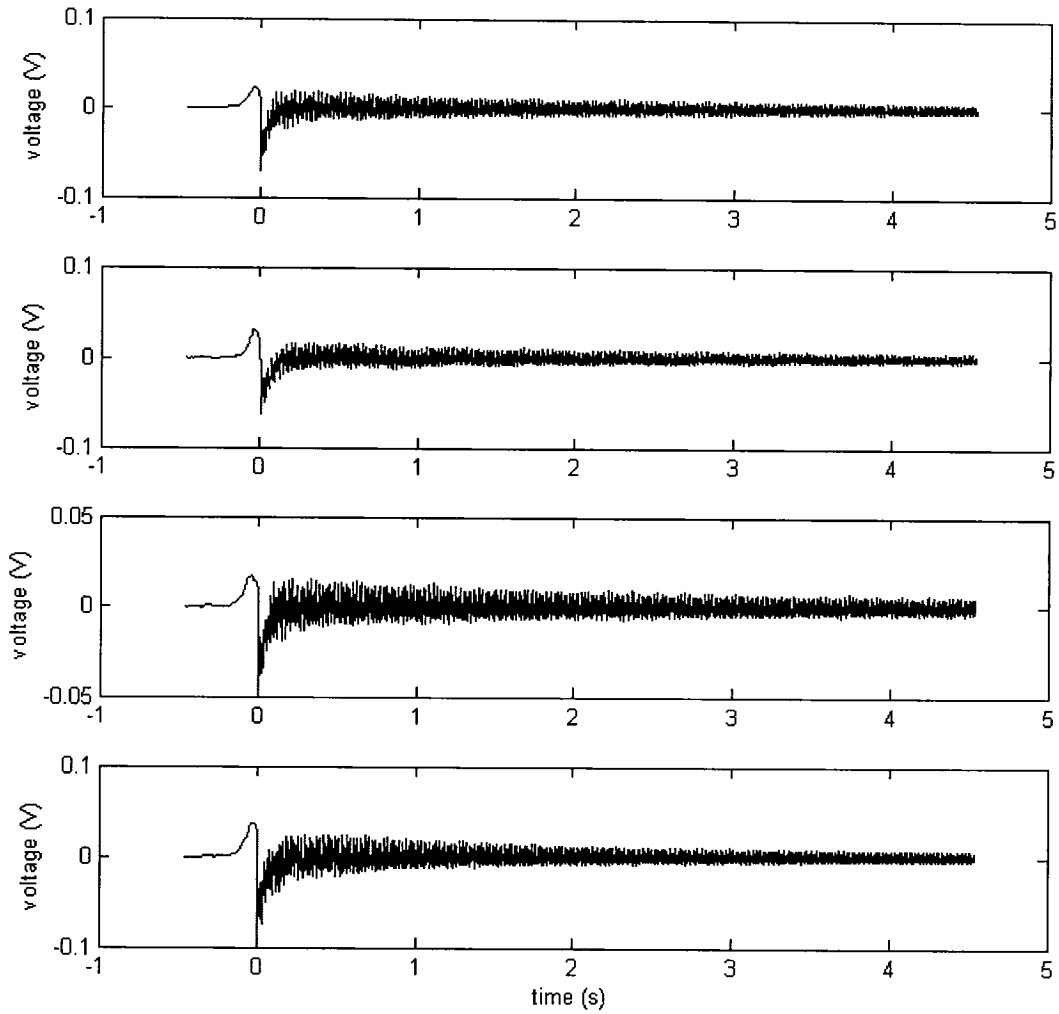

Fig. 6.19. Dynamic force sensor signal recorded by oscilloscope for 1.17 mm string

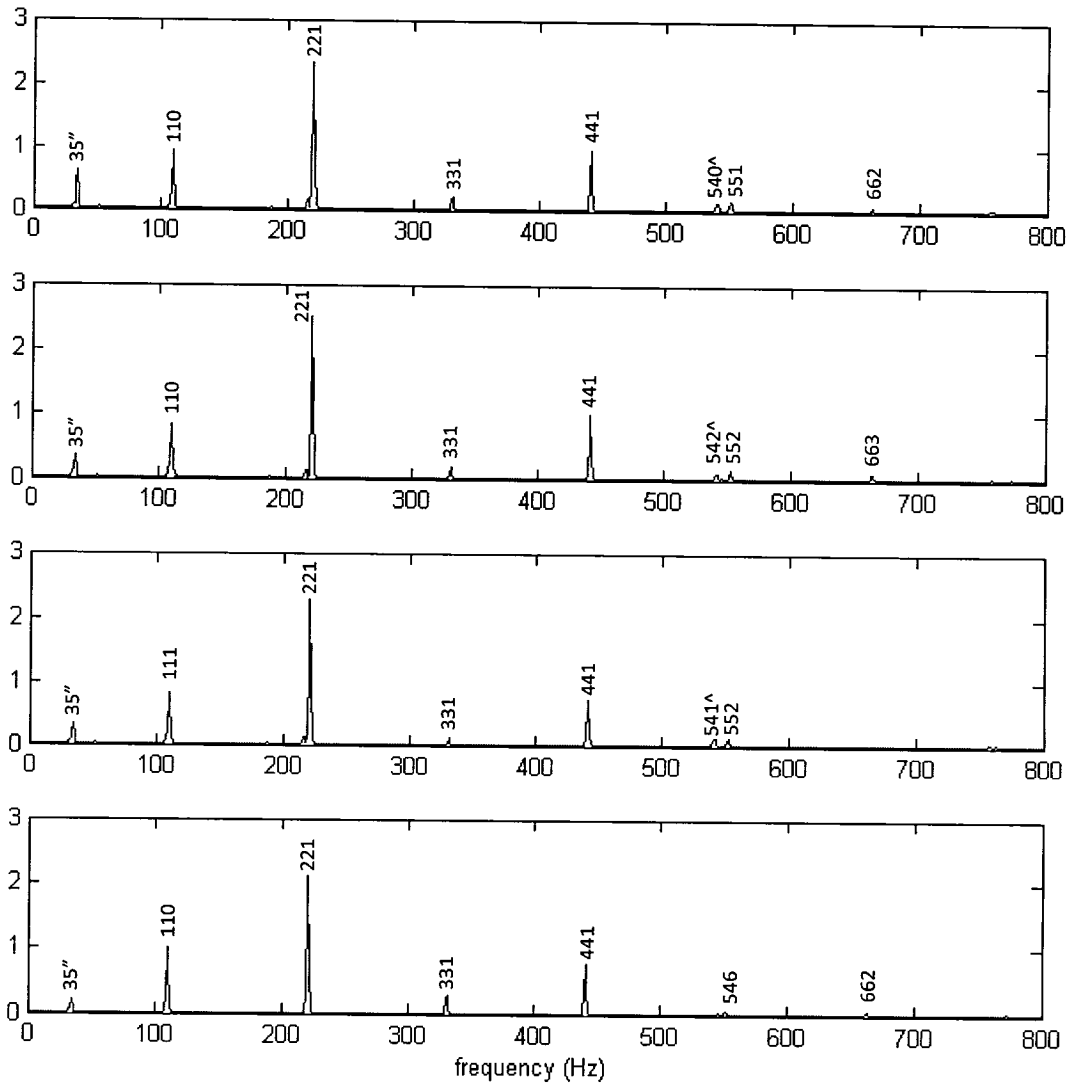

Fig. 6.20. FFT of dynamic force sensor signal from the analyzer for 1.17 mm string

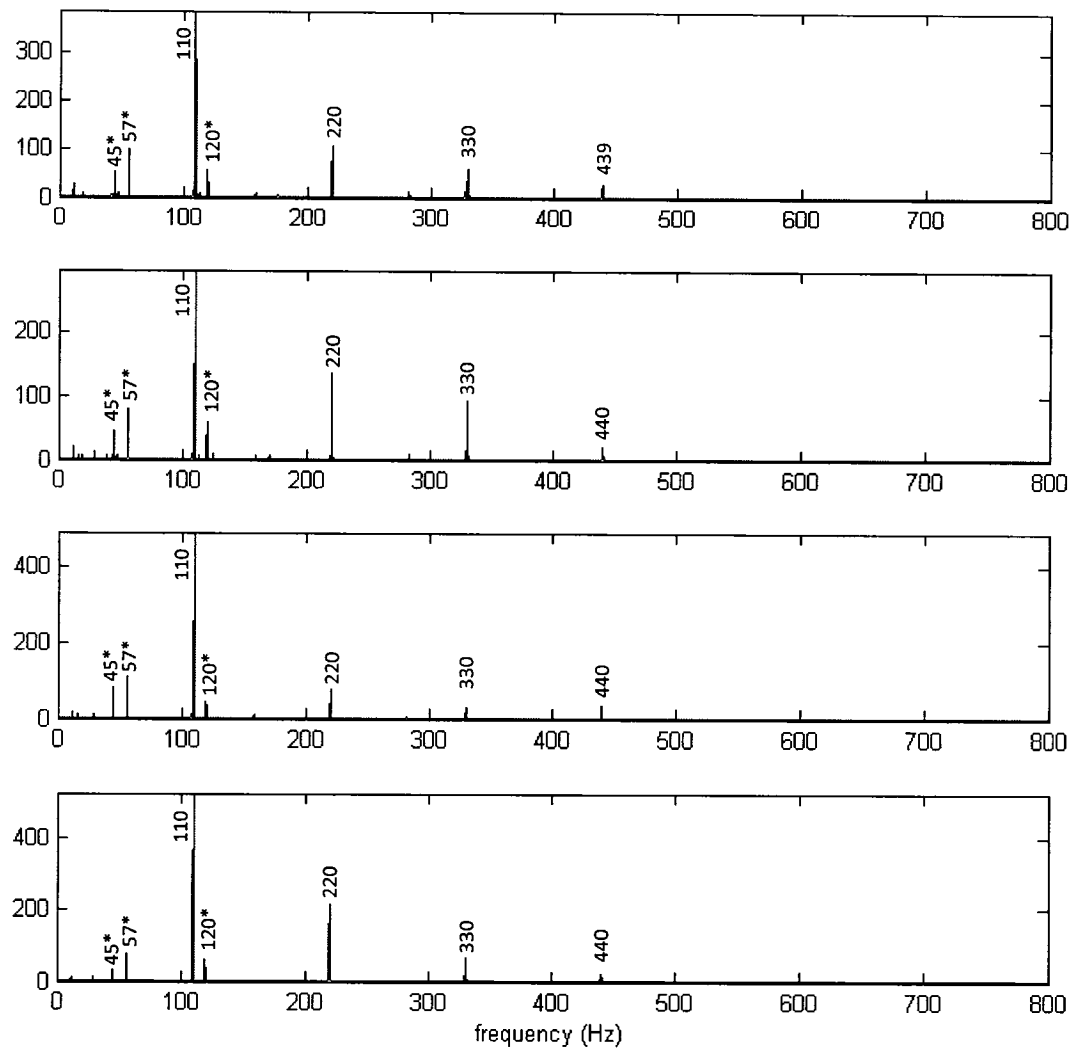

Fig. 6.21. FFT of sound clip recorded for 1.17 mm string

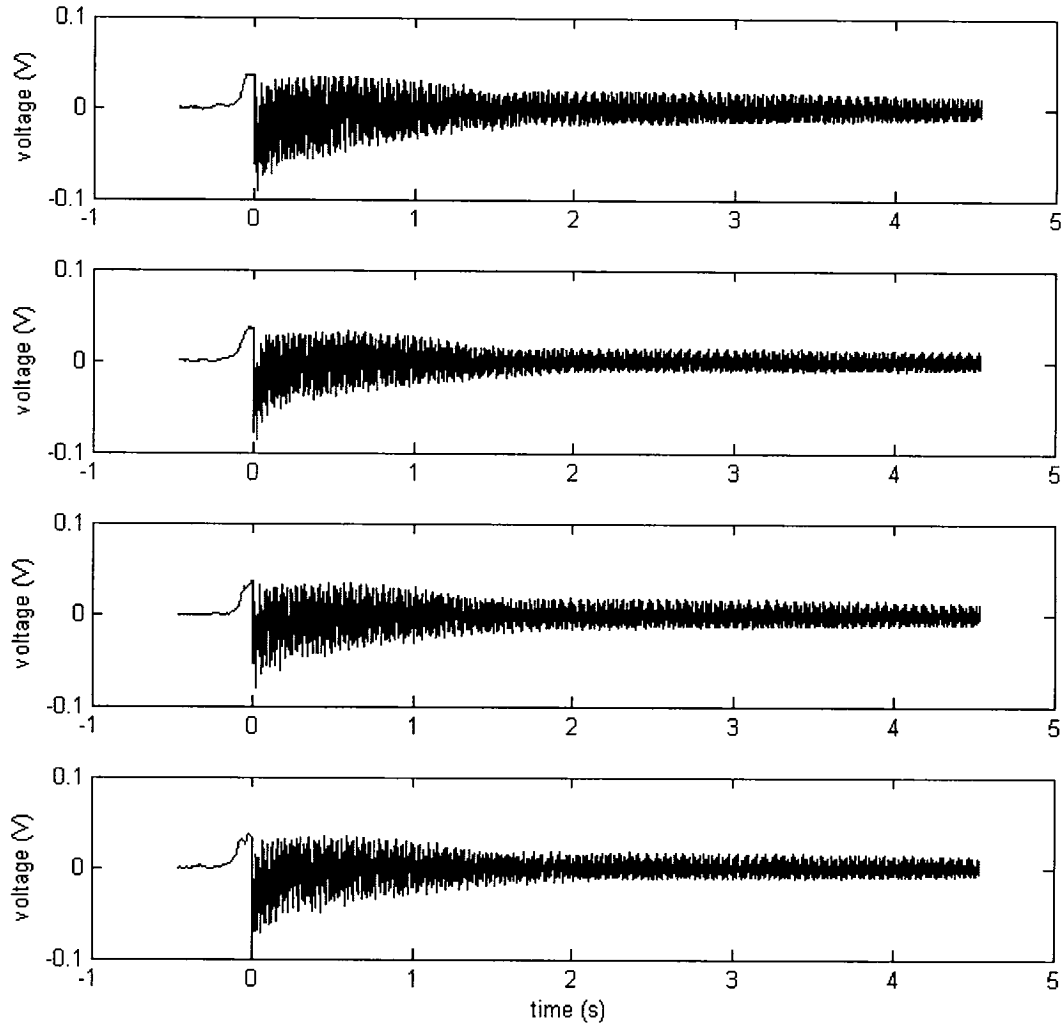

Fig. 6.22. Dynamic force sensor signal recorded by oscilloscope for 1.42 mm string

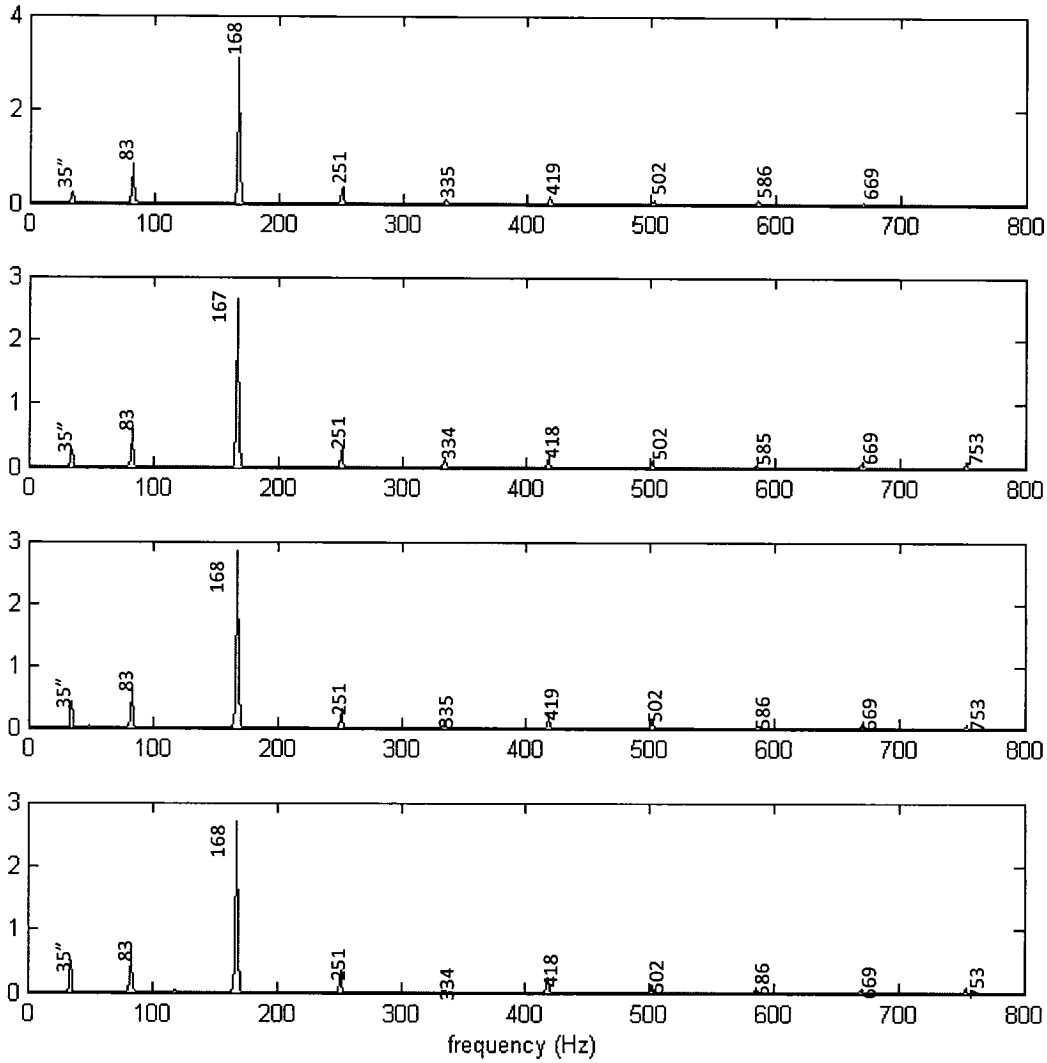

Fig. 6.23. FFT of dynamic force sensor signal from the analyzer for 1.42 mm string

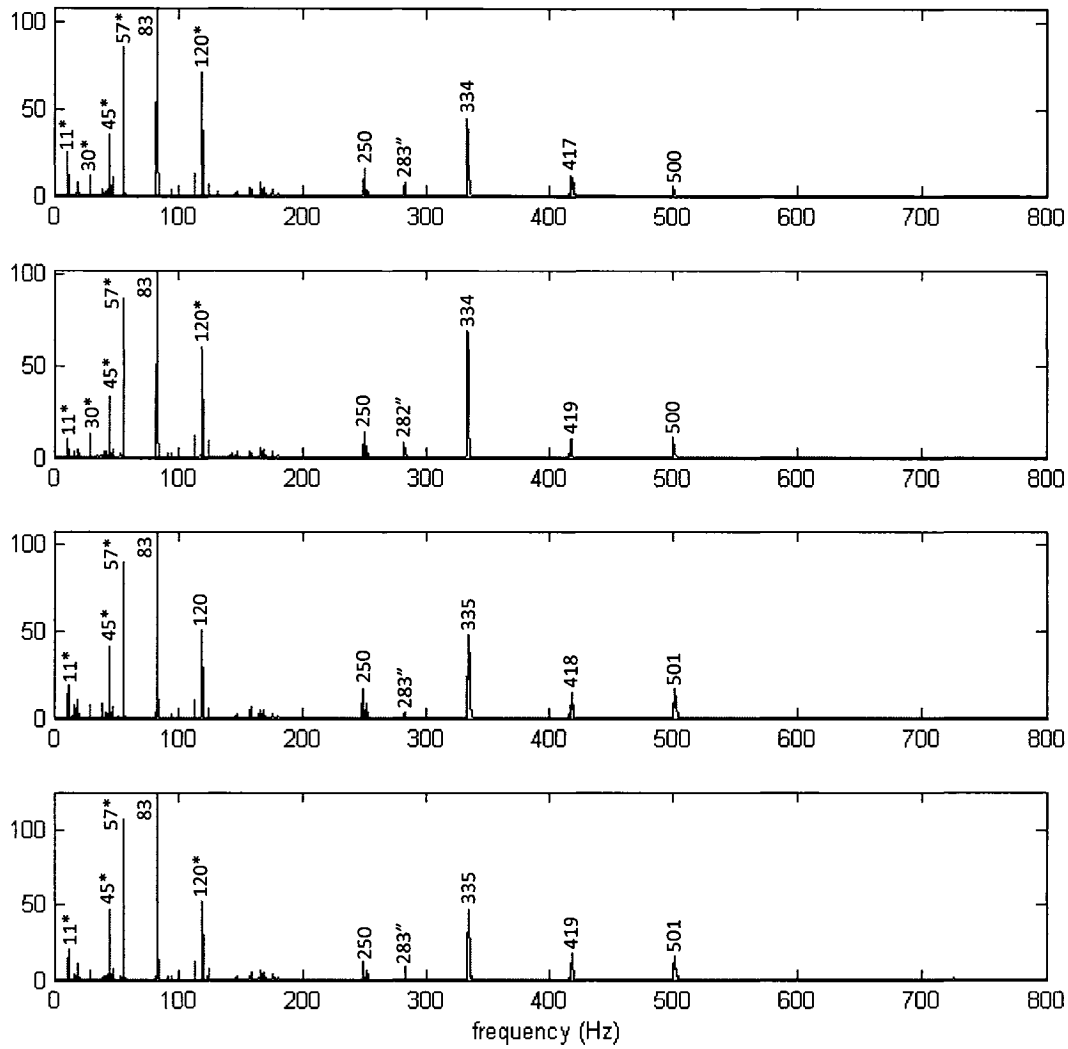

Fig. 6.24. FFT of sound clip recorded for 1.42 mm string

From the sound data obtained, it is clear that the air ventilation system of the laboratory is creating pulsations that interfere with the air displaced by the vibrating string. However, it is possible to identify the frequencies of this noise by performing a FFT on a sound sample of the room shown in Fig. 6.25. The values of those frequencies are shown with a asterisk (*). In addition, there is a frequency that appears at around 35 Hz in all spectrums of dynamic force sensor, and another at around 285 Hz for pressure sensors (microphone and webcam). Since they remain unchanged for all strings, they are considered to be noises from unknown sources, and thus are neglected. Both frequencies are marked with a double apostrophe (") in all spectrums.

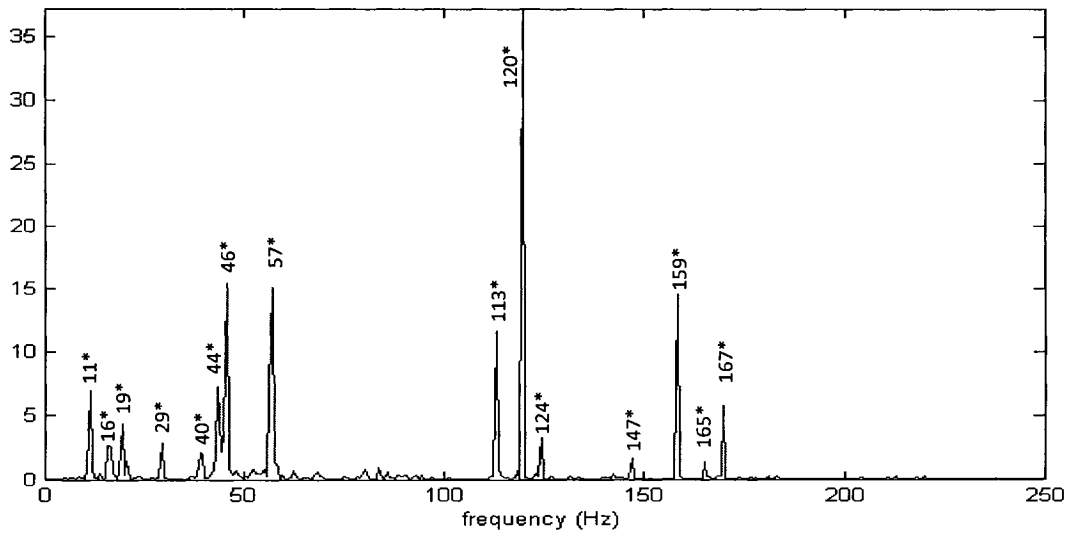

Fig. 6.25. FFT of sound clip recorded for room noise

In order to proceed further in the investigation, sound samples have been recorded from a Yamaha acoustic guitar to obtain the frequency spectrum for each string as shown below in Fig. 6.26.

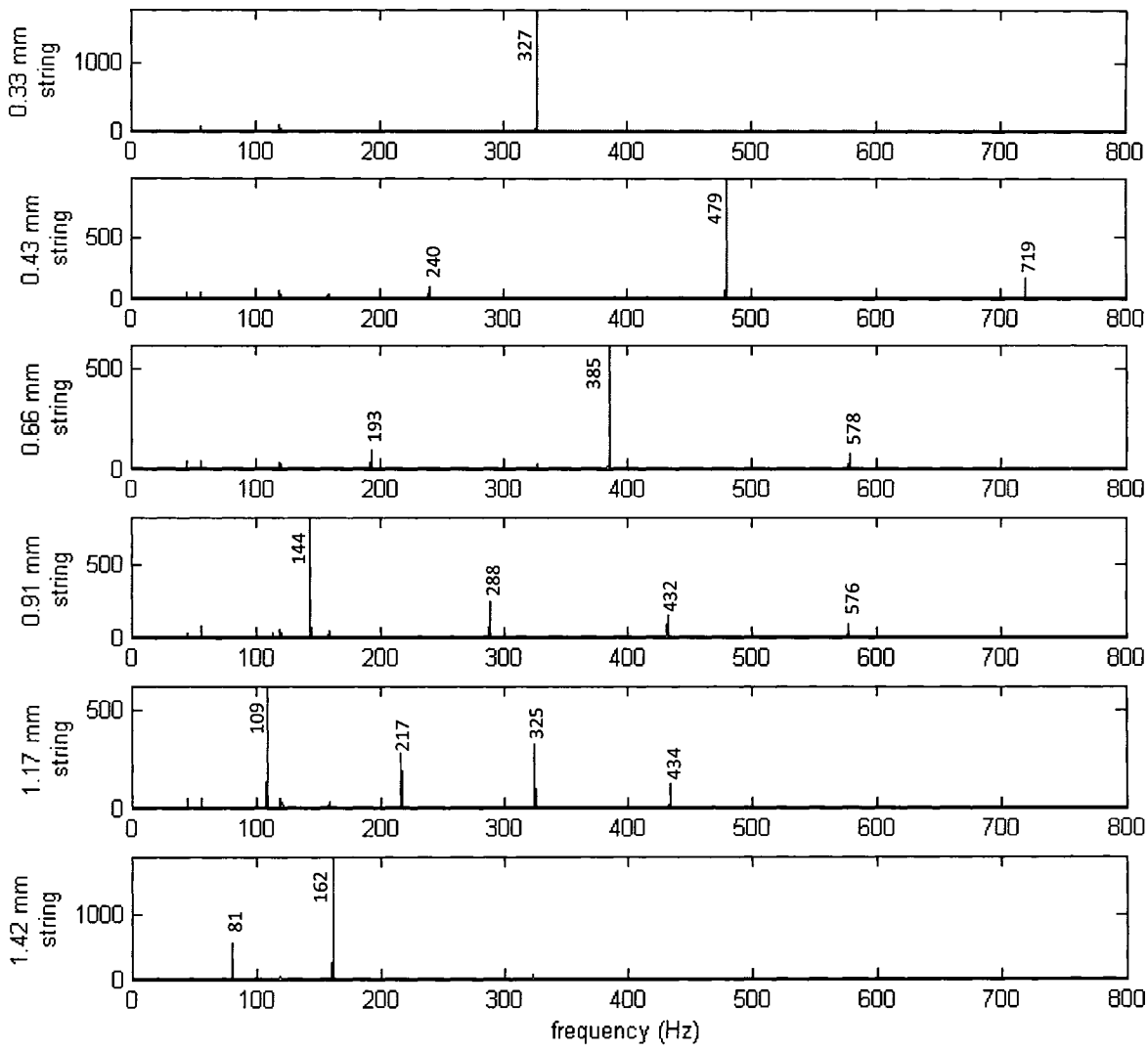

Fig. 6.26. FFT of sounds recorded for each string from a Yamaha guitar

6.3 Data Analyses

From the data presented previously, several observations have been made. First, after neglecting the noises, there are two unknown frequencies marked by the caret sign

(^). In Figs. 6.14, spectrums generated by the analyzer from force sensor have shown a suspicious frequency at around 182 Hz. The partial of this frequency later appears in Fig. 6.20, the spectrum from force sensor, at around 542 Hz. Since in all those graphs, they all appear close to an existing forcing frequency, it looks like they are the natural frequencies of the experiment setup. As mentioned earlier in beat phenomenon, when a vibration near a system's natural frequency is induced, the system will end up vibrating at its own natural frequency.

Table 6.6. Frequencies table

String gauge (mm)	Desired	Tuned	Calculated* Transverse	Calculated* Axial
	Frequency (Hz)			
0.33	329.63	322	323	739
0.43	246.94	246	246	772
0.66	196.00	194	194	470
0.91	146.83	143	143	380
1.17	110.00	110	110	319
1.42	82.41	83	83	279

*Calculated values are from tension used to tune the string rather than the desired tension

From FFT of sound clips recorded by webcam (Figs. 6.9, 6.12, 6.15, 6.18, 6.21 and 6.24), partials have been compared to the fundamentals to verify inharmonicity in each string. From Table 6.7, inharmonicity is observed in two of the four wind strings while in unwind strings, partials are perfectly harmonic. Also, it is observed that the amplitude decreases quickly for higher partials, therefore they will have negligible effect on the string behavior.

Table 6.7. Inharmonicity table

String gauge (mm)	f_0 (Hz)	f_1 / f_0	f_2 / f_0	f_3 / f_0
0.33	322	2.000	N/A	N/A
0.43	245	2.000	3.000	N/A
0.66	192	2.000	N/A	N/A
0.91	141	2.021	3.033	4.043
1.17	110	2.000	3.000	4.000
1.42	83	2.012	3.024	4.036

N/A : Not available

The biggest surprise from experiment data is probably the missing of phantom partials caused by axial vibration. From FFT of dynamic force sensors (Figs. 6.8, 6.11, 6.14, 6.17, 6.20 and 6.23), there is no sign of any phantom frequency. Even from the Yamaha guitar's frequency spectrums (Fig. 6.26), phantom frequencies are not visible. However, the axial motion measured from the dynamic force sensor (Figs. 6.7, 6.10, 6.13, 6.16, 6.19 and 6.22) does show the presence of beat phenomenon as indicated in the simulation, even in strings with harmonic partials (see Table 6.7). For bare string the longer beats are more visible while for wound strings, the smaller beats are more noticeable. Since beating occurs in with harmonic partials, the presence of axial vibration due to tension modulation can be confirmed.

Finally, the orbital motion is observed with the video recorded under stroboscope. The pictures below are made of frames taken from the video putting on top of another with transparency to show the top-bottom and right-left motions. However, from the observation, the orbital motion does not start until the amplitude of oscillation become large enough and it takes more an elliptical form than circular as the amplitude

perpendicular to the plane of motion is much smaller than the one acting on the excited direction as shown in Fig. 6.33.

Fig. 6.27. Top and bottom (left), and right and left (right) string motions

6.4 Summary

In this chapter, the coupled motion of axial and transverse vibrations from a fixed-fixed string with supported points is verified with an actual experimental testing. A set of guitar strings is used and it is merely a test bench to other type of strings and cables. From the data recorded, the presence of phantom partials due to axial-transverse coupling can not be noticed. This maybe due to the amplitude of axial vibration being too small compared to transverse motion to be picked up by the sensors. In guitar strings, partials become negligible after first few. The beat phenomenon and the orbital motion are observed in the axial vibration.

Chapter 7

Conclusions

This chapter finalizes the current thesis by starting with a brief summary of the major investigations covered. It is then followed by conclusions drawn from observation obtained throughout the study. Finally, recommendations of future research topics are suggested.

7.1 Summary

Being a fundamental system in vibration studies, the string is still a topic that can go very deep. In this thesis, the frequency studies start with the investigation of various aspects of beat phenomenon. Mathematical models of various string vibrations are investigated to test the effect of different boundary conditions. Two case studies have been proposed on a fixed-partially fixed string and a fixed-fixed string with two supported points. Since the simulation of analytical model is done with finite difference, this numerical method is briefly discussed along with the important von Neumann and

Courant stability criteria. Both cases have been tested with computer model to obtain the respective string motions. For the fixed-partially fixed string, extensive studies and simulation have been done on the effect of the stiffness on the string natural frequency and the inharmonicity introduced due to the nonhomogeneous boundary conditions. In the second case, 3D axial-transverse coupled motion is modeled as well as its orbits. An experiment has been setup to collect data from vibrating guitar strings fixed at both ends with two supporting points. The use of guitar strings is merely convenient, and easy to tune to its known natural frequency. In the testing, the data analyzer was used to obtain directly the frequency spectrum while the oscilloscope recorded the behavior of string in the time domain from the dynamic force sensor and the microphone. In addition, sound sample was also captured by webcam to be further analyzed on the computer to perform FFT. Finally, the orbital motion of vibrating string was validated with a stroboscope.

7.2 Conclusions

After studying the effect of boundary conditioning and beat phenomenon, the following conclusions are drawn from the present analysis:

1. In the boundary conditioning problem, the inharmonicity is found in the partially fixed string from analytical results. The degree of inharmonicity is defined by string length, tension applied and stiffness of the partially fixed end. General speaking, inharmonicity is more pronounced in shorter strings than longer ones. Also at low stiffness, partials are close to odd multiple of fundamental frequency.

2. For the 3D coupled string, the axial motion is exposed to influences from transverse motions. However, for stiff metallic strings, the motion of axial vibration is not influencing the behavior of lateral motions. Under the influence of lateral motion, the simulation results of axial vibration clearly showed signs of beat phenomenon. For the fixed-fixed string with two supporting points limiting the string section where the lateral motion occurs, the variation of effective string length for each mode of vibration was only affecting their respective natural frequencies. In addition, since axial vibration is influenced by lateral motion, any variation of supporting limiting the lateral vibration will in turn affect the axial motion.
3. From beat phenomenon analysis, the vibration formed by fundamental and inharmonic partials gives different beating mechanisms with each additional partial. Any addition of inharmonic partial, odd multiple or not, will ultimately lead to beat phenomenon in the inner and denser section of the signal.
4. From the experimental data, the frequencies from axial motion were not detected in the recorded results. Also, it is quite unexpected that the partials became negligible after 800 Hz. Slight inharmonicity was observed, especially in wound strings, but due to the lack of higher partials, the inharmonicity pattern was not clear. From the dynamic force sensor data, the axial motion of the string was shown with slight beating. Finally, the orbital motion was observed, but further studies are required to explain the mechanism behind that forces the string to vibrate in circular fashion.

7.3 Recommendations for Future Investigations

Considering the weaknesses and potential further investigations of current research, several recommendations for future studies are suggested.

1. The simple assumption of 90 degree phased shift between the two transverse motions is not enough. Further studies of string stability, nonlinearity and bifurcation are required to further explore the case of pure string vibration.
2. Other boundary conditions need to be explored. In actual life, most of the string and cable systems are operated within boundaries of round edges like in the pulley system and fiber wounding mechanism. Also, moving and accelerating strings need to be investigated to further extend the current studies to main engineering applications of cable and conveyor systems.
3. The simulation of fixed-partially fixed string required validation from actual experiments.
4. Different type of string winding and cable strand and their effect on boundaries can be carried out.

References

[1] B. Bank, "Physics-based sound synthesis of string instruments including geometric nonlinearities", Ph. D. thesis, Department of Measurement and Information Systems, Budapest University of Technology and Economics, Budapest, Hungary, 2006.

[2] B. Bank, and L. Sujbert, "Efficient modeling strategies for the geometric nonlinearities of musical instrument strings", Proceedings of the Forum Acusticum, Budapest, Hungary, August 29th – September 2nd , 2005.

[3] B. Bank, and L. Sujbert, "Generation of longitudinal vibrations in piano strings: from physics to sound synthesis", Journal of the Acoustical Society of America, Vol. 117, Issue 4, 2005, pp. 2268-2278.

[4] B. Bank, and L. Sujbert, "Modeling the longitudinal vibration of piano strings", Proceedings of the Stockholm Music Acoustics Conference, Stockholm, Sweden, August 6th – 9th, 2003, pp. 143-146.

[5] B. Bank, and L. Sujbert, "A piano model including longitudinal string vibrations", Proceedings of the 7th International Conference on Digital Audio Effects, Naples, Italy, October 5th – 8th, 2004, pp. 89-94.

[6] C. N. Bapat, "An approximate approach to study the free vibration of a string with an arbitrary variation in mass density and tension, with attached concentrated masses, and its application to hanging chain and rotating cord", Journal of Sound and Vibration, Vol. 290, Issue 1-2, 2006, pp. 529-537.

[7] E. Bavu, J. Smith, and J. Wolfe, "Torsional waves in a bowed string", Acustica, Issue 91, 2005, pp. 241-246.

[8] E. Bécache, A. Chaigne, G. Derveaux, and P. Joly, "Numerical simulation of a guitar", Computer and Structures, Vol. 83, 2005, pp. 107-126.

[9] J. Bensa, and L. Daudet, "Efficient modeling of 'phantom' partials in piano tones", Proceedings of the International Symposium on Musical Acoustics, Nara, Japan, March 31st – April 3rd, 2004, pp. 207-210.

[10] R. B. Bhat, and G. J. Gouw, "Numerical methods in engineering", Second Edition, Simon & Schuster Custom Publishing, Needham Heights, Massachusetts, 1996.

[11] R. B. Bhat, G. D. Xistris, and T. S. Sankar, "Dynamic behavior of a moving belt supported on elastic foundation", Journal of Mechanical Design, Vol. 104, 1982, pp. 143-147.

[12] F. Bleich, "Dynamic instability of truss-stiffened suspension bridges under wind action", Transactions of American Society of Civil Engineering, Paper No. 2385, 1948, pp. 1177-1222.

[13] J. E. Bolwell, "The flexible string's neglected term", Journal of Sound and Vibration", Vol. 206, Issue 4, 1997, pp. 618-623.

[14] H. R. Bosch, "Aerodynamic stability of a truss-stiffened cable-stayed bridge", Journal of Wind Engineering and Industrial Aerodynamics, Vol. 36, 1990, pp. 1331-1340.

[15] D. Q. Cao, R. W. Tucker, and C. Wang, "A stochastic approach to cable dynamics with moving rivulets", Journal of Sound and Vibration, Vol. 268, Issue 2, 2003, pp. 291-304.

[16] L. Caracoglia, and N. P. Jones, "In-plane dynamic behavior of cable networks. Part 1: formulation and basic solutions", Journal of Sound and Vibration, Vol. 279, Issue 3-5, 2005, pp. 969-991.

[17] L. Caracoglia, and N. P. Jones, "In-plane dynamic behavior of cable networks. Part 2: prototype prediction and validation", Journal of Sound and Vibration, Vol. 279, Issue 3-5, 2005, pp. 993-1014.

[18] Caswita, and A. H. P. van Der Burgh, "Combined parametrical transverse and in-plane harmonic response of an inclined stretched string", Journal of Sound and Vibration, Vol. 267, Issue 4, 2003, pp. 913-931.

[19] T. K. Caughey, "Large amplitude whirling of an elastic string – a nonlinear eigenvalue problem", Journal of Applied Mathematics, Vol. 18, Issue 1, 1970, pp. 210-237.

[20] L. Q. Chen, N. H. Zhang, and J. W. Zu, "Bifurcation and chaos of an axially moving viscoelastic string", Mechanics Research Communications, Vol. 29, 2002, pp. 81-90.

[21] L. Q. Chen, N. H. Zhang, and J. W. Zu, "The regular and chaotic vibrations of an axially moving viscoelastic string based on fourth order Galerkin truncation", Journal of Sound and Vibration, Vol. 261, Issue 4, 2003, pp. 764-773.

[22] L. Q. Chen, W. J. Zhao, and J. W. Zu, "Transient responses of an axially accelerating viscoelastic string constituted by a fractional differentiation law", Journal of Sound and Vibration, Vol. 278, Issue 4-5, 2004, pp. 861-871.

[23] C. G. Chien, R. F. Fung, and C. L. Tsai, "Non-linear vibration analysis of the coupled textile/rotor system by finite element method", Journal of Sound and Vibration, Vol. 221, Issue 1, 1999, pp. 67-84.

[24] H. A. Conklin, "Generation of partials due to nonlinear mixing in stringed instruments", Journal of the Acoustical Society of America, Vol. 105, Issue 1 1999, pp. 536-545.

[25] S. H. Crandall, and G. Pariseanu, "Limit-cycle vibrations of a rolling cylinder", Journal of Non-Linear Mechanics, Vol. 20, Issue 5/6, 1985, pp. 385-393.

[26] L. J. Cveticanin, " The oscillations of a textile machine rotor on which the textile is wound up", Mechanical Machine Theory, Vol. 26, Issue 3, 1991, pp. 253-260.

[27] L. J. Cveticanin, "The vibration of a textile machine rotor with nonlinear characteristics", Mechanism and Machine Theory, Vol. 21, Issue 1, 1986, pp. 29-32.

[28] J. P. den Hartog, "Transmission lines vibrations due to sleet", Transaction of the American Institute of Electrical Engineers", Vol. 51, 1932, pp. 1074-1077.

[29] J. A. Elliott, "Intrinsic nonlinear effects in vibrating strings", American Journal of Physics, Vol. 48, Issue 6, 1980, pp. 478-480.

[30] J. A. Elliott, "Nonlinear resonance in vibrating strings", American Journal of Physics, Vol. 50, Issue 12, 1982, pp. 1148-1150.

[31] C. Erkut, and M. Karjalainen, "Virtual strings based on a 1D FDTD waveguide model: stability, losses, and traveling waves", Proceedings of the Audio Engineering Society 22nd International Conference on Virtual, Synthetic and Entertainment Audio, Espoo, Finland, June 15th-17th, 2002, pp. 317-323.

[32] Z. C. Feng, "Does non-linear intermodal coupling occur in a vibrating stretched string?", Journal of Sound and Vibration, Vol. 182, Issue 5, 1995, pp. 809-812.

[33] H. Flectcher, E. D. Blackham, and R. Stratton, "Quality of piano tones", Journal of the Acoustical Society of America, Vol. 34, Issue 6, 1962, pp. 749-761.

[34] F. Fontana, D. Rocchesso, and E. Apollonio, "Using the waveguide mesh in modeling 3D resonators", Proceedings of the COST G-6 Conference on Digital Audi Effects, Verona, Italy, December 7th – 9th, 2000, pp. 229-232.

[35] H. Friedmann, R. Petricevic, and M. Ries, "On the way to active systems: AVR rotor – active vibration reduction for a textile bobbin", Computer and Structures, doit:10.1016/j.compstruc.2007.02.005, 2007.

[36] R. F. Fung, J. S. Huang, and Y. C. Chen, "The transient amplitude of the viscoelastic travelling string: an integral constitutive law", Journal of Sound and Vibration, Vol. 201, Issue 2, 1997, pp. 153-167.

[37] R. F. Fung, and J. S. Shieh, "Vibration analysis of a non-linear coupled textile-rotor system with synchronous whirling", Journal of Sound and Vibration, Vol. 199, Issue 2, 1997, pp. 207-221.

[38] A. Galembo, A. Askenfelt, L. L. Cuddy, and F. A. Russo, "Effects of relative phases on pitch and timbre in the piano bass range", Journal of the Acoustical Society of America, Vol. 110, Issue 3, 2001, pp. 1649-1666.

[39] P. Galvin, and J. Dominguez, "Dynamic analysis of a cable-stayed deck steel arch bridge", Journal of Constructional Steel Research, Vol. 63, 2007, pp. 1024-1035.

[40] G. C. Gorain, and S. K. Bose, "Uniform stability of damped nonlinear vibrations of and elastic string", Proceedings of the Indian Academy of Sciences, Vol. 113 Issue 4, 2003, pp. 443-449.

[41] H. P. W. Gottlieb, " Non-linear, non-planar transverse free vibrations of a constant-tension string", Journal of Sound and Vibration, Vol. 191, Issue 4, 1996, pp. 563-575.

[42] C. E. Gough, "The mass-loaded and nonlinear vibrating string problem revisited", European Journal of Physics, Vol. 21, 2000, pp. L11-L14.

[43] M. D. Greenberg, "Advanced engineering mathematics", Second Edition, Prentice Hall, Upper Saddle River, New Jersey, 1998.

[44] J. L. Ha, J. R. Chang, and R. F. Fung, "Nonlinear dynamic behavior of a moving viscoelastic string undergoing three-dimensional vibration", Chaos, Solitons and Fractals, Vol. 33, Issue 4, 2007, pp. 1117-1134.

[45] H. Harrison, "Plane and circular motion of a string", Journal of the Acoustical Society of America, Vol. 20, 1948, pp. 874-875.

[46] H. Järveläinen, "Applying perceptual knowledge to string instrument synthesis", Proceedings of MOSART Workshop on Current Research Directions in Computer Music, Barcelona, Spain, November 15th – 17th, 2001, pp. 187-195.

[47] H. Järveläinen, and M. Karjalainen, "Importance of inharmonicity in the acoustic guitar", Proceedings of International Computer Music Conference, Barcelona, Spain, September 5th – 9th, 2005, pp. 363-366.

[48] H. Järveläinen, and M. Karjalainen, "Is inharmonicity perceivable in the acoustic guitar?", Proceedings of the Forum Acusticum, Budapest, Hungary, August 29th – September 2nd, 2005, pp. 435-440.

[49] H. Järveläinen, M. Karjalainen, and V. Välimäki, "Audibility of inharmonicity in string instrument tones", Acoustics Research Letters Online, Vol. 2, Issue 3, 2001, pp.79-84.

[50] H. Järveläinen, M. Karjalainen, and V. Välimäki, "Audibility of the timbral effects of inharmonicity in stringed instrument tones", Acoustics Research Letters Online, Vol. 2, Issue 3, 2001, pp. 79-84.

[51] H. Järveläinen, V. Välimäki, and T. Verma, "Audibility of initial pitch glides in string instrument sounds", Proceedings of International Computer Music Conference, Havana, Cuba, September 17th – 23rd, 2001, pp. 282-285.

[52] J. M. Johnson, and A. K. Bajaj, "Amplitude modulated and chaotic dynamics in resonant motion of strings", Journal of Sound and Vibration, Vol. 128, Issue 1, 1989, pp. 87-107.

[53] M. Karlberg, and J. O. Aidanpää, "Rotordynamical modeling of a fiber refiner during production", Journal of Sound and Vibration, Vol. 303, Issue 3-5, 2007, pp. 440-454.

[54] J. Kim, and S. P. Chang, "Dynamic stiffness matrix of an inclined cable", Engineering Structure, Vol. 23, 2001, pp. 1614-1621.

[55] L. E. Kinsler, and A. R. Frey, "Fundamentals of acoustics", Second Edition, John Wiley & Sons, New York, 1962.

[56] E. Kreyszig, "Advanced engineering mathematics", 8th Edition, John Wiley & Sons, New York, 1998.

[57] A. G. Krishnan, "Orbital dynamics analysis and scale model testing of galloping transmission lines", M. A. Sc. Thesis, Department of Mechanical and Industrial Engineering, Concordia University, Montreal, Canada, 2006.

[58] E. V. Kurmyshev, "Transverse and longitudinal mode coupling in a free vibrating soft string", Physics Letters A, Vol. 310, 2003, pp. 148-160.

[59] J. W. Larsen, and S. R. K. Nielsen, "Non-linear stochastic response of a shallow cable", International Journal of Non-Linear Mechanics, Vol. 41, 2006, pp. 327-344.

[60] A. W. Leissa, and A. M. Saad, "Large amplitude vibrations of strings", Journal of Applied Mechanics, Vol. 61, 1994, pp. 296-301.

[61] C. Lemaitre, M. M. Alam, P. Hémon, E. de Langre, and Y. Zhou, "Rainwater rivulets on a cable subject to wind", Comptes Rendus Mecanique, Vol. 334, 2006, pp. 158-163.

[62] Y. Li, D. Aron, and C. D. Rahn, "Adaptive vibration isolation for axially moving string: theory and experiment", Automatica, Vol. 38, 2002, pp. 379-390.

[63] E. Maor, "Trigonometric delights", Princeton University Press, Reprint Edition, Princeton, New Jersey, 2002.

[64] M. Matsumoto, H. Shirato, T. Yagi, M. Goto, S. Sakai, and J. Ohya, "Field observation of the full-scale wind-induced cable vibration", Journal of Wing Engineering and Industrial Aerodynamics, Vol. 91, 2003, pp. 13-26.

[65] M. Matsumoto, H. Shirato, T. Yagi, M. Goto, and S. Sakai, "Rain-wind-induced vibration of inclined cables at limited high reduced wind velocity region", Journal of Wing Engineering and Industrial Aerodynamics, Vol. 91, 2003, pp. 1-12.

[66] J. H. Mathews, and K. D. Fink, "Numerical methods using MATLAB", Fourth Edition, Prentice Hall, Upper Saddle River, New Jersey, 2004.

[67] T. Miyata, "Historical view of long-span bridge aerodynamics", Journal of Wind Engineering and Industrial Aerodynamics, Vol. 91, 2003, pp. 1393-1410.

[68] T. C. Molteno, and N. B. Tufillaro, "An experimental investigation into the dynamics of a string", American Journal of Physics, Vol. 72, Issue 9, 2004, pp. 1157-1169.

[69] T. C. Molteno, and N. B. Tufillaro, "Torus doubling and chaotic string vibrations: experimental results", Journal of Sound and Vibration, Vol. 137, Issue 2, 1990, pp. 327-330.

[70] P. M. Morse, and K. U. Ingard, "Theoretical acoustics", First Edition with Errata Page, Princeton University Press, Princeton, New Jersey, 1986.

[71] K. W. Morton, and D. F. Mayers, "Numerical solution of partial differential equations", Second Edition, Cambridge University Press, Cambridge, United-Kingdoms, 2005.

[72] I. Nakamura and D. Naganuma, "Characteristics of piano sound spectra", Proceedings of the Stockholm Music Acoustics Conference, Stockholm, Sweden, July 28th – August 1st, 1993, pp. 325-330.

[73] R. Narasimha, "Non-linear vibration of an elastic string", Journal of Sound and Vibration, Vol. 8, Issue 1, 1968, pp. 134-146.

[74] A. H. Nayfeh, and D. T. Mook, "Nonlinear vibrations", John Wiley and Sons, New York, 1979.

[75] F. Noad, "The complete idiot's guide to playing the guitar", Second Edition, Alpha Books, Indianapolis, Indiana, 2002.

[76] O. O'Reilley, and P. J. Holmes, "Non-linear, non-planar and non-periodic vibrations of a string", Journal of Sound and Vibration, Vol. 153, Issue 3, 1992, pp. 413-435.

[77] T. Ohkuma, J. Kagami, H. Nakauchi, T. Kikuchi, K. Takeda, and H. Marukawa, "Analytical study of galloping of four bundle conductors with ice accretion model", Proceedings of 7th Annual Conference of Power and Energy Society, IEEE, Osaka, Japan, August, 1996, pp. 659-660.

[78] T. Ohkuma, J. Kagami, H. Nakauchi, T. Kikuchi, K. Takeda, and H. Marukawa, "Numerical analysis of overhead transmission line galloping considering wind turbulence", Electrical Engineering in Japan, Vol. 131, 2000, pp. 1386-1397.

[79] W. F. Osgood, "Advance calculus", Macmilliam Company, New York, 1933.

[80] M. Otrin, and M. Boltezar, "Damped lateral vibrations of straight and curved cables with no axial pre-load", Journal of Sound and Vibration, Vol. 300, Issue 3-5, 2007, pp. 676-694.

[81] J. Pakarinen, "Spatially distributed computational modeling of a nonlinear vibrating string", M. Sc. thesis, Laboratory of Acoustics and Audio Signal Processing, Helsinki University of Technology, Finland, 2004.

[82] M. Pakdemirli, A. G. Ulsoy, and A. Ceranoglu, " Transverse vibration of an axially accelerating string", Journal of Sound and Vibration, Vol. 169, Issue 2, 1994, pp. 179-196.

[83] S. Parmley, T. Zobrist, T. Clough, A. Perez-Miller, M. Makela, and R. Yu, "Vibrational properties of a loaded string", American Journal of Physics, Vol. 63, Issue 6, 1994, pp. 547-550.

[84] W. H. Press, S. A. Teukolsky, W. T. Vetterling, and B. P. Flannery, "Numerical recipes in C++: the art of scientific computing", Second Edition, Cambridge University Press, Cambridge, United-Kingdoms, 2002.

[85] S. S. Rao, "Mechanical vibrations", Fourth Edition, Prentice Hall, Upper Saddle River, New Jersey, 2004.

[86] J. O. Smith, "Physical modeling using digital waveguides", Computer Music Journal, Vol. 16, Issue 4, 1992, pp. 74-91.

[87] J. O. Smith, "Viewpoints on the history of digital synthesis", Proceedings of the International Computer Music Conference, Montreal, Canada, October $16^{th} - 20^{th}$, 1991, pp. 1-10.

[88] A. Stanoyevitch, "Introduction to numerical ordinary and partial differential equations using MATLAB", John Wiley & Sons, Hoboken, New Jersey, 2005.

[89] C. Su, X. Fan, and T. He, "Wind-induced vibration analysis of a cable-stayed bridge during erection by a modified time-domain method", Journal of Sound and Vibration, Vol. 303, Issue 1-2, 2007, pp. 330-342.

[90] W. T. Thomson and M. D. Dahleh, "Theory of vibration with applications", Fifth Edition, Prentice Hall, Upper Saddle River, New Jersey, 1998.

[91] N. B. Tufillaro, "Nonlinear and chaotic string vibrations", American Journal of Physics, Vol. 57, Issue 5, 1989, pp. 408-414.

[92] N. B. Tufillaro, "Torsional parametric oscillations in wires", European Journal of Physics, Vol. 11, 1990, pp. 122-124.

[93] V. Välimäki, "Discrete-time modeling of acoustic tubes using fractional delay filters", Ph. D. Thesis, Faculty of Electrical Engineering, Helsinki University of Technology, Espoo, Finland, 1995.

[94] W. T. van Horssen, "On the influence of lateral vibrations of supports for an axially moving string", Journal of Sound and Vibration, Vol. 268, Issue 2, 2003, pp. 323-330.

[95] W. T. van Horssen, and S. V. Ponomareva, "On the construction of the solution of an equation describing an axially moving string", Journal of Sound and Vibration, Vol. 287, Issue 1-2, 2005, pp. 359-366.

[96] G. Venkateswara Rao, " Moderately large amplitude vibrations of a constant tension string: a numerical experiment", Journal of Sound and Vibration, Vol. 263, Issue 1, 2003, pp. 227-232.

[97] J. Wang, and J. L. Lilien, "Overhead electrical transmission line galloping: a full multi-span 3-DOF model, some applications and design recommendations", IEEE Transaction of Power Delivery, Vol. 13, Issue 3, 1998, pp. 909-916.

[98] L. Wang, and Y. L. Xu, "Wind-rain-induced vibration of cable: an analytical model (1)", International Journal of Solids and Structures, Vol. 40, 2003, pp. 1265-1280.

[99] A. Watzky, "Non-linear three-dimensional large-amplitude damped free vibration of a stiff elastic stretched string", Journal of Sound and Vibration, Vol. 153, Issue 1, 1992, pp. 125-142.

[100] P. Wesseling, " Von Neumann stability conditions for the convection-diffusion equation", IMA Journal of Numerical Analysis , Vol. 16, Issue 4, 1996, pp. 583-598.

[101] J. Woodhouse, "Plucked guitar transients: Comparison of measurements and synthesis", Acta Acustica united with Acustica, Vol. 90, 2004, pp. 945-965.

[102] W. J. Wu, and C. S. Cai, "Theoretical exploration of a taut cable and a TMD system", Engineering Structures, Vol. 29, 2007, pp. 962-972.

[103] S. K. Yalla, "Liquid dampers for mitigation of structural response: theoretical development and experimental validation", Ph. D. Thesis, Department of Civil Engineering and Geological Sciences, Notre Dame, IN, 2001.

[104] K. J. Yang, K. S. Hong, and F. Matsuno, "Robust adaptive boundary control of an axially moving string under a spatiotemporally varying tension", Journal of Sound and Vibration, Vol. 273, Issue 4-5, 2004, pp. 1007-1027.

[105] M. A. Zarubinskaya, and W. T. van Horssen, "On aspects of boundary damping for a rectangular plate", Journal of Sound and Vibration, Vol. 292, Issues 3-5, 2006, pp. 844-853.

[106] M. A. Zarubinskaya, and W. T. van Horssen, "On the free vibrations of a rectangular plate with two opposite sides simply supported and the other sides attached to linear springs", Journal of Sound and Vibration, Vol. 278, Issues 4-5, 2004, pp. 1081-1093.

[107] L. Zhang, and J. W. Zu, "Non-linear vibrations of viscoelastic moving belts, part I: free vibration analysis", Journal of Sound and Vibration, Vol. 216, Issue 1, 1998, pp. 75-91.

[108] L. Zhang, and J. W. Zu, "Non-linear vibrations of viscoelastic moving belts, part II: forced vibration analysis", Journal of Sound and Vibration, Vol. 216, Issue 1, 1998, pp. 93-105.

[109] N. H. Zhang, and L. Q. Chen, "Nonlinear dynamical analysis of axially moving viscoelastic strings", Chaos, Solitons and Fractals, Vol. 24, 2005, pp. 1065-1074.